

Reversal of aging via *in vivo* epigenetic reprogramming

A dissertation presented by

Yuancheng Lu

to

The Division of Medical Sciences

in partial fulfillment of the requirements for the degree of

Doctor of Philosophy

in the subject of

Biological and Biomedical Sciences

Harvard University

Cambridge, Massachusetts

May 2020

© 2020 Yuancheng Lu

All rights reserved.

Reversal of aging via *in vivo* epigenetic reprogramming**Abstract**

Aging is a degenerative process leading to tissue dysfunction and death. A proposed cause of aging is the accumulation of epigenetic noise, which disrupts youthful gene expression patterns that are required for cells to function optimally and recover from damage. Changes to DNA methylation patterns over time form the basis of 'aging clocks', but whether old individuals retain information to reset the clocks and, if so, whether it would improve tissue function is not known. Of all the tissues in the body, the central nervous system (CNS) is one of the first to lose regenerative capacity. Using the eye as a model tissue, we show that expression of Oct4, Sox2, and Klf4 genes (OSK) in mice resets youthful gene expression patterns and the DNA methylation age of retinal ganglion cells, promotes axon regeneration after optic nerve crush injury, and restores vision in a mouse model of glaucoma and in normal aged mice. This process, which we call the reversal of information loss via epigenetic reprogramming or REVIVER, requires non-global, active DNA demethylation by TET enzymes and the downstream enzyme TDG, indicating that alterations in DNA methylation patterns may not simply indicate age, but participate in aging. Thus, old tissues retain a faithful record of youthful epigenetic information that can be accessed for functional age reversal.

Dedication

This thesis is dedicated to my grandfather, Honghua Lu, who passed away bravely fighting aging during preparation of this manuscript. Sadly, I was at the critical attempt to test the effect of *in vivo* reprogramming for axon regeneration, when travelling back and waiting for visa renewal was unaffordable. I missed seeing him one last time and his funeral too. My project, however, took off since then, maybe due to his blessing in the heaven. He was unschooled and a farmer for life who couldn't read and write. But he was hard-working and resilient, which also brought me where I am. I hope he feels proud that the knowledge we gain from my thesis may one day alleviate aging diseases from those like him, who be loved and cherished by their family.

Acknowledgement

As the famous proverb said, “It takes a village to raise a child”. There are a lot of people I want to thank for their support to raise me up as a scientist. I am truly grateful for the love, wisdom, inspiration and memory they afforded me.

First, I’d like to thank my thesis advisor David Sinclair, for giving me the opportunity to join your team and that vision of an ambitious goal: reversing aging. My thesis may be a small step forward for this goal, but it was huge and long like ten marathons to me. I never imagined I would finish it; however, you did. You believed in me when I didn’t, then we celebrated each milestone along this journey. Looking back, I am amazed what we have accomplished together.

I am greatly indebted to two of my great friends and colleagues: Michael Bonkowski and Michael Schultz. You two welcomed me immediately during my rotation and treated me as your naughty little brother since then. I had some cultural shock during the first year of my PhD, but you two helped me overcome it by taking me out for boating, fishing, and drinking etc. Besides, you offered me so many scientific and life advice, helped me settle my family here, and wanted me to have success just like it was yours. You are my extended family.

This dissertation could not be completed without other members of the Sinclair lab: Susan DeStefano, our wonderful coordinator, I appreciate the love you showed me from day 1!

Xiao Tian, a PhD superstar that I have admired since we first met at the 2016 CSHL meeting, I feel very lucky we became colleagues and friends from 2018 and started collaborating on the reprogramming project since then. I kept learning from you every day I worked with you.

Jae-Hyun Yang, my mentor on epigenetics, your hard work on proving the epigenetic aging theory really paved my way to try epigenetic reprogramming, not to mention you guided

me on the initial trials of chemical and mRNA reprogramming *in vitro*. I learned most of my cell culture and qPCR knowledge from you. Thank you for investing your time on me.

Jun Li, Abhirup Das and Alice Kane, thank you for your support during my hard time. Daniel Vera, your expertise on RNA-seq amazed me. Luis Rajman, I got to understand your underappreciated management job close to the end of my PhD. Karolina Chwalek, your help on getting grants for this project turned the narrative of my PhD around.

My PhD colleagues Michael Cooney, Patrick Griffin, Joao Amorim, and incoming Chris Petty turned the lab into a more fun place to work in. Those board game nights are fond memories! Israel, Giuseppe, Jaime, Maeve, Parvez, Amber, and Minyang, the special skillset each of you brought made our lab immeasurably strong scientifically.

It was my great privilege to work with two amazing intern students: Doudou Yu and Qiurui Zeng. I thank you both for your incredible hard work you put into this project: those busy trips between three labs, working holidays and nights quantifying data till wrists aching. My graduation would have delayed a year without you. Thank you for letting me be your mentor.

I owe a large amount of gratitude to Zhigang He, Bruce Ksander and Meredith Ksander, who have brought their decades of knowledge on the retinal injury and disease to this project, and I learnt a great deal from each of them. And also, my wonderful collaborators in their labs: Benedikt Brommer, Anitha Krishnan, Chen Wang, Songlin Zhou, Emma Hoffmann, Margarete Karg, Ekaterina Korobkina. Working with each of you side by side was so enjoyable, and I appreciate all your contributions from the bottom of my heart.

Steve Horvath, Vadim Gladyshev, Margarita Meer, and Noah Davidsohn, each of you has played an irreplaceable critical role in my thesis, and I look forward to many more exciting collaborations with you in the future.

My dissertation advisory committee is formed by four professors that I look up to a lot: Raul Mostoslavsky, Amy Wagers, Konrad Hochedlinger and Yang Shi. Having this “A” team was a blessing that could make me smile during sleep. Your knowledge and insightful advice really help shaped my thesis project. Raul Mostoslavsky served on all my committees from PQE to 5 of DACs, and now thesis. You inspired me not only in these meetings that you travelled all the way from MGH to attend, but also through your Epigenetic class and our email discussions. I just couldn’t thank you enough. I would also like to thank other professors who served on my PQE and thesis committee: Ya-Chieh Hsu, Vadim Gladyshev, Andrew Lassar, and Feng Zhang. Thank you for taking your valuable time reading my proposal and thesis.

I would not have gotten into graduate school without the training and recommendations from my undergraduate mentors Tian Xu, Xiaohui Wu, and Guoping Fan. You all taught me how to critically think and be a scientist. Thank you for letting me stand on your shoulders.

I made great friends during graduate school in classes, basketball games, and in the student dorm Vanderbilt Hall. Jason Qian, Jeff Yuzhong Meng, Liang Wei Wang and many others, thank you for those fond memories, from making dumplings and biking along the Charles River, to playing cards and pool at my home. My talented BBS classmates, especially my deceased colleague John Hatch, gave me a lot of inspirations and encouragements along the way.

To my big family: My mom Hong Xu and dad Zhigang Lu, thank you for your unconditional love and tremendous effort you put into my education. I appreciate it even more since I have become a parent. My stepfather Guosheng Xu, stepmother Yuyan Zhang, and brother Steven Lyu, thank you for brining me peace and happiness in tough times. I feel lucky to have you joining my life. Last but not least, my dear wife Shurong Hou, and our son Raymond Wade Lu, you brought me a home I have always dreamed for, and I will cherish us forever.

Table of Contents

	Page #
Abstract	iii
Dedication	iv
Acknowledgement	v
Chapter 1: The epigenetic information theory of aging	1
I. Introduction to the information theory of aging.....	2
II. Epigenetic noise caused by Relocalization of Chromatin Modifiers (RCM).....	4
III. Epigenetic information loss during aging.....	5
IV. Evidence of epigenetic information correction	11
V. Summary.....	12
VI. References	13
Chapter 2: Development of a safe <i>in vivo</i> epigenetic reprogramming method	17
I. <i>In vivo</i> reprogramming was limited by toxicity and delivery.....	18
II. c-Myc is disposable for resetting aging signature	21
III. Dual AAV system enables inducible expression of polycistronic OSK	23
IV. AAV-mediated OSK expression achieves long term safety.....	23
V. References	27
Chapter 3: Promoting axon regeneration in mammalian CNS by Tet-dependent reprogramming. 28	
I. Polycistronic OSK promotes RGC survival and axon regeneration post optic nerve injury	29
II. Epigenetic reprogramming promotes DNAm age reversal and DNA demethylation post axonal injury	36
III. OSK promotes Tet2-dependent axon regrowth in human neurons	41
IV. New hypothesis: Acute CNS injury leads to accelerated aging	44
V. References	46
Chapter 4: Reversal of glaucoma- and aging-induced vision loss by epigenetic reprogramming..... 48	
I. Reversal of vision loss in a mouse model of glaucoma.....	49
II. Restoration of youthful regenerative capacity and vision in aged mice by resetting epigenome	52
III. Summary.....	57
IV. References	58
Chapter 5: Mechanism and future directions of <i>in vivo</i> reprogramming..... 60	
I. Active DNA demethylation is required for epigenetic correction.....	61
II. Alternative strategies for <i>in vivo</i> reprogramming.....	62
III. More applications of <i>in vivo</i> reprogramming	64
IV. Prospection: What’s the biological observer for aging reversal.....	65
V. References	68
Methods	70
Supplementary Tables	86

Portions of this thesis have been submitted for publications and patents:

Lu, Y., Brommer, B., Tian, X., Krishnan, A., Wang, C., Meer, M., Vera, D., Zeng, Q., Yu, D., Bonkowski, M., Zhou, S., Yang, J., Hoffmann, E., Karg, M., Schultz, M., Kane, A., Davidsohn, N., Korobkina, E., Chwalek, K., Rajman, L., Church, G., Hochedlinger, K., Gladyshev, V., Horvath, S., Ksander, M.G., Ksander, B., He, Z., Sinclair, D.A. Reversal of ageing- and injury-induced vision loss by Tet-dependent *in vivo* epigenetic reprogramming. Nature. (*in revision*) bioRxiv: <https://www.biorxiv.org/content/10.1101/710210v1>

Lu, Y., Tian, X., Sinclair, D.A., The epigenetic information theory of aging. Trends in Biochemical Sciences. (Editor invited, in preparation)

Lu, Y., Sinclair, D.A., Cellular reprogramming to reverse aging and promote organ and tissue regeneration. Appln. No.: PCT/US2019/053545, 2019

Lu, Y., Davidsohn, N., Sinclair, D.A., Mutant reverse tetracycline transactivators for expression of genes. Appln. No.: PCT/US2019/053492, 2019

Other publications during doctoral study:

Schultz, M.B., Rinaldi, C., **Lu, Y.**, Amorim, JA., Sinclair DA. Molecular and Cellular Characterization of SIRT1 Allosteric Activators. Methods Mol Biol. 2019;1983:133-149.

Das, A., Huang, G.X., Bonkowski, M.S., Longchamp, A., Li, C., Schultz, M.B., Kim, L., Osborne, B., Joshi, S., **Lu, Y.**, Treviño-Villarreal, J.H., 10 authors..., Sinclair, D.A., Impairment of an Endothelial NAD⁺-H₂S Signaling Network Is a Reversible Cause of Vascular Aging. Cell. 2018, 173(1):74-89.e20

Schultz, M.B., **Lu, Y.**, Braidy, N., Sinclair, D.A., Assays for NAD⁺-Dependent Reactions and NAD⁺ Metabolites. Methods Mol Biol. 2018, 1813:77-90.

Disclosure:

I am a shareholder of Iduna Therapeutics, a Life Biosciences company that focus on translating *in vivo* reprogramming technologies into human. The potential conflict of interest in under management by Office for Academic and Clinical Affairs at Harvard Medical School.

Chapter 1: The epigenetic information theory of aging

I. Introduction to the information theory of aging

Over the past 20 years, the aging field has moved out from the backwaters of biology to the forefront of science. Nine “hallmarks” of aging are proposed to explain what causes us to grow old, and various interventions are being developed to counter them [1, 2]. But what causes these changes to happen in the first place? Is there a unified cause of aging that explains them all? Various theories have been proposed but none have adequately explained the phenomenon, leaving the field without a guiding paradigm.

A new theory to explain why we age is gaining traction, which we will refer to as the Information Theory of Aging. The Hypothesis emerges from an understanding of the biological information cycle. Life is, by necessity, information-based, dependent on both digital and analog information, the latter controlling the survival and replication of the former. Long-term digital biological information is encoded by the genome, whereas rapidly responsive analog information is encoded by the epigenome, a complex system of transcriptional networks, RNAs, DNA, and chromatin modifications that preserves and perpetuates life’s digital information [3].

Maintaining digital information over many decades is relatively straightforward. DNA is a robust molecule that can be repaired by excising the damage or copying across a duplicate copy. Analog information, on the other hand, is far more difficult to maintain. The problem with all analog-based systems, whether they are electronic or biological, is that they are inherently susceptible to noise. This phenomenon was first described by communications engineer Claude Shannon shortly after the Second World War [4] but is well known to anyone who has repeatedly copied a cassette tape or photocopied an image for multiple times. With this in mind, a loss of analog information over time, which is accelerated by threats to losing long-term digital information, is the best explanation for why life is transitory.

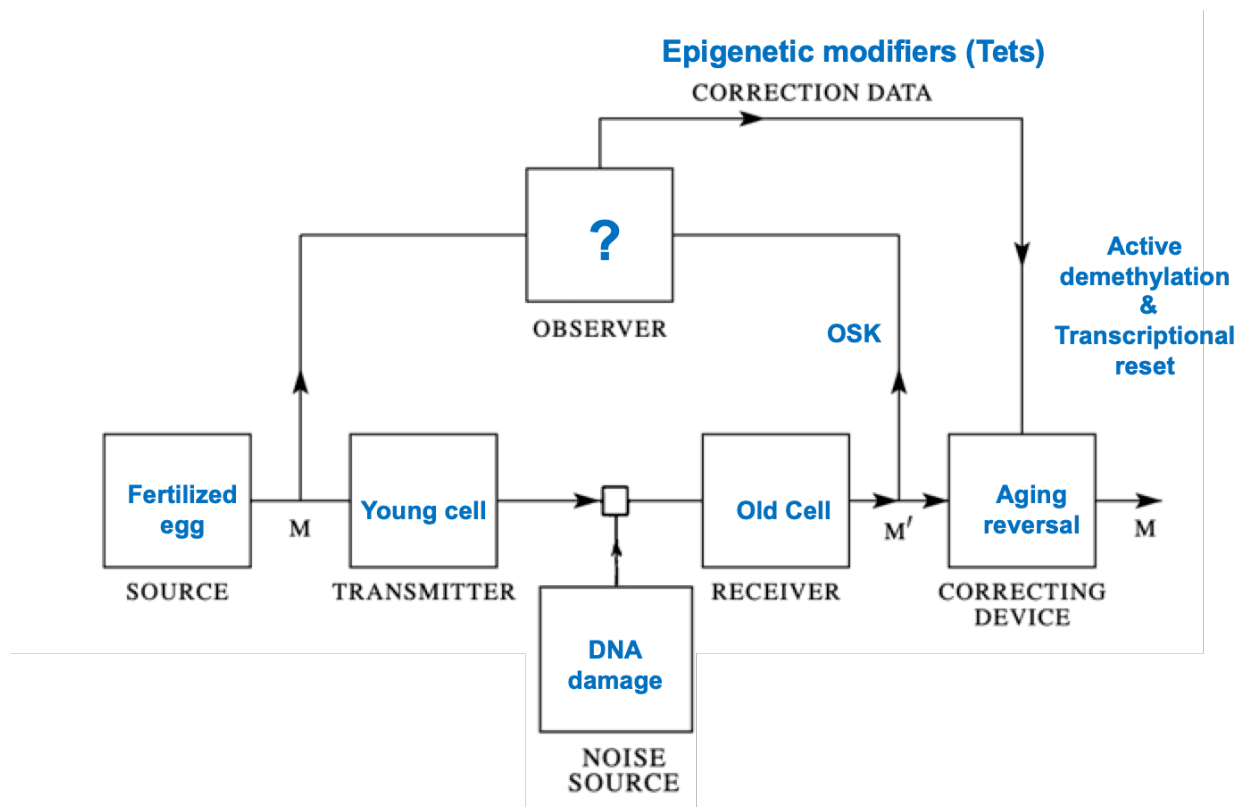


Figure 1 The Information Theory of Aging. The original algorithms to quantify information loss due to entropy were proposed by Claude Shannon [4]. In communication, the signal is sent by a source, go through a transmitter, and then the receiver gets the signal. Shannon was trying to solve the information loss during signal communication. all information representing in a physical way is normally subject to noise (so does epigenetic information). Shannon propose to introduce an observer to the system, so the observer can see both what is sent and what is recovered. This observer distinguishes the errors in the received message and use a correction channel to guide the receiver to correct the errors. This is basically how the internet and TCP/IP works. When data packets are lost, they are recovered and resent moments later. But Shannon’s work may ultimately prove to be even more important than that, for what he discovered about preserving and restoring information can be applied to aging. In aging, the source of epigenetic information is the egg and sperm, from our parents. And that information gets transmit through time, subject to epigenetic noise, and then lost in the old cells. The noise source for aging is DNA damage induces Relocalization of Chromatin Modifiers (RCM), which causes young cells to lose their identity and eventually senesce. Relevant works are summarized in subsection II of this Chapter. The rest part of this thesis focuses on the finding and understanding of aging correction process, in which epigenetic reprogramming with OSK helps the old cells access the cellular observer to retrieve the youthful epigenetic information via Tet-dependent DNA demethylation etc, thus achieving “aging reversal”.

II. Epigenetic noise caused by Relocalization of Chromatin Modifiers (RCM)

The first evidence that the loss of analog information in response to cellular damage causes aging came from studies of budding yeast performed by the Guarente lab at MIT in the 1990s [5]. This landmark work identified “silent information regulatory” (SIR) genes as key determinates of lifespan. Sir2, the prototypical sirtuin longevity protein, was shown to be a key DNA repair factor that is recruited away from silent mating-type loci to assist with the repair of DNA breaks, which increasingly occur as yeast cells age [6]. The protracted absence of Sir2 from silent mating-type loci causes the cell to lose its identity and become sterile, a hallmark of yeast aging. Addition of an extra copy of SIR2 increases epigenomic resilience by improving DNA repair while also maintaining cellular identity [7]. As a result, yeast cells maintain their cellular identity and live 30% longer. These data are consistent with yeast aging being the result of a loss of epigenomic information.

In the past few years, evidence points to epigenomic noise as an upstream cause of aging in mammals, too. The Sir2 homologs, SIRT1, SIRT6, and SIRT7, maintain cellular identity and extend a mouse’s lifespan. Similar to the yeast story, as animals age SIRT1 moves to sites of DNA damage to assist with repair, causing the ectopic transcription of hundreds of genes, satellite repeat RNA, and transposons [8-10]. This "relocalization of chromatin modifying proteins" or RCM concept is by no means limited to sirtuins. In recent years, other proteins have been implicated in this age-related loss of epigenomic information including PARP-1, HDAC1, Wnt, and the REST complex [8, 11, 12].

These findings raise the question: Why is life set up this way? The answer appears to be antagonistic pleiotropy, an evolution theory proposed by George Williams [13], where a beneficial process that provides young organisms a greater chance to survive is detrimental later

in life as noise builds up in the system. The re-localization of chromatin modifying proteins during aging is likely to be an active cellular defense response because the DNA damage checkpoint protein, ATM, is required [14]. The benefit this provides is that in young organisms, gene expression is coordinated with DNA repair. The recruitment of SIRT1 away from the silent mating-type loci expresses genes that improve DNA repair and halt mating while damage is repaired. Most proteins will return to their original sites, however, the epigenomic shuffle is never completely reset, introducing noise into the system. The cost of this adaptive mechanism is epigenetic noise, which causes cells to lose their identity and eventually senesce [8, 15-17]. Thus, according to the Information Hypothesis of Aging, the loss of epigenetic information over time ultimately causes organisms to age. If this is correct, long-lived species should have increased epigenetic resilience. Interestingly, a study in naked mole rats, which are known for their exceptional longevity and cancer resistance, showed that compared to mice, in aging, they maintain a stable epigenomic landscape during aging [18]. This may be a result of having a stronger DNA repair protein SIRT6, a Sir2 homolog that repairs DNA double strand breaks, in the naked mole rat compared to other rodent species [19].

III. Epigenetic information loss during aging

During development, cell identity is established by laying down a complex set of epigenetic information in each cell, each one with a specialized pattern of gene expression and function, a concept first depicted by the Waddington landscape. Owing to advances in single cell RNA sequencing and CRISPR-mediated lineage tracing, hundreds of distinct cell types have been identified in mammals [20, 21]. During development, cell identity is established by laying down a complex set of epigenetic information in each cell, each one with a specialized pattern of gene expression and function [22]. However, this information is seemingly lost over time,

leading to a gradual loss of cell identity and functional decline. In this section, I summarize the epigenetic changes that occur during aging, including changes to chromatin structure, histone post-translational modifications, and DNA methylation patterns. I also focus on the potential causes and interventions of these changes.

(1) Chromatin structure

Chromatin is a nucleoprotein complex that packages 3-meter-long DNA into a nucleus of 1-5 micrometers. The nucleosome, composed of 147 bp of DNA wrapped around a histone octamer (two of H2A-H2B dimers and one H3-H4 tetramer), is the fundamental subunit of chromatin. Both DNA and histones are subject to chemical modifications, which facilitate the formation of two different chromatin states: euchromatin, an open and transcriptionally active state, and heterochromatin, a condensed and transcriptionally silent state. During aging, a global loss of heterochromatin has been seen in multiple model organisms including yeast [15], *C. elegans* [27], *Drosophila* [28, 29], and mammals, indicating a common feature in all of them. Box 1 summarizes the current understanding of the mechanisms contributing to age-associated heterochromatin loss. Heterochromatin loss is known to relieve silencing at repetitive elements such as retrotransposons [30, 31] and endogenous retroviral elements [32], triggering an inflammatory response. Importantly, heterochromatin that establishes cell identity [33, 34], is lost with age [16, 17], which explains loss of cell identity in aged organisms including yeast and mice [8, 35].

The development of high-throughput chromosome conformation capture technologies, such as Hi-C, have transformed our understanding of gene regulation and chromatin structure [36]. The chromatin fiber, which has the appearance of beads on a string, is further compacted by forming higher-order organizations in interphase nuclei mediated by genomic interaction, i.e.,

topologically associating domains (TADs) and chromatin compartmentalization. The spatial organization of chromatin carries critical information for gene regulation. For example, specific long-range interactions between functional loci, such as active enhancers and promoters, are facilitated by chromatin looping and insulated by TAD boundaries. TADs are highly conserved even across cell types, and limited alterations of TAD boundaries have been detected between young and old cells [37]. However, significant changes occur among intra-TAD interactions as well as compartment switching [37]. TAD switching is an efficient way to change chromatin state of a genomic locus, which happens genome wide during stem cell differentiation [38]. With the advancement of high-resolution microscopy imaging and other 3C-based methods such as HiChIP [39], Capture Hi-C [40], and ChIA-PET [41], a more comprehensive and high-resolution picture will be revealed for the changes of chromatin structure that lead to an dysregulated state during aging [17].

Some major unsolved questions remain. For example, what causes TADs and chromatin compartmentalization to change over time? Are these changes reversible? One driver of change might be reduced levels of TAD boundary anchor proteins, including CTCF and cohesin, which is known to occur during aging [42-44]. A recent study from our lab revealed DNA damage being a potential cause of the progression of such 3D changes [17]. Although no significant changes happen to the TAD boundaries following recovery from DNA damage, reproducible changes to chromatin compartmentalization occur, together with a loss of superenhancers and a shift in H3K27Ac patterns at genes involved in metabolic and developmental processes, leading to a loss of cell identity [17]. Future study may identify the RCM factors that lead to such changes and test interventions that restore proper genomic interaction.

(2) Histone changes

Histones are among the most highly conserved proteins in eukaryotes. During aging, a global loss of core histone proteins has been observed in yeast [45], worms [27], quiescent stem cells [46], and replicatively senescent human cells [47]. Histone loss results in a global upregulation of transcription due to reduced nucleosome occupancy and increased accessibility of the genome, increasing transcriptional noise. Histone loss is ostensibly a driver of aging in yeast cells, as elevated expression of histones extends lifespan [48]. However, the causative role of histone loss in aging in multi-cellular organisms has not been determined.

Histones are post-translationally modified by a variety of histone-modifying enzymes, decorating histone proteins with over 100 types of chemical groups [49]. Histone methylation and acetylation are two types of most studied modifications, which play critical roles in regulating chromatin structure and gene expression. For example, some marks are associated with transcriptional silencing and formation of heterochromatin, including H3K9me₃, H3K27me₃, and H4K20me₂. Other marks are associated with euchromatin and active transcription, such as H3K4me₃ and H4K16ac. Consistent with heterochromatin loss during aging, constitutive heterochromatin mark H3K9me₃ and the expression level of its methyltransferase SUV39H1 are both reduced [50-52]. One would expect that rescuing H3K9me₃ level by overexpressing SUV39H1 extends lifespan. However, in a progeria mouse model, a significant lifespan extension was obtained by knocking out Suv39h1 [53]. Whether or not H3K9me₃ decline plays a causative role in normal, physiological aging is not yet known.

Age-associated changes have been seen with other histone modifications, including H3K27me₃, H3K4me₃, H3K36me₃, H4K20me₃, H3K56Ac, and H4K16ac [54]. These changes often occur to a different extent and even in opposite directions in particular tissues and models

[55]. Considerable evidence indicates that altering specific histone marks by manipulating the level of related “writers” and “erasers” can extend lifespan in yeast and worms [54-56], demonstrating a causative role in aging and organismal health. Intriguingly, recent advances using different forms of transient reprogramming have proven that histone-related changes can be safely reversed, including a reversal of histone loss, changes in the levels of heterochromatin-associated proteins, and abnormal histone modifications (Table 1).

(3) DNA methylation clocks

The most common DNA modification in mammals is the 5-methyl cytosine (5mC) of CpG dinucleotides. As a stable epigenetic mark, DNA methylation plays an important role in establishing epigenetic landscapes and defining cell identity during development. Recent studies have revealed that DNA methylation is not static during aging but subjected to bidirectional changes at different genomic regions. While a global decline of DNA 5mC (hypomethylation) has been observed in mice and humans [57, 58], an increase of DNA 5mC (hypermethylation) occurs at a subset of CpGs including polycomb-group protein targets [59] and bivalent promoters [60]. These bidirectional changes serve as the basis of using DNA methylation profiles as a biomarker of aging.

The use of DNA methylation to predict age was first achieved in specific cell types, including human saliva [61] and blood samples [62]. However, it was unknown whether DNA methylation could be used as a universal biomarker of aging across different tissues of the body. The biomathematician Steve Horvath first showed there are age-related clusters of CpG sites shared between blood and brain tissue [63]. Then in 2013, after analyzing near 8000 samples covering 51 different tissues and cell types, he identified a set of 353 CpGs that can act as multi-tissue age estimators, often referred to as the “Horvath” clock [64]. Among these 353 CpG

sites, 193 of them positively correlate with age, whereas the remaining 160 CpGs have a negative correlation. Although the clock was based originally on chronological age, it may also indicate biological age, i.e., the true aging status of a given individual [65]. Using similar strategies, DNA methylation clocks have also been developed for mice [66-69], dogs [70], and naked mole rats [71], as well as over a dozen other species, suggesting that DNA methylation works as a clock in both short- and long-lived species. Whether other types of DNA methylation, such as N⁶-methylation of adenine, are involved in defining or regulating biological age is not yet known.

Table 1. Epigenetic information loss that can be rescued by interventions

Epigenetic factor	Epigenetic function	Changes during aging	Interventions	Outcome	Context
Histone level	Nucleosome assembly	Decrease	Transient reprogramming (OSK)	Increase	Fibroblasts isolated from old mice [23]
Lamin B1	LAD formation	Decrease	Transient reprogramming (OSK)	Increase	Fibroblasts isolated from old mice [23]
HP1 γ	Heterochromatin maintenance	Decrease	Transient reprogramming (OSKMLN)	Increase	Fibroblasts and endothelial cells from aged humans [24]
H3K9me3	Heterochromatin maintenance, transcriptional silencing	Decrease	Transient reprogramming (OSKM)	Increase	Progeroid fibroblasts (mouse), progeroid kidney and spleen (mouse), high-passage fibroblasts (mouse, human) [25]
			Transient reprogramming (OSKMLN)	Increase	Fibroblasts and endothelial cells from aged humans [24]
			SIRT1 overexpression	Increase	MEF [26]
H4K20me3	Heterochromatin maintenance, transcriptional silencing	Increase	Transient reprogramming (OSKM)	Decrease	Progeroid fibroblasts (mouse), progeroid kidney and spleen (mouse) [25]
DNA methylation clock	Indicate (or regulate) biological age	Increase	Transient reprogramming (OSK)	Decrease	Retina ganglion cells of old mice [23]
			Transient reprogramming (OSKMLN)	Decrease	Fibroblasts and endothelial cells from aged humans [24]

IV. Evidence of epigenetic information correction

The most remarkable studies to support the information theory of aging are somatic cell nuclear transplantation (SCNT) and induced pluripotent stem cells (iPSCs), two technologies that can induce epigenetic reprogramming. The results from them not only suggest the plasticity of cell fate, but also the plasticity of aging, in other words, the age of cell can be reset to young again after reprogramming.

In 1958, John Gurdon and his colleagues obtained cloned adult frogs by transferring the nuclei of adult frog cells into enucleated eggs [72]. It showed that the genetic information of a differentiated cell has not been irreversibly altered, and the cell fate can restart again. Will the age of cloned animals (such as Dolly) restart as well [73]? The answer is yes. In 2016, a comprehensive study for a cohort of 13 cloned sheep showed that they have normal lifespan and are healthy at advanced age [74].

In 2006, Shinya Yamanaka and his student found that using 4 nuclear transcription factors, Oct3/4, Sox2, Klf4, and c-Myc (Yamanaka factors), they can convert a somatic cell into induced pluripotent stem cells (iPSCs) [75], which are considered functionally identical to embryonic stem cells [76, 77]. Importantly, old human cells can also be reprogrammed back to young by resetting the epigenetic landscape [78]. The study in cells from aged patients demonstrated that Yamanaka factors plus two other factors Nanog and Lin28 [79], reprogrammed senescent and centenarian fibroblasts into iPSCs, which could then be differentiated into fibroblasts that showed gene expression profiles similar to that of young embryonic fibroblasts [78]. Even after differentiation into other cell types such as neurons, the differentiated cells retain the young phenotype [80].

It is worth noting that non-artificial reprogramming processes have also existed in nature for billions of years. For every species, extensive epigenetic reprogramming during germline specification and fertilization resets the age of subsequent generation. Natural reprogramming processes may also happen on a living animal. Hydra seem to have the ability to escape the aging process with high regenerative capacity [81], flatworms called planarians can grow back any piece of their body [82], zebrafish can regrow their fins, heart and kidney throughout their lives [83], and axolotls, a species of salamander, can replace complex body parts such as limbs that are lost at any age [84]. In mammals, mice can regrow toe tips [85] and the human liver, when resected, can regenerate to the same size it once was [86]. Considering the reprogramming process does not correct somatic mutations [87], the amelioration of age-associated phenotypes by epigenetic remodeling during cellular reprogramming indicates that epigenetic dysregulation is a major cause of aging.

V. Summary

Together, relocalization of epigenetic modifiers induces epigenetic information loss at the level of DNA methylation, histone modification, and overall chromatin structure. The change in the epigenome not only serves as biomarkers of aging but may drive the aging process. The Information Theory of Aging is supported by recent discoveries of cellular reprogramming. Although the genetic mutations that accumulate during aging cannot be reverted, the aged epigenome can be fully reset to a pluripotent state during continuous reprogramming *in vitro* [23]. It is important to determine whether and how the epigenetic information loss can be reversed *in vivo* by epigenetic reprogramming to register any functional improvement, such as vision improvement [23] and lifespan extension [25].

VI. References

1. Lopez-Otin, C. et al. (2013) The hallmarks of aging. *Cell* 153 (6), 1194-217.
2. Johnson, F.B. et al. (1999) Molecular biology of aging. *Cell* 96 (2), 291-302.
3. Bernstein, B.E. et al. (2007) The mammalian epigenome. *Cell* 128 (4), 669-81.
4. Shannon, C.E. (1948) A Mathematical Theory of Communication. *The Bell System Technical Journal* 27, 379-423.
5. Kennedy, B.K. et al. (1995) Mutation in the silencing gene SIR4 can delay aging in *S. cerevisiae*. *Cell* 80 (3), 485-96.
6. Sinclair, D.A. and Guarente, L. (1997) Extrachromosomal rDNA circles--a cause of aging in yeast. *Cell* 91 (7), 1033-42.
7. Kennedy, B.K. et al. (1997) Redistribution of silencing proteins from telomeres to the nucleolus is associated with extension of life span in *S. cerevisiae*. *Cell* 89 (3), 381-91.
8. Oberdoerffer, P. et al. (2008) SIRT1 redistribution on chromatin promotes genomic stability but alters gene expression during aging. *Cell* 135 (5), 907-18.
9. Sinclair, D.A. et al. (1997) Accelerated aging and nucleolar fragmentation in yeast sgs1 mutants. *Science* 277 (5330), 1313-6.
10. Kaerberlein, M. et al. (1999) The SIR2/3/4 complex and SIR2 alone promote longevity in *Saccharomyces cerevisiae* by two different mechanisms. *Genes Dev* 13 (19), 2570-80.
11. Lu, T. et al. (2014) REST and stress resistance in ageing and Alzheimer's disease. *Nature* 507 (7493), 448-54.
12. Nalapareddy, K. et al. (2017) Canonical Wnt Signaling Ameliorates Aging of Intestinal Stem Cells. *Cell Rep* 18 (11), 2608-2621.
13. Williams, G.C. (1957) Pleiotropy, Natural Selection, and the Evolution of Senescence. *Evolution* 11 (4), 398-411.
14. Dobbin, M.M. et al. (2013) SIRT1 collaborates with ATM and HDAC1 to maintain genomic stability in neurons. *Nat Neurosci* 16 (8), 1008-15.
15. Oberdoerffer, P. and Sinclair, D.A. (2007) The role of nuclear architecture in genomic instability and ageing. *Nat Rev Mol Cell Biol* 8 (9), 692-702.
16. Hayano, M. et al. (2019) DNA Break-Induced Epigenetic Drift as a Cause of Mammalian Aging. *bioRxiv*.
17. Yang, J.-H. et al. (2019) Erosion of the Epigenetic Landscape and Loss of Cellular Identity as a Cause of Aging in Mammals. *bioRxiv*, 808642.
18. Tan, L. et al. (2017) Naked Mole Rat Cells Have a Stable Epigenome that Resists iPSC Reprogramming. *Stem Cell Reports* 9 (5), 1721-1734.
19. Tian, X. et al. (2019) SIRT6 Is Responsible for More Efficient DNA Double-Strand Break Repair in Long-Lived Species. *Cell* 177 (3), 622-638 e22.
20. Cao, J. et al. (2019) The single-cell transcriptional landscape of mammalian organogenesis. *Nature* 566 (7745), 496-502.
21. Chan, M.M. et al. (2019) Molecular recording of mammalian embryogenesis. *Nature* 570 (7759), 77-82.
22. Becker, J.S. et al. (2016) H3K9me3-Dependent Heterochromatin: Barrier to Cell Fate Changes. *Trends Genet* 32 (1), 29-41.
23. Lu, Y. et al. (2019) Reversal of ageing- and injury-induced vision loss by Tet-dependent epigenetic reprogramming. *bioRxiv*.

24. Sarkar, T.J. et al. (2020) Transient non-integrative expression of nuclear reprogramming factors promotes multifaceted amelioration of aging in human cells. *Nat Commun* 11 (1), 1545.
25. Ocampo, A. et al. (2016) In Vivo Amelioration of Age-Associated Hallmarks by Partial Reprogramming. *Cell* 167 (7), 1719-1733 e12.
26. Vaquero, A. et al. (2007) SIRT1 regulates the histone methyl-transferase SUV39H1 during heterochromatin formation. *Nature* 450 (7168), 440-4.
27. Ni, Z. et al. (2012) Two SET domain containing genes link epigenetic changes and aging in *Caenorhabditis elegans*. *Aging Cell* 11 (2), 315-25.
28. Larson, K. et al. (2012) Heterochromatin formation promotes longevity and represses ribosomal RNA synthesis. *PLoS Genet* 8 (1), e1002473.
29. Wood, J.G. et al. (2010) Chromatin remodeling in the aging genome of *Drosophila*. *Aging Cell* 9 (6), 971-8.
30. De Cecco, M. et al. (2019) L1 drives IFN in senescent cells and promotes age-associated inflammation. *Nature* 566 (7742), 73-78.
31. Simon, M. et al. (2019) LINE1 Derepression in Aged Wild-Type and SIRT6-Deficient Mice Drives Inflammation. *Cell Metab* 29 (4), 871-885 e5.
32. Benayoun, B.A. et al. (2019) Remodeling of epigenome and transcriptome landscapes with aging in mice reveals widespread induction of inflammatory responses. *Genome Res* 29 (4), 697-709.
33. Allan, R.S. et al. (2012) An epigenetic silencing pathway controlling T helper 2 cell lineage commitment. *Nature* 487 (7406), 249-53.
34. Liu, J. et al. (2015) Chromatin landscape defined by repressive histone methylation during oligodendrocyte differentiation. *J Neurosci* 35 (1), 352-65.
35. Salzer, M.C. et al. (2018) Identity Noise and Adipogenic Traits Characterize Dermal Fibroblast Aging. *Cell* 175 (6), 1575-1590 e22.
36. Lieberman-Aiden, E. et al. (2009) Comprehensive mapping of long-range interactions reveals folding principles of the human genome. *Science* 326 (5950), 289-93.
37. Criscione, S.W. et al. (2016) Reorganization of chromosome architecture in replicative cellular senescence. *Sci Adv* 2 (2), e1500882.
38. Dixon, J.R. et al. (2015) Chromatin architecture reorganization during stem cell differentiation. *Nature* 518 (7539), 331-6.
39. Mumbach, M.R. et al. (2016) HiChIP: efficient and sensitive analysis of protein-directed genome architecture. *Nat Methods* 13 (11), 919-922.
40. Davies, J.O. et al. (2016) Multiplexed analysis of chromosome conformation at vastly improved sensitivity. *Nat Methods* 13 (1), 74-80.
41. Fullwood, M.J. et al. (2009) An oestrogen-receptor-alpha-bound human chromatin interactome. *Nature* 462 (7269), 58-64.
42. Fu, V.X. et al. (2004) A loss of insulin-like growth factor-2 imprinting is modulated by CCCTC-binding factor down-regulation at senescence in human epithelial cells. *J Biol Chem* 279 (50), 52218-26.
43. Pal, S. et al. (2018) Impaired cohesion and homologous recombination during replicative aging in budding yeast. *Sci Adv* 4 (2), eaaq0236.
44. Hodges, C.A. et al. (2005) SMC1beta-deficient female mice provide evidence that cohesins are a missing link in age-related nondisjunction. *Nat Genet* 37 (12), 1351-5.
45. Dang, W. et al. (2009) Histone H4 lysine 16 acetylation regulates cellular lifespan. *Nature* 459 (7248), 802-7.

46. Liu, L. et al. (2013) Chromatin modifications as determinants of muscle stem cell quiescence and chronological aging. *Cell Rep* 4 (1), 189-204.
47. O'Sullivan, R.J. et al. (2010) Reduced histone biosynthesis and chromatin changes arising from a damage signal at telomeres. *Nat Struct Mol Biol* 17 (10), 1218-25.
48. Feser, J. et al. (2010) Elevated histone expression promotes life span extension. *Mol Cell* 39 (5), 724-35.
49. Tan, M. et al. (2011) Identification of 67 histone marks and histone lysine crotonylation as a new type of histone modification. *Cell* 146 (6), 1016-28.
50. Sidler, C. et al. (2014) A role for SUV39H1-mediated H3K9 trimethylation in the control of genome stability and senescence in WI38 human diploid lung fibroblasts. *Aging (Albany NY)* 6 (7), 545-63.
51. Zhang, W. et al. (2015) Aging stem cells. A Werner syndrome stem cell model unveils heterochromatin alterations as a driver of human aging. *Science* 348 (6239), 1160-3.
52. Scaffidi, P. and Misteli, T. (2006) Lamin A-dependent nuclear defects in human aging. *Science* 312 (5776), 1059-63.
53. Liu, B. et al. (2013) Depleting the methyltransferase Suv39h1 improves DNA repair and extends lifespan in a progeria mouse model. *Nat Commun* 4, 1868.
54. Kane, A.E. and Sinclair, D.A. (2019) Epigenetic changes during aging and their reprogramming potential. *Crit Rev Biochem Mol Biol* 54 (1), 61-83.
55. Benayoun, B.A. et al. (2015) Epigenetic regulation of ageing: linking environmental inputs to genomic stability. *Nat Rev Mol Cell Biol* 16 (10), 593-610.
56. Pal, S. and Tyler, J.K. (2016) Epigenetics and aging. *Sci Adv* 2 (7), e1600584.
57. Bollati, V. et al. (2009) Decline in genomic DNA methylation through aging in a cohort of elderly subjects. *Mech Ageing Dev* 130 (4), 234-9.
58. Heyn, H. et al. (2012) Distinct DNA methylomes of newborns and centenarians. *Proc Natl Acad Sci U S A* 109 (26), 10522-7.
59. Teschendorff, A.E. et al. (2010) Age-dependent DNA methylation of genes that are suppressed in stem cells is a hallmark of cancer. *Genome Res* 20 (4), 440-6.
60. Rakyan, V.K. et al. (2010) Human aging-associated DNA hypermethylation occurs preferentially at bivalent chromatin domains. *Genome Res* 20 (4), 434-9.
61. Bocklandt, S. et al. (2011) Epigenetic predictor of age. *PLoS One* 6 (6), e14821.
62. Hannum, G. et al. (2013) Genome-wide methylation profiles reveal quantitative views of human aging rates. *Mol Cell* 49 (2), 359-367.
63. Horvath, S. et al. (2012) Aging effects on DNA methylation modules in human brain and blood tissue. *Genome Biol* 13 (10), R97.
64. Horvath, S. (2013) DNA methylation age of human tissues and cell types. *Genome Biol* 14 (10), R115.
65. Bell, C.G. et al. (2019) DNA methylation aging clocks: challenges and recommendations. *Genome Biol* 20 (1), 249.
66. Petkovich, D.A. et al. (2017) Using DNA Methylation Profiling to Evaluate Biological Age and Longevity Interventions. *Cell Metab* 25 (4), 954-960 e6.
67. Stubbs, T.M. et al. (2017) Multi-tissue DNA methylation age predictor in mouse. *Genome Biol* 18 (1), 68.
68. Wang, T. et al. (2017) Epigenetic aging signatures in mice livers are slowed by dwarfism, calorie restriction and rapamycin treatment. *Genome Biol* 18 (1), 57.

69. Meer, M.V. et al. (2018) A whole lifespan mouse multi-tissue DNA methylation clock. *Elife* 7.
70. Thompson, M.J. et al. (2017) An epigenetic aging clock for dogs and wolves. *Aging (Albany NY)* 9 (3), 1055-1068.
71. Lowe, R. et al. (2020) DNA methylation clocks as a predictor for ageing and age estimation in naked mole-rats, *Heterocephalus glaber*. *Aging (Albany NY)* 12 (5), 4394-4406.
72. Gurdon, J.B. et al. (1958) Sexually mature individuals of *Xenopus laevis* from the transplantation of single somatic nuclei. *Nature* 182 (4627), 64-5.
73. Wilmut, I. et al. (1997) Viable offspring derived from fetal and adult mammalian cells. *Nature* 385 (6619), 810-3.
74. Sinclair, K.D. et al. (2016) Healthy ageing of cloned sheep. *Nat Commun* 7, 12359.
75. Takahashi, K. and Yamanaka, S. (2006) Induction of pluripotent stem cells from mouse embryonic and adult fibroblast cultures by defined factors. *Cell* 126 (4), 663-76.
76. Wernig, M. et al. (2007) In vitro reprogramming of fibroblasts into a pluripotent ES-cell-like state. *Nature* 448 (7151), 318-24.
77. Okita, K. et al. (2007) Generation of germline-competent induced pluripotent stem cells. *Nature* 448 (7151), 313-7.
78. Lapasset, L. et al. (2011) Rejuvenating senescent and centenarian human cells by reprogramming through the pluripotent state. *Genes Dev* 25 (21), 2248-53.
79. Yu, J. et al. (2007) Induced pluripotent stem cell lines derived from human somatic cells. *Science* 318 (5858), 1917-20.
80. Mertens, J. et al. (2015) Directly Reprogrammed Human Neurons Retain Aging-Associated Transcriptomic Signatures and Reveal Age-Related Nucleocytoplasmic Defects. *Cell Stem Cell* 17 (6), 705-718.
81. Schaible, R. et al. (2014) Aging and potential for self-renewal: hydra living in the age of aging - a mini-review. *Gerontology* 60 (6), 548-56.
82. Reddien, P.W. and Sanchez Alvarado, A. (2004) Fundamentals of planarian regeneration. *Annu Rev Cell Dev Biol* 20, 725-57.
83. Beffagna, G. (2019) Zebrafish as a Smart Model to Understand Regeneration After Heart Injury: How Fish Could Help Humans. *Front Cardiovasc Med* 6, 107.
84. Nowoshilow, S. et al. (2018) The axolotl genome and the evolution of key tissue formation regulators. *Nature* 554 (7690), 50-55.
85. Takeo, M. et al. (2013) Wnt activation in nail epithelium couples nail growth to digit regeneration. *Nature* 499 (7457), 228-32.
86. Michalopoulos, G.K. and DeFrances, M.C. (1997) Liver regeneration. *Science* 276 (5309), 60-6.
87. Gore, A. et al. (2011) Somatic coding mutations in human induced pluripotent stem cells. *Nature* 471 (7336), 63-7.

Chapter 2: Development of a safe *in vivo* epigenetic reprogramming method

The terms ‘epigenetic reprogramming’ and ‘cellular reprogramming’ refer to the remodeling of epigenetic markers to provide new cellular functions. To date, there have been several examples of epigenetic age reversal by cellular reprogramming *in vitro*. DNA methylation changes correlate with age in somatic tissues, as a result, the DNA methylation level of only a few hundred loci is sufficient to accurately calculate biological age [1]. During complete reprogramming *in vitro*, the DNA methylation age of human iPSC and ES cells, based on the original “Horvath” clock, is close to zero [1]. DNA methylation clocks for mice, including a blood clock [2] and rDNA clock [3], also indicate that mouse iPSCs have their DNA methylation age reset to zero. A time-course measurement during iPSC reprogramming indicates that this methylation age reversal process is a steady one that lasts for about 20 days, with the complete loss of cellular identity in the last five [4]. The loss of identity is believed to be assisted by the rapid proliferation and passive demethylation that occurs during cell division. Recently, the transient expression of all four Yamanaka factors (OSKM) plus Lin28 and Nanog, mediated by the introduction of mRNAs, was shown to reverse the methylation clock in human endothelial cells without changing cell identity, allowing them to be re-transplanted into old mice where they improved potency of aged muscle stem cell [5].

I. *In vivo* reprogramming was limited by toxicity and delivery

While *in vitro* reprogramming has been used with success to rejuvenate cells for transplantation, it was still unclear whether the age of a cell can be safely reversed without changing cell identity (Table 2). In OSKM transgenic mice, continual induction of OSKM using high concentrations of doxycycline (1-2 mg/mL) causes death within days [6, 7], ostensibly due to weight loss by intestinal dysplasia. Reduced expression of OSKM (0.2 mg/mL doxycycline)

for 2.5 weeks induces teratomas that are characterized with three germ layers at death [6]. When the OSKM combination was delivered separately using four separate AAVs, mice also developed teratoma in liver and pancreas after 4 weeks [8]. Even when OSKM was induced for only two days per week for 8 weeks, homozygous transgenic mice with two copies of an OSK transgene still developed teratomas [9].

Two studies have tried transient OSKM to address the toxicity *in vivo*. The first study used a cyclic induction protocol for heterozygous OSKM transgenic mice, developed in the Belmonte lab at the Salk Institute. DOX was given for 2 days to induce the heterozygous OSKM transgene, and then withdrawn for 5 days for reasons of OSKM toxicity, cycling every week. No deaths or tumors were observed for 9 months. This method alleviated the progeroid (premature aging) phenotype of the lamin A mutant mice and increased their lifespan by 40%. Similarly, in 12-month-old transgenic mice, three cycles of pre-treatment promoted pancreatic and muscle cell proliferation after a chemical injury. Even if the illness caused by OSKM could be overcome, the fact that teratomas are seen after 8 weeks of cyclic treatment in homozygous OSKM transgenics means that it would be dangerous to use this approach in humans.

The second study used intramuscular injection of a OSKM plasmid (pOKSM) [10], which transiently upregulated the pluripotency genes Nanog, Ecat1, and Rex1. This induced transient proliferation but not dysplasia or tumorigenesis, even after four months. Increased muscle regeneration and reduced fibrosis was observed, however, *in vivo* delivery of genes via a plasmid is inefficient and prone to transgene silencing and immune responses.

In summary, though *in vivo* reprogramming has great potential to improve tissue function and reverse aging, continuous OSKM expression *in vivo* is toxic, and transient OSKM expression is not translational (Table 2).

Table 2 Summary of *In vivo* reprogramming trials

In vivo studies	Overexpression method	Safe?	Tissue examined	Observation safety	Improved regeneration or rejuvenation	Can be treated post-injury?	DNAm age reversal and mechanism?
OSKM	Transgenic [6]	No.	Systemically	2.5 weeks of induction leads to all death later with systemic teratoma; 1 week of induction gives slower death and less teratoma.	/	/	/
	Transgenic [7]	No.	Kidney, pancreas	Become morbid within days; Teratoma in kidney and pancreas after 4 weeks.	/	/	/
	Monocistronic AAV8 [8]	No.	Liver	Liver teratoma in 6 weeks	/	/	/
	Plasmid [10]	Yes? (Transient active proliferation)	Muscle	No dysplasia or tumorigenesis after 4 months	Accelerated repair and reduced fibrosis after muscle injury	Yes	/
	Transgenic; Cyclically induction [9]	Yes? (single copy only)	Pancreas, Muscle	No death after 9 months (teratomas seen after two months in homo/homo)	Increased lifespan of progeroid mice; Increased proliferation post pancreas/muscle damage in aged mice	No (pre-treatment)	/
OSK	Transgenic [11]	No. (Has to avoid digestion system)	Systemically	Become morbid within days	/	/	/
	Polycistronic AAV2 or AAV9 [11]	Yes.	Retina (AAV2) Systemically (AAV9)	No death after 18m from young; No tumor incidence in the retina after 15 months; No tumor promotion systemically after 10 months in old.	Promoted axon regeneration after optic nerve injury in both young and aged mice; Improved vision in glaucoma disease; Improved vision in normal aging	Yes	Yes. Non-global, active DNA demethylation

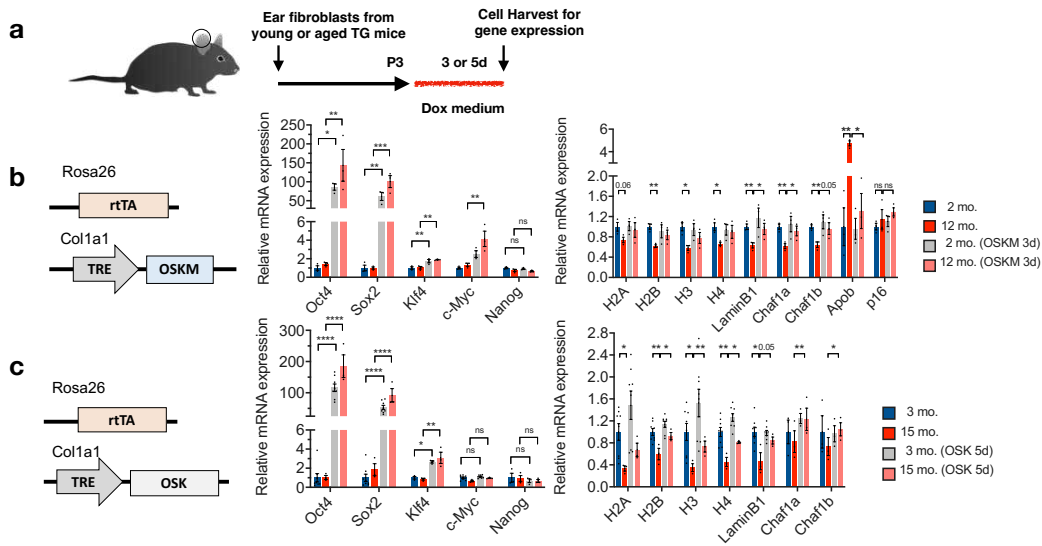


Figure 2.1 Partial reprogramming by OSK (no Myc) can reset gene expression pattern in aged fibroblasts without changing cellular identity. **a**, Experimental outline for testing the effects of OSK and OSKM and expression in fibroblasts from young and old transgenic mice ($R26^{rtTA}$; $Col1a1^{OKS-mCherry}$ and $R26^{rtTA}$; $Col1a1^{OSKM}$). **b** and **c**, Expression of OSKM and OSK expression rescues age-associated transcriptional changes without inducing Nanog mRNA.

II. c-Myc is disposable for resetting aging signature

To solve the safety issue from OSKM expression *in vivo*, we want to exclude the c-Myc gene from future experiments because it is an oncogene that negatively regulates lifespan [12]. But could it reset epigenome similarly as OSKM *in vitro*? We isolated ear fibroblasts from young and old transgenic mice that harbor either OSKM or OSK (no Myc) under the TRE promoter. Then the fibroblasts are grown in cell culture till P3 and treated with 2 $\mu\text{g/mL}$ doxycycline to induce transgene expression for 3 and 5 days respectively (Figure 2.1a). We then measured the effect on RNA levels of genes known to be altered with age, including H2A, H2B, LaminB1, and Chaf1b etc. OSK-treatment promoted a more youthful gene expression pattern, similar to what OSKM achieved. Importantly, we did not detect an induction of Nanog, an early embryonic transcription factor that can induce teratomas, suggesting no apparent loss of cellular identity had happened (Figure 2.1b, c).

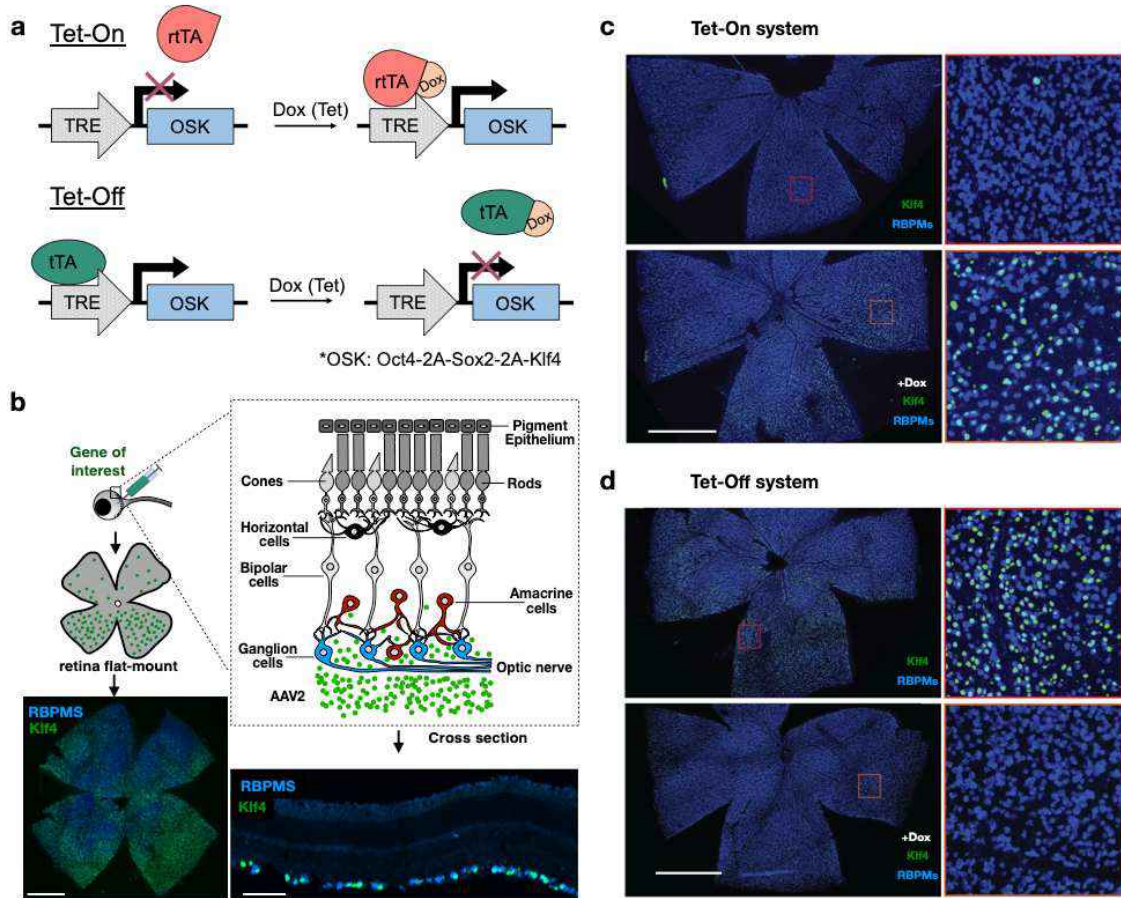


Figure 2.2 Dual AAV system enables inducible polycistronic OSK expression in the retina ganglion cells. **a**, Schematic of the Tet-On and Tet-Off AAV vectors. **b**, Intravitreal AAV2 injections targeting retinal ganglion cells. A representative retinal wholemount and cross section 2 weeks after intravitreal injection of AAV2-tTA and AAV2-TRE-OSK. Staining of virally-delivered Klf4 (green) and RGC-marker RBPMs (blue) shows the transduction efficiency to the AAV-targeted retinal layer. Scale bars, 1 mm and 100 μ m respectively. **c** and **d**, Wholemount retina display of RBPMs and Klf4 immunofluorescence, showing that expression from the AAV2 Tet-On system can be turned on by doxycycline (2 mg/mL, 2 days), and the expression from the AAV2 Tet-Off system can be turned off by doxycycline in drinking water (2 mg/mL, 3 days). Scale bar, 1 mm.

III. Dual AAV system enables inducible expression of polycistronic OSK

Next, we tested the safety of ectopically expressing OSK in mice. To deliver and control OSK expression *in vivo*, we engineered a tightly regulated adeno-associated viral (AAV) vector under the control of a tetracycline response element (TRE) promoter (Figure 2.2a) [8, 13]. The TRE promoter can be activated either by reverse tetracycline-controlled transactivator (rtTA) in the presence of doxycycline (Dox) ("Tet-On") or by tetracycline transactivator (tTA) in the absence of Dox ("Tet-Off"). Extraneous AAV sequences were removed from the vector to accommodate OSK as a poly-cistron.

We then packaged such AAV vectors into AAV2 capsids and injected them into the vitreous body. AAV2 mostly got into RGCs, as shown by the wholemount and cross section (Figure 2.2b). And the inducible system could be regulated tightly by the control of doxycycline (2 mg/mL in the drinking water), resulting in Dox-responsive gene expression in RGCs (Figure 2.2c, d).

IV. AAV-mediated OSK expression achieves long term safety

In order to determine whether prolonged expression of OSK within the eye produced retinal tumors, groups of mice received intravitreal injection of +OSK AAV2 (tTA+TRE-OSK AAV2) and, as negative controls, mice received either no injection, or -OSK AAV2 (rtTA+TRE-OSK AAV2) that was not turned on (Figure 2.3a-e). After extended expression of AAV-OSK for 15 months, immunohistochemical staining confirmed the Klf4 gene was still expressed in RGCs from all 6 retinas we had (Figure 2.3a). Importantly, retinal imaging by OCT demonstrated there was no detectable change in the retinal layers or overall retinal thickness as compared with the negative controls (Figure 2.3b-d and f). To confirm the validity of the OCT images, eyes from all groups were embedded and serial sections obtained from the entire globe, which were stained with H&E and examined microscopically (Figure 2.3e). Moreover, for a group of mice received a subretinal injection of 10,000 retinoblastoma tumor cells, OCT images taken at 14 days post tumor cell injection clearly revealed the small retinal tumors that were approximately 100 μm at the apex, validating that OCT imaging is a highly sensitive method to detect even small retinal tumors (Figure 2.3g).

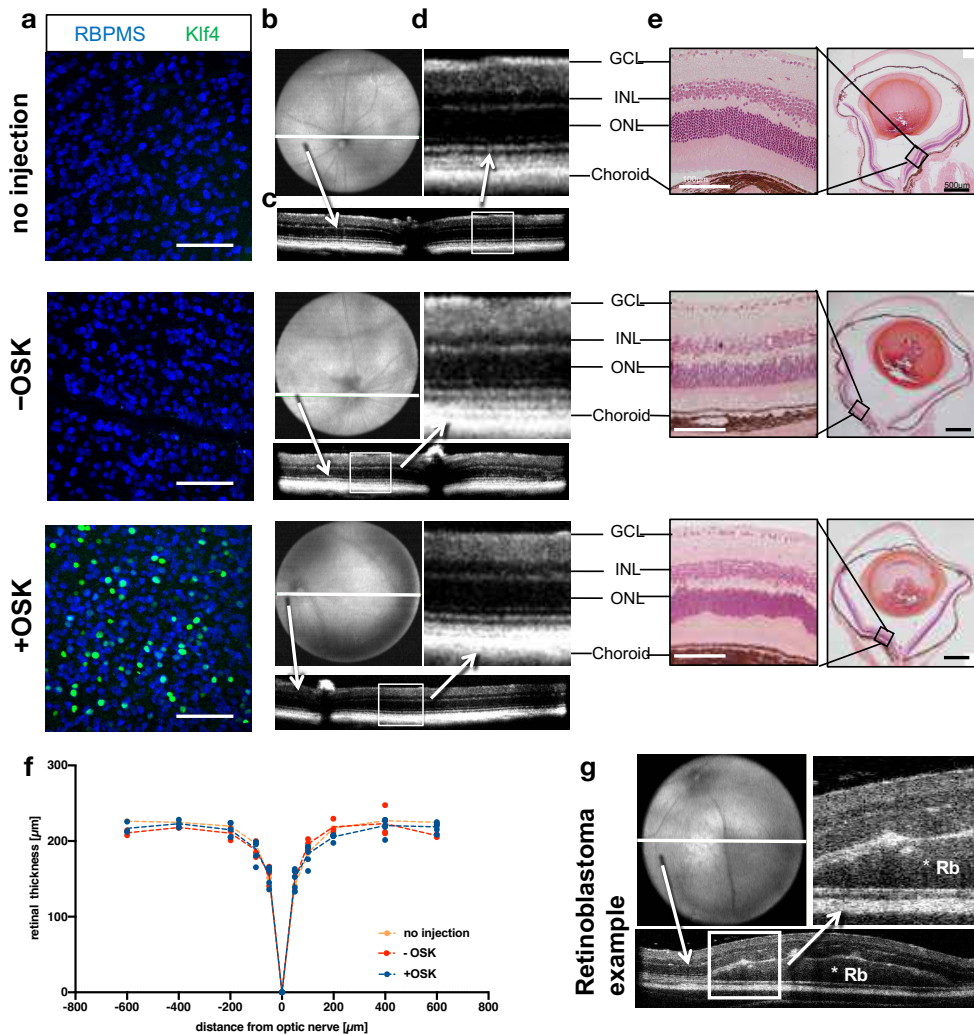


Figure 2.3 Normal architecture and absence of tumors in the retina after long-term OSK expression mediated by AAV2 delivery. **a**, Corresponding retinal wholemount images stained for RBPMS and KLF4 are shown for each group tested (i) no injection, (ii) -OSK (intravitreal injection of AAV-rtTA and AAV-TRE-OSK without Dox induction), 10 months post injection, (iii) +OSK (intravitreal injection of AAV-tTA and AAV-TRE-OSK with Dox induction), 15 months post injection. All retinas show similar expression within the group. **b**, Volume intensity projection of en-face OCT (optical coherence tomography) retinal image with a white line indicating the location of **c**. **c**, The representative retinal cross section B-scan images. The white box indicates the location of the high magnification scans in **d** (retinal layers: GCL = ganglion cell layer, INL = inner nuclear layer, ONL = outer nuclear layer, and choroid). **e**, Low- and high-power representative images of H&E-stained cross-sections of the corresponding eyes, verifying retinal layers. **f**, Quantitative measurements of retinal thickness showing no significant change between treated and control groups ($n=6$ no injection, $n=3$ -OSK, $n=5$ +OSK; $P>0.05$ mixed effect analysis, Tukey's multiple comparisons test). **g**, Immunosuppressed NSG mice received a subretinal injection of 10,000 human retinoblastoma tumor cells and OCT images of a small retinal tumor with the associated increased retinal thickness, 14 days post injection, demonstrating the sensitivity of OCT scan, * Rb (retinoblastoma).

To examine the expression of this dual AAV system systemically, we performed retro-orbital injection of AAV9-UBC-rtTA and AAV9-TRE-Luc, 1.0×10^{12} gene copies total (Figure 2.4a). 2 months after injection, we treated the mice with 1mg/mL Dox drinking water for 7 days, others treated with regular water for measuring luciferase background. 10min after injecting D-luciferin, the substrate of luciferase, the luminescence is emittedw from the internal organs (Figure 2.4b). Imaging of the internal organs with a short exposure reveals that luciferase signal was primarily located in the liver (right panel), and a longer exposure time (right panel) revealed luciferase signal in pancreas with the liver removed (Figure 2.4c).

Thinking that AAV9's weak tropism for the digestive system would avoid the dysplasia and weight loss seen in transgenic OSK(M) mice [6, 8], we tested if OSK is safe when delivered by AAV9 *in vivo*, we infected young (5-month-old) and aged (20-month-old) mice with AAV9-rtTA and AAV9-TRE-OSK via intravenous delivery (Figure 2.4d).

Young mice were injected intravenously with AAV9-rtTA and AAV9-TRE-OSK (3 and 7×10^{11} gene copies each AAV/mouse) at 5 months of age. After 1 month, mice remained untreated (-Dox) or treated with Dox (+Dox) for 18 months. WT mice did not receive AAV injection. With similar expression level of OSK in the liver compared to OSK transgenic mice (Figure 2.4e), surprisingly, AAV9 injected mice did not significantly lose body weight during the 18 month period, and no negative effects on overall health were observed (Figure 2.4f).

Aged mice were injected intravenously with 5×10^{11} gene copies of AAV9-rtTA and 7×10^{11} gene copies of either AAV9-TRE-GFP (GFP) or TRE-OSK (OSK) per mouse at 21 months of age. After 1 month, GFP, OSK and un-injected WT mice were treated with Dox for a 10 month-period. We sacrificed the mice at 32 months of age and validated the GFP and OSK expression in the liver (Figure 2.4g, h). No increase in tumor incidence locally or systemically was observed (Figure 2.4i), nor was there a significant change in the liver tumor size (Figure 2.4j) or white blood cell count, an indicator of inflammation (Figure 2.4k).

Taken together, these data indicate that prolonged expression of OSK delivered through AAV injection either locally (retina) or systemically, does not induce or promote tumors in both young and old body environment, or disrupt normal tissue architecture. We have finally developed an *in vivo* epigenetic reprogramming method achieving long-term safety.

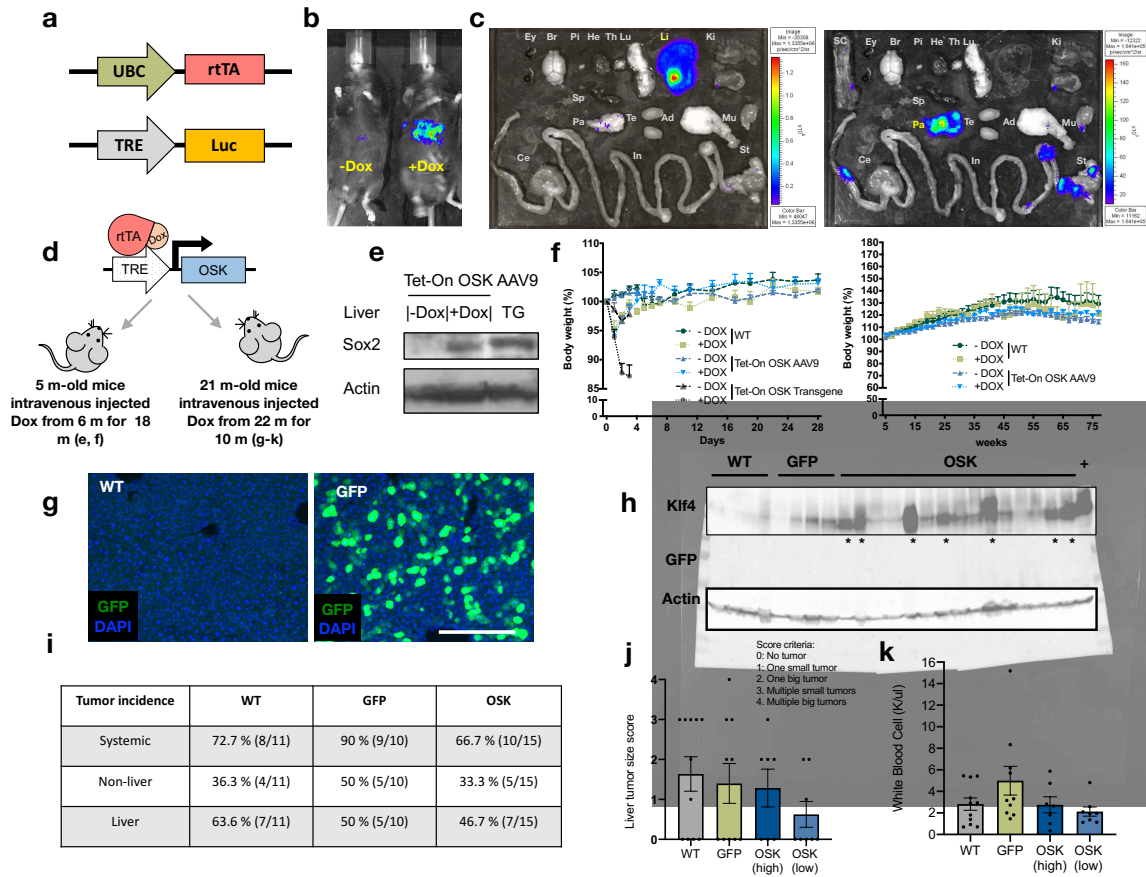


Figure 2.4 No negative effects were observed with intravenous delivery of AAV9-OSK in either young or old mice. **a**, AAV-UBC-rtTA and AAV-TRE-Luc vectors for measuring tissue distribution. **b**, Luciferase imaging of WT mice 2 months after retro-orbital injection of AAV9-UBC-rtTA and AAV9-TRE-Luc (1.0×10^{12} gene copies total). Doxycycline (Dox) was delivered in drinking water (1 mg/mL) for 7 days to the +Dox mouse. **c**, Luciferase imaging of eye (Ey), brain (Br), pituitary gland (Pi), heart (He), thymus (Th), lung (Lu), liver (Li), kidney (Ki), spleen (Sp), pancreas (Pa), testis (Te), adipose (Ad), muscle (Mu), spinal cord (SC), stomach (St), small intestine (In), and cecum (Ce). **d**, Details of safety test in both young and old mice after *in vivo* delivery of OSK-expressing AAVs. **e**, Sox2 expression in the liver of WT mice two months post-intravenous delivery of OSK-expressing AAV9s with or without 1 month of Dox induction, and in the liver of OSK transgenic (TG) mice. **f**, Body weight of WT mice, OSK transgenic mice, and AAV-mediated OSK-expressing mice with or without doxycycline in the first 4 weeks (left panel, $n = 5, 3, 6, 4, 4$ and 3 , respectively) and the following 17 months (right panel, $n = 5, 3, 6, 4$, respectively). **g**, Examples of liver sections from WT or GFP mice showing the infection of AAV9. **h**, Klf4 and GFP protein levels in livers of WT, GFP, and OSK mice at 32 months of age. * indicates high OSK expression, + indicates induced protein expression levels in livers of OSK transgenic mice. **i**, Tumor incidence in WT, GFP, and OSK mice at 32 months of age after 10 months of Dox induction. **j**, Liver tumor scoring for WT, GFP, and OSK groups at 32 months of age after 10 months of Dox induction. OSK mice were defined as either high expression (indicated by * in panel **h**) or low expression. **k**, White blood cell counts for WT, GFP or OSK mice at 32 months of age after 10 months of Dox induction. There was no difference between the groups using one-way ANOVA in **j** and **k**.

V. References

1. Horvath, S. (2013) DNA methylation age of human tissues and cell types. *Genome Biol* 14 (10), R115.
2. Petkovich, D.A. et al. (2017) Using DNA Methylation Profiling to Evaluate Biological Age and Longevity Interventions. *Cell Metab* 25 (4), 954-960 e6.
3. Wang, M. and Lemos, B. (2019) Ribosomal DNA harbors an evolutionarily conserved clock of biological aging. *Genome Res* 29 (3), 325-333.
4. Olova, N. et al. (2019) Partial reprogramming induces a steady decline in epigenetic age before loss of somatic identity. *Aging Cell* 18 (1), e12877.
5. Sarkar, T.J. et al. (2020) Transient non-integrative expression of nuclear reprogramming factors promotes multifaceted amelioration of aging in human cells. *Nat Commun* 11 (1), 1545.
6. Abad, M. et al. (2013) Reprogramming in vivo produces teratomas and iPS cells with totipotency features. *Nature* 502 (7471), 340-5.
7. Ohnishi, K. et al. (2014) Premature termination of reprogramming in vivo leads to cancer development through altered epigenetic regulation. *Cell* 156 (4), 663-77.
8. Senis, E. et al. (2018) AAV vector-mediated in vivo reprogramming into pluripotency. *Nat Commun* 9 (1), 2651.
9. Ocampo, A. et al. (2016) In Vivo Amelioration of Age-Associated Hallmarks by Partial Reprogramming. *Cell* 167 (7), 1719-1733 e12.
10. de Lazaro, I. et al. (2019) Non-viral, Tumor-free Induction of Transient Cell Reprogramming in Mouse Skeletal Muscle to Enhance Tissue Regeneration. *Mol Ther* 27 (1), 59-75.
11. Lu, Y. et al. (2019) Reversal of ageing- and injury-induced vision loss by Tet-dependent epigenetic reprogramming. *bioRxiv*.
12. Hofmann, J.W. et al. (2015) Reduced expression of MYC increases longevity and enhances healthspan. *Cell* 160 (3), 477-88.
13. Smalley, E. (2017) First AAV gene therapy poised for landmark approval. *Nat Biotechnol* 35 (11), 998-999.

**Chapter 3: Promoting axon regeneration in mammalian CNS by
Tet-dependent reprogramming**

Almost all species experience a decline in regenerative potential during ageing. In mammals, one of the first systems to lose its regenerative potential is the CNS [1]. Retinal ganglion cells (RGCs) of the CNS project axons away from the retina towards the brain to form the optic nerve. In embryos and neonates, RGCs can regenerate axons if damaged, but this capacity is lost within days after birth [2]. Even with interventions, older individuals continue to experience a decline in axonal regrowth [3], consistent with the Kennard Principle, the observation that the older the CNS is, the lower its regenerative capacity [4]. To date, attempts to reverse damage to the optic nerve have been only moderately successful and no treatments have successfully restored eyesight in the context of late-stage glaucoma or old age.

I. Polycistronic OSK promotes RGC survival and axon regeneration post optic nerve injury

To test whether it is possible to safely provide adult RGCs with the regenerative capacity of younger cells, we induced OSK in an optic nerve crush injury model. The Tet-Off system carrying OSK, either in separate monocistronic AAVs or one polycistronic AAV, was injected into the vitreous body. We performed optic nerve crush in mice two weeks after delivering AAV2. After another two weeks, intravitreal injection of Alexa Fluor 555-conjugated cholera toxin subunit B (CTB), an anterograde axonal tracer, was performed to assess axon regeneration (Figure 3.1a).

The greatest extent of axon regeneration and RGC survival, occurred when all three genes were delivered and expressed via the same AAV as a polycistron. Suppression of polycistronic OSK expression by Dox treatment blocked regeneration (Figure 3.1b-d). When Oct4, Sox2, and Klf4 were co-delivered via separate monocistronic AAVs, no effect on axon regeneration was observed, ostensibly due to the lower frequency of co-infection and inconsistent stoichiometry (Figure 3.1e-g). When delivered singly, Oct4 or Sox2 alone increased RGC survival slightly, but none of the single factors alone had any effect on regenerative capacity. Because Klf4 has been reported to repress rather than promote axonal growth [5, 6], we tested a dual-cistron of Oct4 and Sox2 and observed no regenerative effect (Figure 3.1b, c).

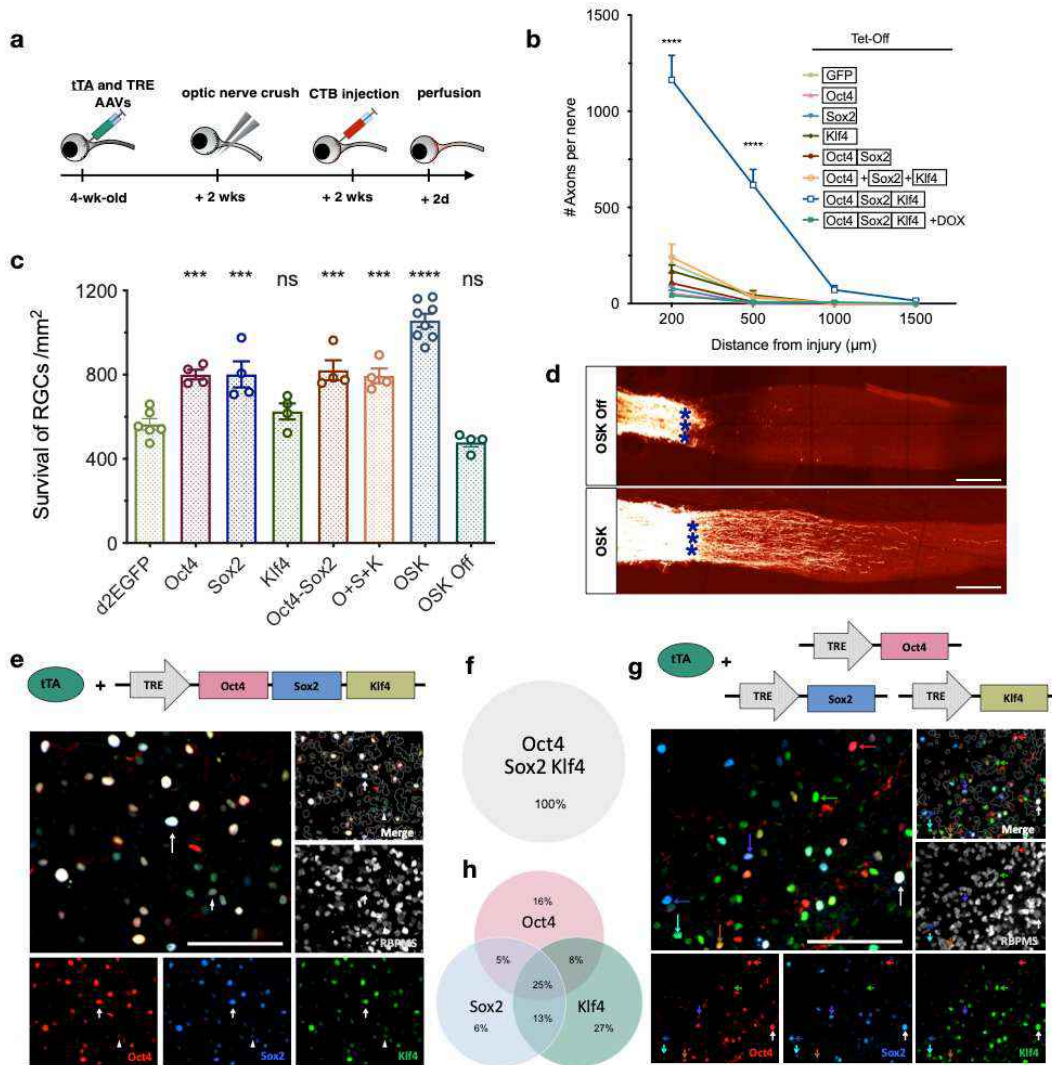


Figure 3.1. AAV-delivered polycistronic OSK promotes axon regeneration and RGC survival after optic nerve injury. **a**, Experimental outline of the optic nerve crush study using the Tet-Off system. Alexa-conjugated (555 nm) cholera toxin subunit B (CTB) was used for anterograde axonal tracing. **b**, Number of axons 16 days after crush injury at multiple distances distal to the lesion site in mice treated with either AAV2 encoding d2EGFP, Oct4, Sox2, Klf4, Oct4-Sox2, or OSK on monocistronic AAV2s or a single polycistronic AAV2 ($n = 4-7$). Suppression of polycistronic OSK expression by Dox is shown as OSK Off in **c** and **d**. **c**, Survival of RBPMS-positive cells in the RGC layer transduced with different AAV2s on day 16 post-crush (16 dpc). **d**, Representative images of longitudinal sections through optic nerves after receiving intravitreal injections of AAV2-tTA and AAV2-TRE-OSK in the presence or absence of doxycycline (Dox). CTB-labeled axons are shown, 16 dpc. Asterisks indicate crush site. **e** and **f**, Immunofluorescence and sub-population proportion of wholemount retinas transduced with a polycistronic AAV vector expressing Oct4, Sox2, and Klf4 in the same cell. White arrows point at triple-positive cells. **g** and **h**, Immunofluorescence and sub-population proportion of wholemount retinas transduced with AAVs separately encoding Oct4, Sox2, and Klf4. Red, blue and green arrows point at single-positive cells, with a white arrow marking a triple-positive cell, and other arrows marking double-positive cells. Scale bar, 100 μm .

Is the axon regeneration observed with polycistronic OSK expression just a secondary effect of RGC proliferation? The answer is no. We performed daily intra-peritoneal BrdU injections during the first or the second week post-crush injury, no BrdU expression was detected in the RGCs, including OSK-expressing RGCs. Proliferating cells such as glial cells in optic nerve from the BrdU injected mice served as positive controls for proliferating cells. Co-localization of BrdU staining with Ki67 confirms that we were detecting proliferation (Figure 3.2a, b). When polycistronic OSK was induced for 12-16 weeks, regenerating RGC axon fibers extended over 5 mm into the chiasm, where the optic nerve connects to the brain (Figure 3.2c, d).

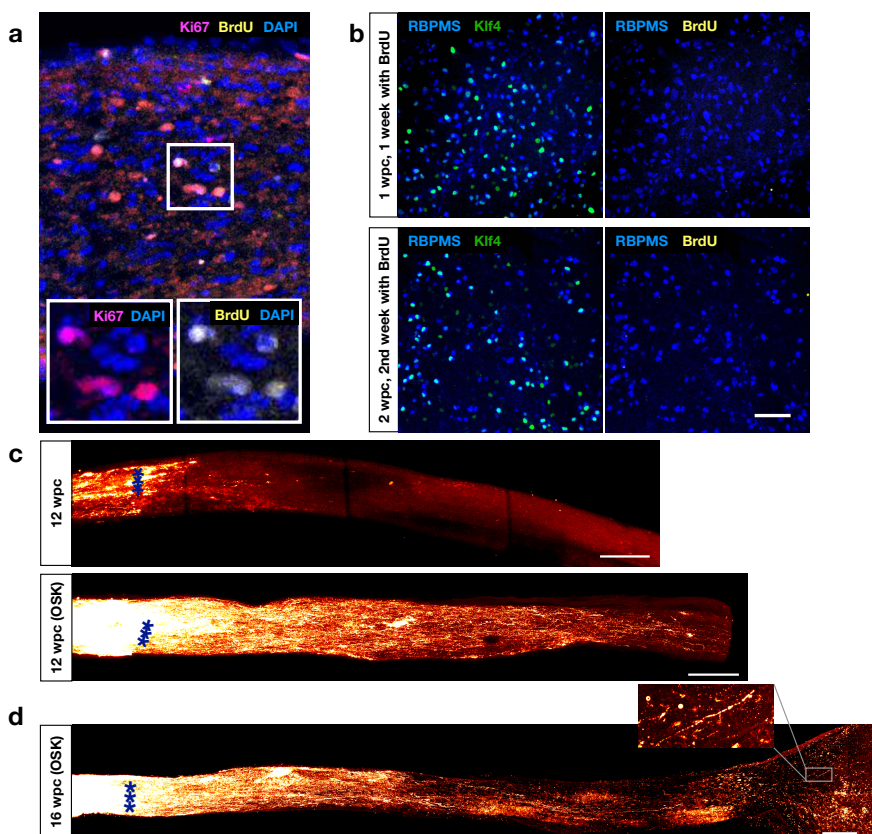


Figure 3.2 Polycistronic OSK induces long-distance axon regeneration post-injury without RGC proliferation. **a**, Proliferating cells in the optic nerve (e.g. glial cells) in BrdU-injected mice as a positive control. BrdU staining co-localized with Ki67, a proliferation marker. **b**, Retina wholemount staining shows OSK-expressing RGCs do not stain for BrdU the first or second week after crush injury. Scale bars, 100 μ m. **c** and **d**, Imaging of optic nerves showing CTB- labeled regenerating axons with or without intravitreal injection of AAV2-tTA and TRE-OSK OSK: **c**, 12 weeks post crush (wpc). **d**, 16 wpc. Scale bars, 200 μ m.

Next, to test whether OSK was acting directly on RGCs or via another cell type [7], we injected AAV2-Flex-tTA with AAV2-TRE-OSK into two CRE transgenic mouse lines: Vglut2-CRE mice selectively expressing CRE in excitatory neurons such as RGCs, while Vgat-CRE mice selectively express CRE in inhibitory amacrine and horizontal cells (Figure 3.3a). AAV-FLEX-tTA is inverted in CRE positive cells to express tTA and therefore induces OSK only either in RGCs (Vglut2-CRE) or amacrine cells (Vgat-CRE), the other type of retinal cells that AAV2 infects following intravitreal injection (Figure 3.3b). OSK expression in RGCs alone promoted axon regeneration, while expression in amacrine cells did not (Figure 3.3c-e).

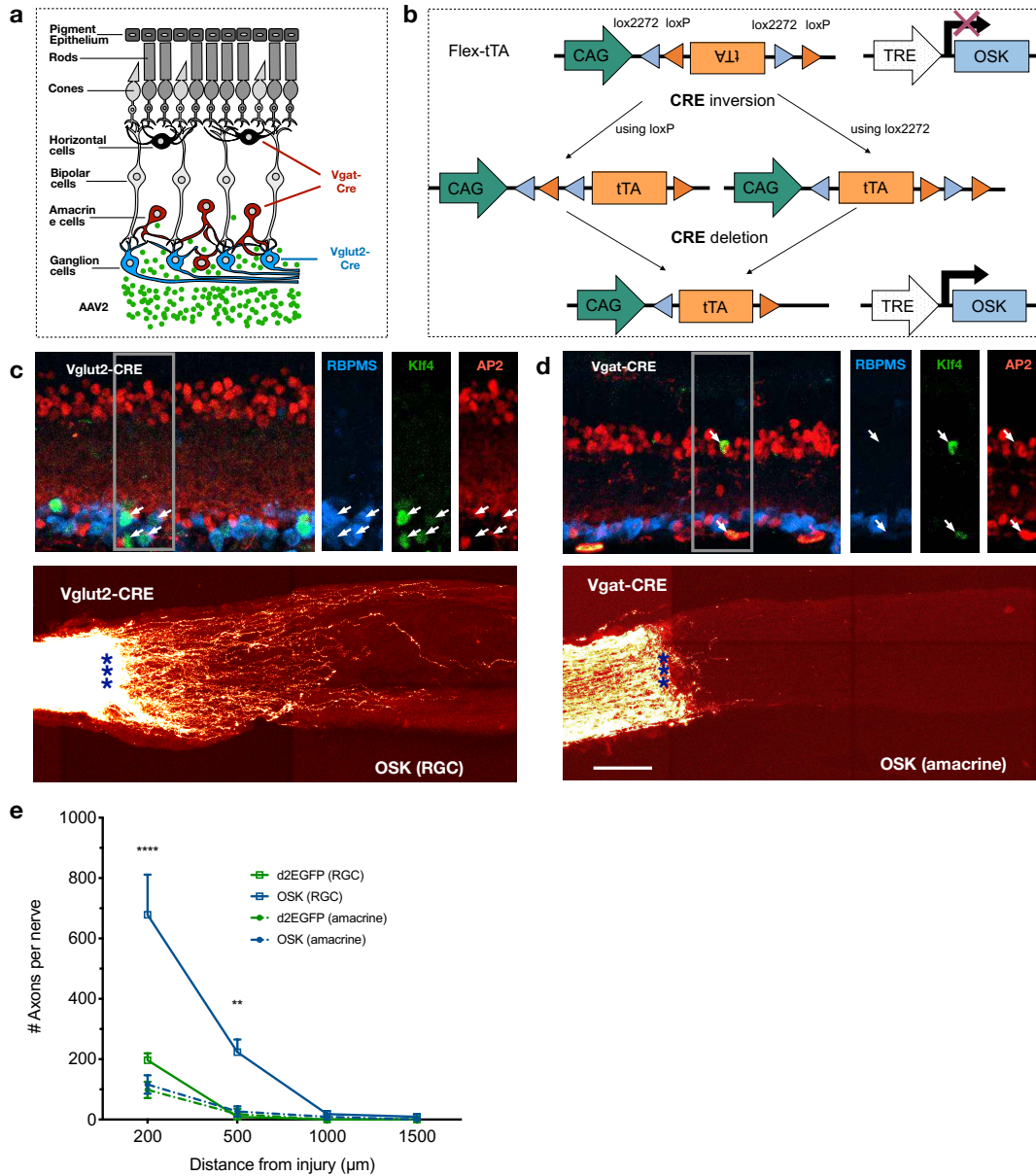


Figure 3.3 Regenerative and pro-survival effects of OSK are RGC-specific and cell-autonomous. **a**, Schematic of retinal structure showing Vglut2-CRE mice selectively expressing CRE in excitatory neurons such as RGCs, while Vgat-CRE mice selectively express CRE in inhibitory amacrine and horizontal cells. **b**, Schematic of the FLEEx (flip-excision) CRE-switch system. **c**, Confocal image stack demonstrating delivery of AAV2-FLEEx-tTA and AAV2-TRE-OSK to intact Vglut2-Cre transgenic retinas, resulting in RGC-specific OSK expression (upper) and robust axon regeneration in the optic nerve (lower). White arrows indicate RBPMS+ (AP2-) labeled RGCs that express Klf4 (green). **d**, Confocal image stack demonstrating delivery of AAV2-FLEEx-tTA and AAV2-TRE-OSK to intact Vgat-Cre transgenic retinas, resulting in amacrine-specific OSK expression (upper) and poor axon regeneration in the optic nerve (lower). White arrows indicate AP2+ (RBPMS-) labeled amacrine cells that express Klf4 (green). **e**, At 16 dpc, the number of axons at multiple distances distal to the lesion site in transgenic CRE lines that selectively express OSK either in RGCs (Vglut2-CRE) or amacrine cells (Vgat-CRE) with intravitreal injection of AAV2-FLEEx-tTA and AAV2-TRE-OSK. One-way ANOVA with Bonferroni correction in **g**. Scale bars, 200 μ m.

The survival frequency of OSK-positive RGCs was approximately three times that of nearby OSK-negative cells or RGCs in GFP-treated control retinas (52% vs.15-21%), resulting in their relative abundance increasing post-injury (Figure 3.4a-c). Together, these data indicate that the protective effect of OSK is mediated within the RGC and is largely cell-autonomous. Comparative RNA-seq of treated and untreated RGCs showed that mRNA levels of Stat3, a pro-regeneration gene [8-10], robustly increase in response to OSK (Supplemental Table 1) and this increase is maintained post-injury (Figure 3.4d). Stat3 upregulation does not, however, appear to be mediated by PTEN-mTOR-S6K and SOCS3, two canonical Stat3 regulatory pathways [11] (Figure 3.4e, f and Supplemental Table 1).

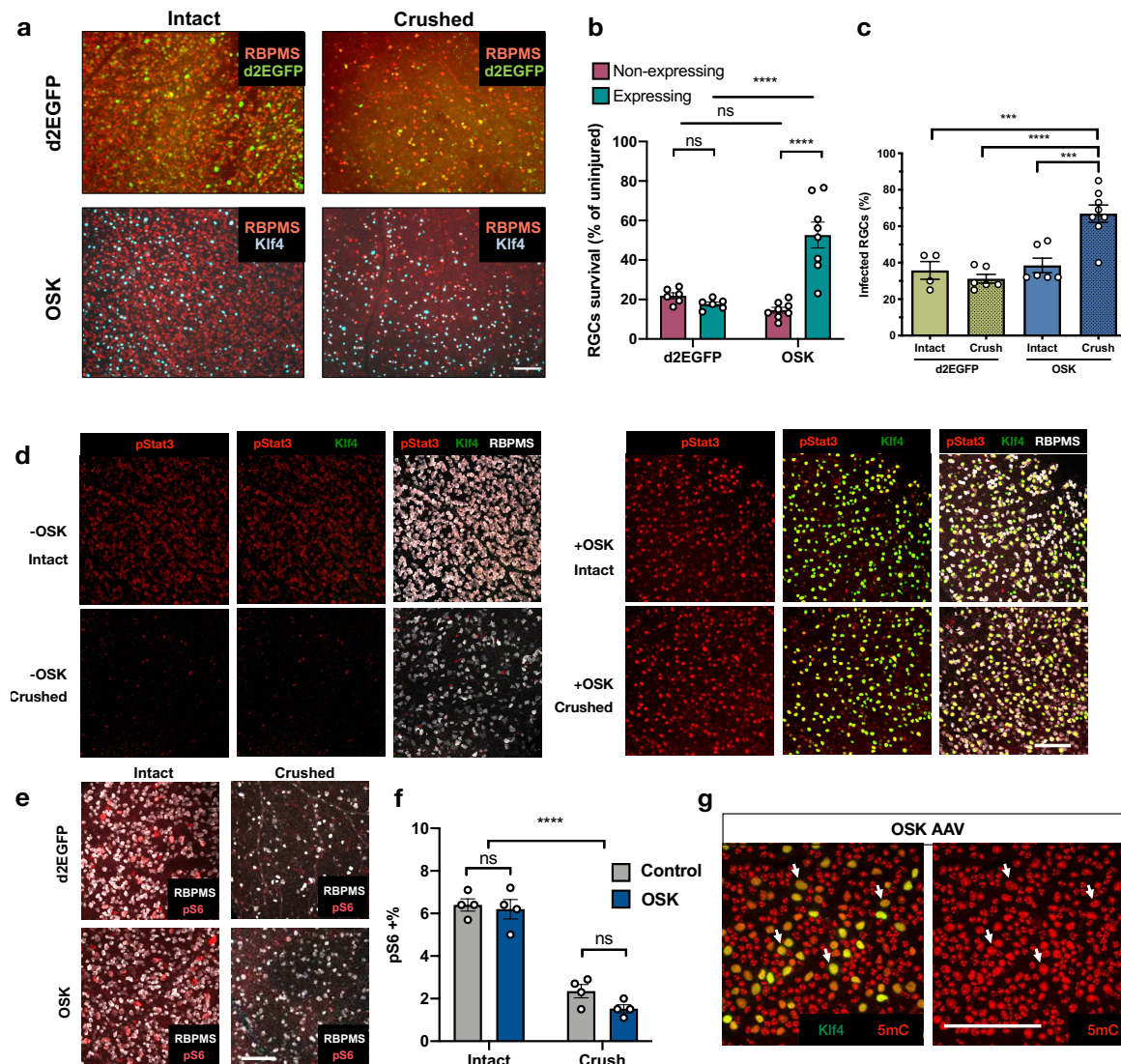


Figure 3.4 OSK activates Stat3 in the absence of mTOR activation or global demethylation. **a**, Representative image of AAV-expressing or non-expressing RGCs in intact and crushed retinas 2 weeks post-crush (2 wpc) with AAVs expressing d2EGFP or OSK. d2EGFP: tTA+TRE-d2EGFP; OSK: tTA+TRE-OSK. **b**, Quantification of d2EGFP- or KLF4-expressing and non-expressing cells in intact or crushed retinas (2 wpc) indicating a cell-autonomous pro-survival effect of OSK-expressing RGCs after crush. **c**, Frequency of d2EGFP- or KLF4-positive RGCs pre- or two weeks post-injury. **d**, Representative images of retinal wholemounts transduced with AAV2-tTA (-OSK) or AAV2-tTA+AAV2-TRE-OSK (+OSK) in the absence or presence of crush injury (post 3 days). Retinal wholemounts were immunostained for pStat3, Klf4 and the RGC marker RBPMS. **e**, Representative images of retinal wholemounts transduced with d2EGFP- or OSK-encoding AAV2 in the presence or absence of a crush injury. Retinal wholemounts were immunostained for the RBPMS and mTOR activation marker phosphorylated S6 (pS6). **f**, Percent of pS6-positive RGCs in intact and crushed samples. **g**, Representative image of retinal wholemounts transduced with AAV2-OSK. Retinal wholemounts were immunostained for 5-methylcytosine (5mC) and Klf4, showing a lack of global demethylation.

To test whether inducing OSK post the injury can still promote axon regeneration and RGC survival, we used the Tet-On AAV system because of its ability to rapidly induce OSK (Figure 3.5a, b). Significant improvement in axon regeneration and RGC survival occurred even if OSK was induced post-injury, and the longer the duration of OSK induction, the greater the distance the axons extended, without any signs of RGCs proliferation (Figure 3.5c-e).

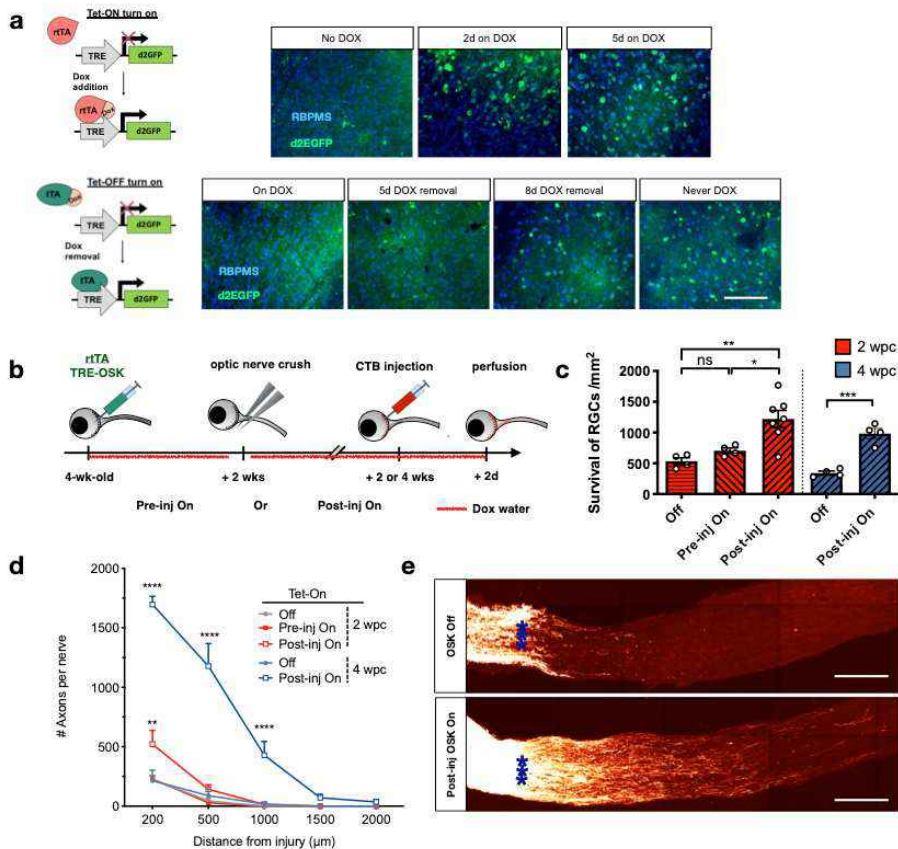


Figure 3.5 Post-injury OSK expression is required for axon regeneration.

a, Representative images showing the d2EGFP in retina expressed from the Tet-On (first row) or Tet-Off (second row) AAV system, Dox water concentration: 2 mg/mL. In Tet-On, no GFP expression was observed in the absence of Dox. GFP expression reached a peak level 2 days after Dox induction and remained at a similar level 5 days after induction. In Tet-Off, when pre-treated with Dox to suppress expression (on Dox), GFP showed up sparsely on day 8 after Dox withdrawal, lower than peak expression (Never Dox). **b**, Experimental strategies for pre- and post-injury induction of OSK expression. **c**, RGC survival in response to OSK induction, pre- or post-injury 2- and 4-weeks post crush (wpc). **d**, Axon regeneration in response to OSK induction, pre- or post-injury. **e**, Representative longitudinal sections through the optic nerve showing CTB-labeled axons, 4 wpc, with or without post-injury induction of OSK. Scale bars, 200 μm.

II. Epigenetic reprogramming promotes DNAm age reversal and DNA demethylation post axonal injury

Given that OSK was effective post-injury and the known role of Yamanaka factors to reverse DNA methylation age (DNAm age) during partial or full reprogramming *in vitro* [12-14], we tested whether neuronal injury advances DNAm age and whether OSK's benefits are associated with a younger DNAm age. Genomic DNA from FACS-isolated RGCs from axon-intact retinas or from axon-injured retinas four days post-injury in the presence or absence of OSK induction, were subjected to reduced-representation bisulfite sequencing (RRBS). A ribosomal DNA methylation (rDNAm) clock [15] provided the best site coverage (70/72 CpG sites) relative to other mouse clocks [16, 17], and its age estimate remained highly correlated with the chronological age of RGCs (Figure 3.6a and Methods). As shown in Figure 3.6b, injured RGCs experienced an acceleration of the DNAm age and OSK expression counteracted this effect.

Is the change of DNA methylation pattern revealed by the DNAm clock just a correlation? Or is it required for the OSK effect? We decided to answer this by examining the role of DNA methylation modifiers. Ten-Eleven-Translocation dioxygenases, TET1-3, catalyze DNA demethylation either by replication-dependent passive dilution, or active enzymatic removal by the downstream enzyme thymine DNA glucosidase (TDG) [18]. Retinal wholemount staining and RRBS revealed that OSK expression do not cause changes in global DNA methylation (Figure 3.4g and Figure 3.6c, d), suggesting its effect on DNAm age may require site-specific demethylation. Similar to *in vitro* reprogramming to create iPSCs [19, 20], OSK expression in RGCs upregulated Tet1 and Tet2, but had no effect on Tet3 (Figure 3.6e). To test whether Tet1 and Tet2 are required for the regenerative effects of OSK, we co-injected OSK-expressing AAVs along with AAVs expressing short-hairpin RNAs against Tet1 or Tet2 (sh-Tet1 or sh-Tet2) [21-23]. Tet1 knockdown was 75% and Tet2 knockdown was 78% (Figure 3.6f-h). Knockdown of either Tet1 or Tet2 blocked the ability of OSK to promote RGC survival and regeneration, as well as the upregulation of Stat3 mRNA (Figure 3.6i-k).

Figure 3.6 Epigenetic reprogramming promotes DNA methylation age reversal and Tet-dependent axon regeneration in retina ganglion cells. **a**, Correlation between rDNA methylation age and chronological age of sorted mouse RGCs. **b**, rDNA methylation age of 1-month-old RGCs isolated from axon-intact retinas infected with or without GFP-expressing AAV, or from axon-injured retinas infected with GFP- or OSK- expressing AAV, 4 dpc. **c** and **d**, Average DNA methylation levels across the mouse genome (**c**) or at CpGs located in CpG islands, gene promoters and gene bodies (**d**) of RGCs from different ages and treatments, based on 708,156 shared sites from RRBS of all samples (combined strands). **e**, Mouse Tet mRNA levels with or without OSK expression in RGCs. **f**, Representative images of retinal wholemounts transduced with TRE-OSK and tTA AAV2 in combination with sh-Scr or sh-Tet1 or sh-Tet2 YFP AAV2 at titer ratio 5:5:1. Retinal wholemounts immunostained for Klf4. **g**, Quantification of shRNA-YFP AAV transduction in OSK-expressing RGCs. **h**, Mouse Tet mRNA levels with sh-Scr or sh-Tet1 or sh-Tet2 YFP AAV2 in RGCs in the presence of OSK

expression. **i** and **j**, Quantification of axon regeneration and RGC survival 2 weeks post-injury in retinas co-transduced with AAV2 vectors encoding polycistronic OSK, tTA, and shRNA vectors with a scrambled sequence (Scr), Tet1, or Tet2 hairpin sequences to knockdown Tet expression. **k**, Mouse Stat3 mRNA levels after sh-Scr or sh-Tet1 or sh-Tet2 knockdown in RGCs in the presence of OSK expression.

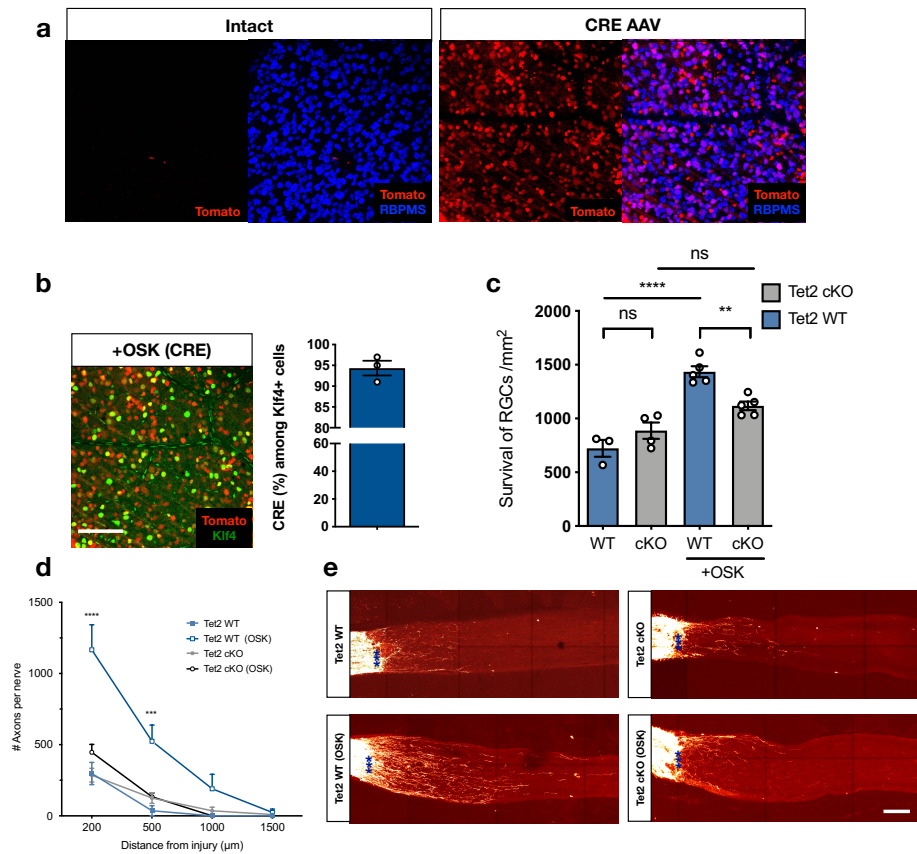


Figure 3.7 Protective and regenerative effect of OSK is abolished by Tet2 conditional knockout. **h**, CRE-dependent Tomato expression in RGCs after intravitreal AAV-CRE injection to Tomato reporter mice (Rosa-CAG-lox-STOP-lox-Tomato), and the co-expressed frequency of CRE and Klf4. **c-e**, RGC survival (**c**) and axon regeneration in quantification (**d**) or in longitudinal sections (**e**) in response to OSK (AAV2-tTA+AAV2-TRE-OSK), 16 dpc in Tet2^{flx/flx} mice that infected with saline (Tet2 WT) or AAV2-CRE (Tet2 cKO). Scale bars, 100 μm in **b**, **h** and **j**. **P* < 0.05; ***P* < 0.01; ****P* < 0.001, *****P* < 0.0001. Two-tailed Student's t-test in **a** and **g**, Two-Way ANOVA in **a**, **d**, **i**, and One-way ANOVA in **e**, **f**, **d**,

A Tet knockout model would indisputably validate the requirement of Tet2 for OSK *in vivo* reprogramming. We avoided the whole-body Tet KO mice because they may have developmental defects. Instead, we obtain Tet2 conditional KO (Tet2^{flx/flx}) mice [24] (JAX:017573) that have normal RGCs to begin with, and then delete Tet2 in adult RGCs, with

and without OSK treatment. We used a published CRE-AAV (Supplementary Fig. S3 of [9]) to remove exon 3 of Tet2, thereby removing the start codon of the TET2 protein. We first validated CRE enzymatic activity in RGCs using a Tomato reporter mouse carrying a stop cassette flanked by loxP sites (Figure 3.7a). When CRE AAV and +OSK AAV were co-infected, 95% of the OSK-positive cells had Tomato expression, indicating the knockout efficiency was around 95% (Figure 3.7b). Importantly, the conditional knockout of Tet2 also abrogated OSK-mediated RGC survival and axon regeneration (Figure 3.7c-e).

Could TET overexpression recapitulate the OSK effect? We suspect it could not, because over-saturated TET protein would induce a non-specific global decline in DNA methylation, but we did not see that in OSK expressing RGCs from retinal wholemount staining and RRBS (Figure 3.4g, Figure 3.6c, d). To further test it, we intravitreally injected AAV2s that overexpressing HA tagged Tet1 catalytic domain (Tet1-CD) or its catalytic mutant [21]. We could not overexpress the full-length Tet1 because it is over the AAV packaging limit. As we expected, Tet1 catalytic domain overexpression decreased global DNA methylation (5mC), but it did not provide any benefit to RGC survival and axon regeneration (Figure 3.8a-c). Therefore TET1/2 are necessary but not sufficient for the effect of OSK.

The lack of DNA replication in OSK expressing RGCs indicated Tet-dependent demethylation cannot complete through passive dilution (Figure 3.2a, b). To confirm the active enzyme-dependent demethylation was indeed required, we investigated the necessity of TDG, the downstream mediator of TETs, for axon regeneration. We packaged TDG and corresponding scramble knockdown AAV vectors [23] with AAV2 capsid, and co-injected them intravitreally together with +OSK AAV. The expected effect of the TDG knockdown in normal RGCs was seen, i.e. the level of 5hmC was elevated in RGCs (Figure 3.8d). We found that TDG knockdown completely abolished the beneficial effects of OSK on both axon regeneration and RGC survival (Figure 3.8e-g).

Together, these data strongly indicate that for OSK to protect RGCs and regenerate axons, site-specific, enzyme-dependent active demethylation is necessary (Figure 3.8h).

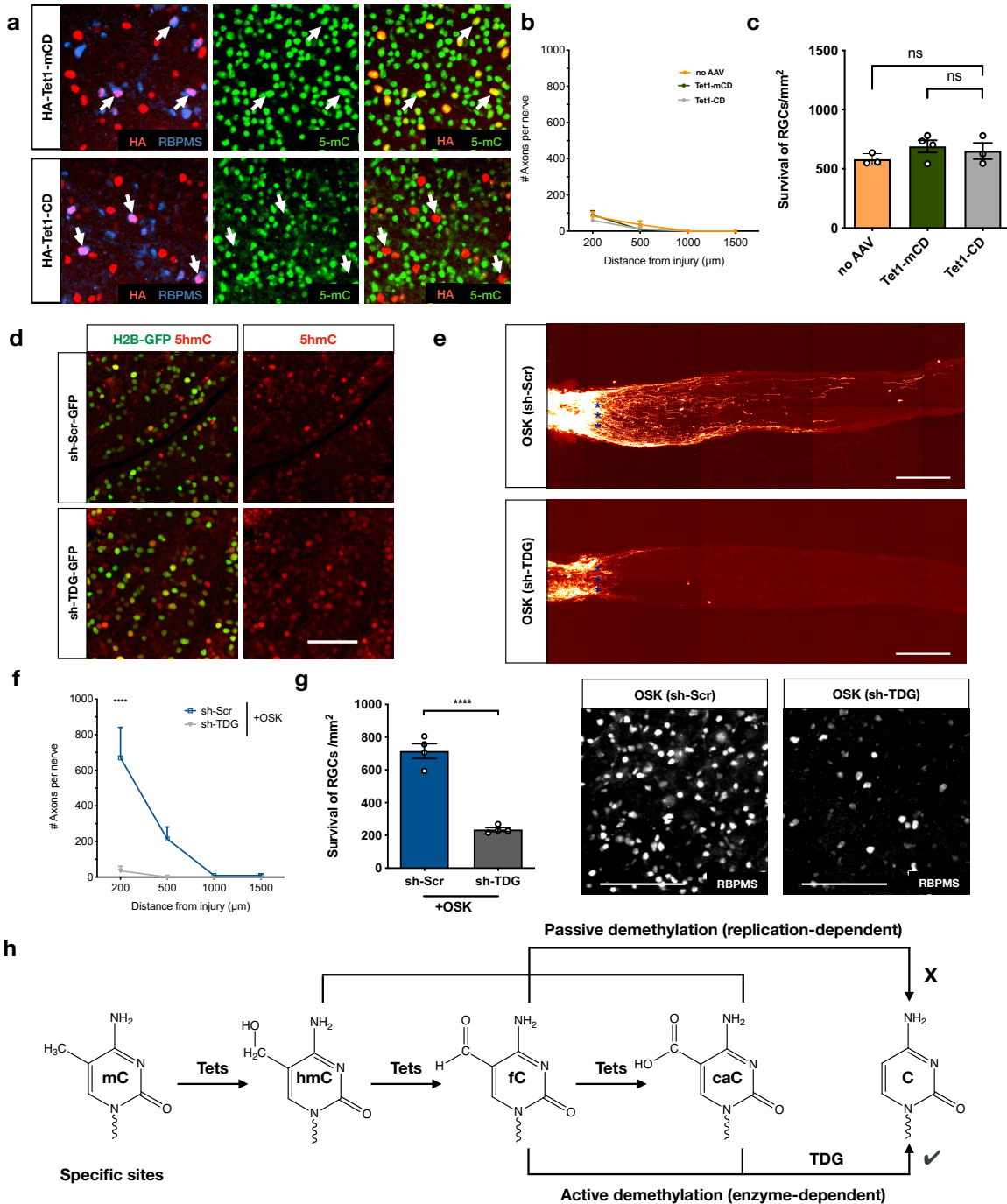


Figure 3.8 OSK-induced axon regeneration and survival require non-global active DNA demethylation through TDG. **a**, Representative images of retinal wholemounts transduced with AAV2 vectors encoding the HA-Tet1 catalytic domain (Tet1-CD) or its catalytic mutant (Tet1-mCD) for 4 weeks, demonstrating overexpression of Tet1-CD decreases global 5-mC levels. **b** and **c**, Quantification of axon regeneration and RGC survival 2 wpc in retinas co-transduced with AAV2 vectors encoding HA-Tet1 CD mutant or HA-Tet1 CD. **d**, Representative images of retinal wholemounts transduced with sh-Scr-H2B-GFP or sh-TDG-H2B-GFP AAV2s for 4 weeks, demonstrating TDG knockdown increased levels of 5-hydroxymethylcytosine (5-hmC). **e**, Representative images of longitudinal sections through the optic nerve showing CTB-labeled

regenerative axons in wild-type mice, 16 dpc after an intravitreal injection of AAV2-tTA and AAV2-TRE-OSK in combination with AAV2-sh-Scr (sh-Scr) or AAV2-sh-TDG (sh-TDG) at titer ratio 5:5:1. **f**, Quantification of regenerating axons in OSK-treated mice 16 dpc with AAVs carrying sh-Scr or sh-TDG. **g**, Quantification of RGC survival and representative retinal wholemount images from mice in **f**. **h**, A schematic diagram illustrating passive demethylation and TDG dependent active DNA demethylation. Scale bars, 100 μm in **d**, **e**, **g**.

III. OSK promotes Tet2-dependent axon regrowth in human neurons

To explore if neuronal reprogramming might be applicable to humans, we performed axon regeneration assays. We chose to assay neurons that were differentiated from SH-SY5Y human cells instead of iPSCs or ESCs because latter are pluripotent and have a DNAm age at or close to zero [12, 25]. Similar to the results in mouse RGCs, OSK expression did not induce human neuron cell proliferation (Figure 3.9a-c). Next, axon degeneration was induced by a 24-hr treatment with vincristine (VCS), a chemotherapeutic agent, and cells were then allowed to recover for 9 days (Figure 3.9d). Again, we measured the DNAm age of AAV-transduced neurons using a clock for *in vitro* studies [26]. DNAm age was significantly increased after VCS-induced damage of human neurons, OSK expression not only prevented this increase but led to a younger DNAm age (Figure 3.9e, f), without a global reduction in DNA methylation (Figure 3.9g). Nine days after damage, the neurite area was 15-fold greater in the rejuvenated OSK-transduced cells compared to controls (Figure 3.9h-j). In that particular experiment shown in Figure 3.9i, cell clusters were not split after damage, importantly to prevent cells from forming connections that would prevent us from quantifying the maximum axon regeneration that occurred without cell-cell contact.

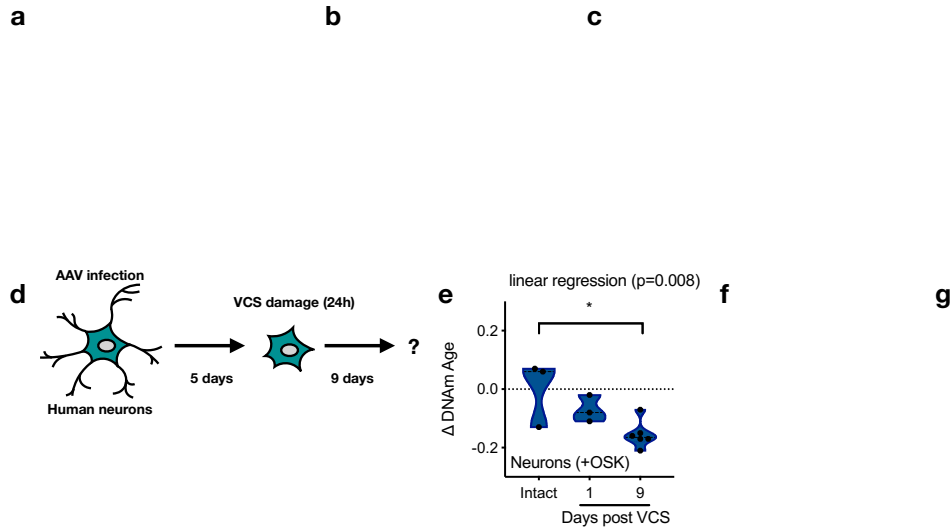


Figure 3.9 Epigenetic reprogramming promotes DNA methylation age reversal and Tet-dependent axon regeneration in human neurons. **a**, mRNA levels of Oct4, Sox2 and Klf4 in human neurons transduced with AAV-DJ vectors. -OSK: AAV-tTA; +OSK: AAV-tTA+AAV-TRE-OSK. **b**, Percentage of cells in S phase by PI-staining. **c**, FACS profiles of G1, S, and G2 phases in undifferentiated SH-SY5Y cells and differentiated cells transduced with -OSK and +OSK vectors. **d**, Experimental outline for testing axon regeneration in human neurons post-vincristine (VCS) damage. **e** and **f**, DNA methylation age of human neurons without damage (intact), and 1- or 9-days post-vincristine (VCS) damage in the presence (**e**) or absence (**f**) of OSK expression, measured using a skin and blood clock suited to *in vitro* studies. Linear regression p value refers to a continuous decrease in DNAm Age. **g**, Average DNA methylation levels among 850,000 probes from the EPIC array in human neurons without damage (intact), and 1- or 9-days post-vincristine (VCS) damage in the absence or presence of OSK expression. **h**, Morphology of regenerated axons, clusters were dissociated and transferred to new plate after VCS damage. Axons were ablated at D1 after VCS damage. Regeneration of -OSK and +OSK axons at day 9. Red arrows indicate regenerated axons. **i** and **j**, Quantification of neurite area and representative images of human neurons at different times after VCS damage with or without OSK expression. Cell clusters were not split after damage for quantifying the maximum axon regeneration that occurred without cell-cell contact.

To test if Tet is also involved in the OSK effect in human neurons, we use AAVs expressing short-hairpin RNA against human Tet2 (sh-Tet2). Knockdown of Tet2 also reduced mRNA levels of Tet1 but not Tet3 (Figure 3.10a-c), consistent with previously observed co-regulation between Tet1 and Tet2 [27].

OSK-mediated recovery of neurite area and the number, length of axons were all completely blocked by Tet2 knockdown (Figure 3.10d-g), even in the presence of high OSK expression (Figure 3.10h), and was not dependent on the mTOR-S6K pathway (Figure 3.10i, j), paralleling the effect observed in mouse RGCs. Consistent with the mouse data, global demethylation achieved by overexpression of Tet1-CD was not sufficient to promote axon regeneration (Figure 3.10k). Thus, the ability of OSK to reprogram neurons and promote axon growth is a conserved non-global, active DNA demethylation-dependent process. We refer to this process as the reversal of information loss via epigenetic reprogramming, or "REVIVER".

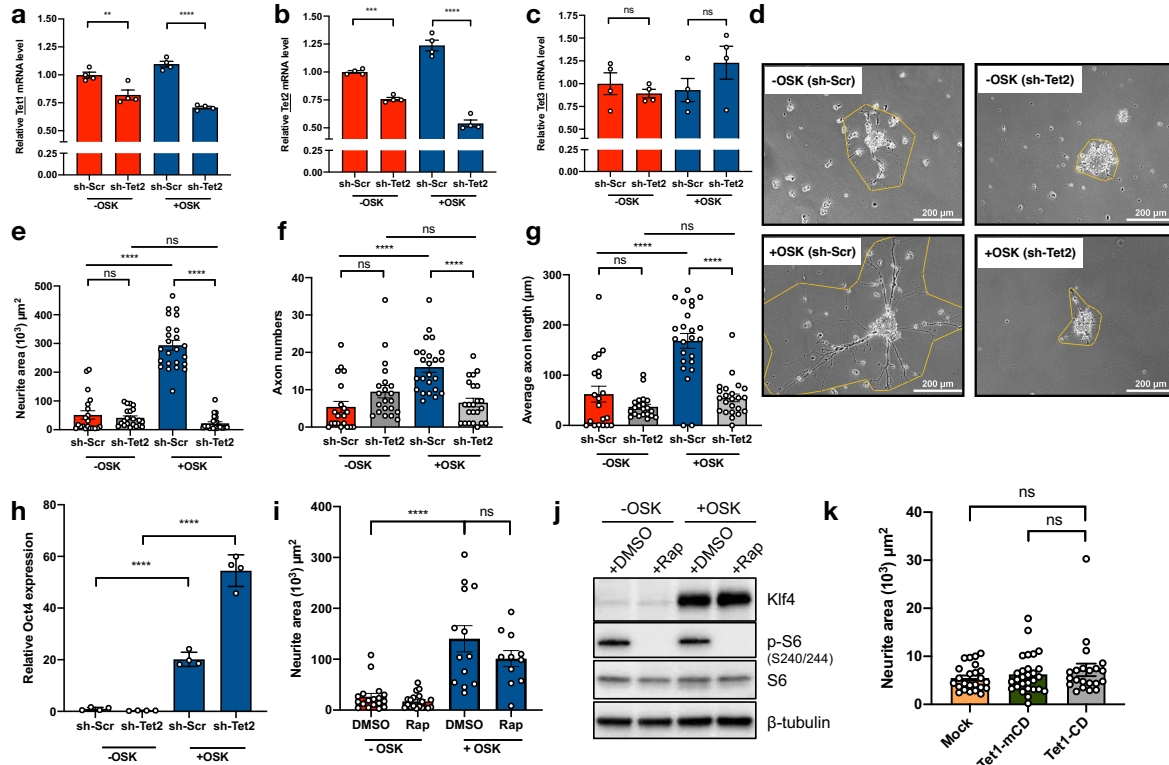


Figure 3.10 OSK induces axon regeneration of human neurons via non-global DNA demethylation and independently of mTOR. **a-c**, human *Tet1-3* mRNA level with sh-Scr or sh-Tet2 AAV in human neurons in the absence or presence of OSK-expressing AAV. **d-g**, Representative images of human neurons (**d**), and quantification of neurite area (**e**), axon number (**f**), axon length (**g**) in each AAV-treated group, 9 days post VCS damage. **h**, mouse *Oct4* mRNA level with sh-Scr or sh-Tet2 AAV in human neurons in the absence or presence of OSK AAV. **i**, The effect of mTOR inhibition on axon regeneration of differentiated neurons with or without OSK AAV. **j**, Phosphorylation levels of S6 in human neurons after rapamycin treatment (10 nM) for 5 days. **k**, Quantification of neurite area in neurons expressing Tet1 catalytic domain (Tet1-CD) or its catalytic mutant (Tet1-mCD) 9 days post-VCS damage.

IV. New hypothesis: Acute CNS injury leads to accelerated aging

One universal change that happens to aged cells is a decline in regenerative capacity after injury. In mammals, one of the first systems to lose regenerative potential is the central nervous system (CNS) [1], a phenomenon articulated as the Kennard Principle [4]. This is possibly due to the post-mitotic feature of CNS, where the intrinsic damage markers that are induced by the injury cannot be diluted through proliferation. Therefore, understanding what happens to the

CNS neuron's epigenome post injury is extremely meaningful for improving its regenerative capacity.

Injury-induced axon degeneration is an acute process starting from the injury site, while axon degeneration during aging or chronic stress is a much slower process where the axon dying back from the distal site. However, there is a lot of similarity between these processes and both result in neuronal function decline. In fact, serious traumatic brain injury (TBI) leads to cognitive aging [28], and chronic traumatic encephalopathy (CTE) in professional athletes (e.g. American football player) that repetitively getting mild TBI could lead to high risk of neurodegenerative diseases such as Alzheimer's disease (AD) and Parkinson's disease (PD).

The study of retinal ganglion cells (RGCs) has shed light on whether acute injury leads to an aged epigenome [29]. RGCs are a type of CNS neuron, projecting axons away from the retina towards the brain to form the optic nerve. In embryos and neonates, RGCs can regenerate their axons if they are damaged, but this capacity is lost within days after birth [2]. After optic nerve injury, RGCs from axon-injured retinas have significantly increased DNA methylation age [29]. Injuries to neurons include not only mechanical damage, but also protein aggregation, and exposure to chemicals. Vincristine is a chemotherapy drug that destabilizes microtubules, thereby preventing spindle assembly and cell division, which is particularly toxic to rapidly growing cancer cells but also induces axon degeneration and neuropathy in patients. After vincristine damage, DNA methylation age of differentiated human neurons was accelerated [29].

Together these findings indicate that acute physical or chemical injury can accelerate epigenetic age of cells, and we showed that a youthful epigenome can make cells better able to survive and recover from injury, thus providing a molecular explanation for the Kennard Principle.

V. References

1. Yun, M.H. (2015) Changes in Regenerative Capacity through Lifespan. *Int J Mol Sci* 16 (10), 25392-432.
2. Goldberg, J.L. et al. (2002) Amacrine-signaled loss of intrinsic axon growth ability by retinal ganglion cells. *Science* 296 (5574), 1860-4.
3. Geoffroy, C.G. et al. (2016) Evidence for an Age-Dependent Decline in Axon Regeneration in the Adult Mammalian Central Nervous System. *Cell Rep* 15 (2), 238-46.
4. Dennis, M. (2010) Margaret Kennard (1899-1975): not a 'principle' of brain plasticity but a founding mother of developmental neuropsychology. *Cortex* 46 (8), 1043-59.
5. Moore, D.L. et al. (2009) KLF family members regulate intrinsic axon regeneration ability. *Science* 326 (5950), 298-301.
6. Qin, S. et al. (2013) Cross-talk between KLF4 and STAT3 regulates axon regeneration. *Nat Commun* 4, 2633.
7. Zhang, Y. et al. (2019) Elevating Growth Factor Responsiveness and Axon Regeneration by Modulating Presynaptic Inputs. *Neuron* 103 (1), 39-51 e5.
8. Mehta, S.T. et al. (2016) Hyperactivated Stat3 boosts axon regeneration in the CNS. *Exp Neurol* 280, 115-20.
9. Sun, F. et al. (2011) Sustained axon regeneration induced by co-deletion of PTEN and SOCS3. *Nature* 480 (7377), 372-5.
10. Luo, X. et al. (2016) Enhanced Transcriptional Activity and Mitochondrial Localization of STAT3 Co-induce Axon Regrowth in the Adult Central Nervous System. *Cell Rep* 15 (2), 398-410.
11. Park, K.K. et al. (2008) Promoting axon regeneration in the adult CNS by modulation of the PTEN/mTOR pathway. *Science* 322 (5903), 963-6.
12. Horvath, S. (2013) DNA methylation age of human tissues and cell types. *Genome Biol* 14 (10), R115.
13. Petkovich, D.A. et al. (2017) Using DNA Methylation Profiling to Evaluate Biological Age and Longevity Interventions. *Cell Metab* 25 (4), 954-960 e6.
14. Olova, N. et al. (2019) Partial reprogramming induces a steady decline in epigenetic age before loss of somatic identity. *Aging Cell* 18 (1), e12877.
15. Wang, M. and Lemos, B. (2019) Ribosomal DNA harbors an evolutionarily conserved clock of biological aging. *Genome Res* 29 (3), 325-333.
16. Meer, M.V. et al. (2018) A whole lifespan mouse multi-tissue DNA methylation clock. *Elife* 7.
17. Thompson, M.J. et al. (2018) A multi-tissue full lifespan epigenetic clock for mice. *Aging (Albany NY)* 10 (10), 2832-2854.
18. Wu, X. and Zhang, Y. (2017) TET-mediated active DNA demethylation: mechanism, function and beyond. *Nat Rev Genet* 18 (9), 517-534.
19. Koh, K.P. et al. (2011) Tet1 and Tet2 regulate 5-hydroxymethylcytosine production and cell lineage specification in mouse embryonic stem cells. *Cell Stem Cell* 8 (2), 200-13.
20. Gao, Y. et al. (2013) Replacement of Oct4 by Tet1 during iPSC induction reveals an important role of DNA methylation and hydroxymethylation in reprogramming. *Cell Stem Cell* 12 (4), 453-69.

21. Guo, J.U. et al. (2011) Hydroxylation of 5-methylcytosine by TET1 promotes active DNA demethylation in the adult brain. *Cell* 145 (3), 423-34.
22. Yu, H. et al. (2015) Tet3 regulates synaptic transmission and homeostatic plasticity via DNA oxidation and repair. *Nat Neurosci* 18 (6), 836-43.
23. Weng, Y.-L. et al. (2017) An Intrinsic Epigenetic Barrier for Functional Axon Regeneration. *Neuron* 94 (2), 337-346.e6.
24. Moran-Crusio, K. et al. (2011) Tet2 loss leads to increased hematopoietic stem cell self-renewal and myeloid transformation. *Cancer Cell* 20 (1), 11-24.
25. Mertens, J. et al. (2015) Directly Reprogrammed Human Neurons Retain Aging-Associated Transcriptomic Signatures and Reveal Age-Related Nucleocytoplasmic Defects. *Cell Stem Cell* 17 (6), 705-718.
26. Horvath, S. et al. (2018) Epigenetic clock for skin and blood cells applied to Hutchinson Gilford Progeria Syndrome and ex vivo studies. *Aging (Albany NY)* 10 (7), 1758-1775.
27. Etchegaray, J.P. et al. (2015) The histone deacetylase SIRT6 controls embryonic stem cell fate via TET-mediated production of 5-hydroxymethylcytosine. *Nat Cell Biol* 17 (5), 545-57.
28. Wood, R.L. (2017) Accelerated cognitive aging following severe traumatic brain injury: A review. *Brain Injury* 31 (10), 1270-1278.
29. Lu, Y. et al. (2019) Reversal of ageing- and injury-induced vision loss by Tet-dependent epigenetic reprogramming. *bioRxiv*.

Chapter 4: Reversal of glaucoma- and aging-induced vision loss by epigenetic reprogramming

Under acute intense stress like crush injury in Chapter 3, the axons degenerate from the injury site. Under chronic biological stress, however, the axons slowly die back from the distal end to the cell body. The axon degeneration of brain neurons results in the occurrence of neurodegenerative diseases, and the axon degeneration of retina ganglion cells results in loss of vision acuity in glaucoma or aging. In this chapter, we explore whether we can use *in vivo* reprogramming (REVIVER) to reverse vision decline from diseases or aging in the retina.

I. Reversal of vision loss in a mouse model of glaucoma

Glaucoma, a progressive loss of RGCs and their axons that often coincides with increased intraocular pressure, is a leading cause of age-related blindness worldwide. Given the ability of OSK to regenerate axons after acute nerve damage, we tested whether REVIVER could restore the function of RGCs in a chronic setting like glaucoma (Figure 4.1a).

Elevated intraocular pressure (IOP) was induced unilaterally for 21 days by injection of microbeads into the anterior chamber (Figure 4.1b)[1]. At 4 weeks post-microbead injection, we saw a significant decrease in RGC number, axonal density (~20%), and vision acuity (~30%). This is a time point that glaucomatous damage was established and considered as a late stage of glaucoma (Figure 4.2a-c). AAVs or PBS were then injected intravitreally and expression was started. Two groups of mice received AAV injection: -OSK group, AAV2-rtTA+AAV2-TRE-OSK, where OSK is not induced; +OSK group, AAV2-tTA+AAV2-TRE-OSK, where OSK is induced. We did not choose TRE-d2EGFP as a replacement for TRE-OSK as a control, concerning GFP autofluorescence may interfere with our electrical response recording.

Four weeks after AAV injection, OSK-treated mice (+OSK) presented with a significant increase in axon density compared to mice that received either PBS or AAVs with no OSK induction (-OSK). The increased axon density was equivalent to the axon density in the saline-only, non-glaucomatous mice (Figure 4.1c, d) and was not associated with proliferation of RGCs (Figure 4.2d).

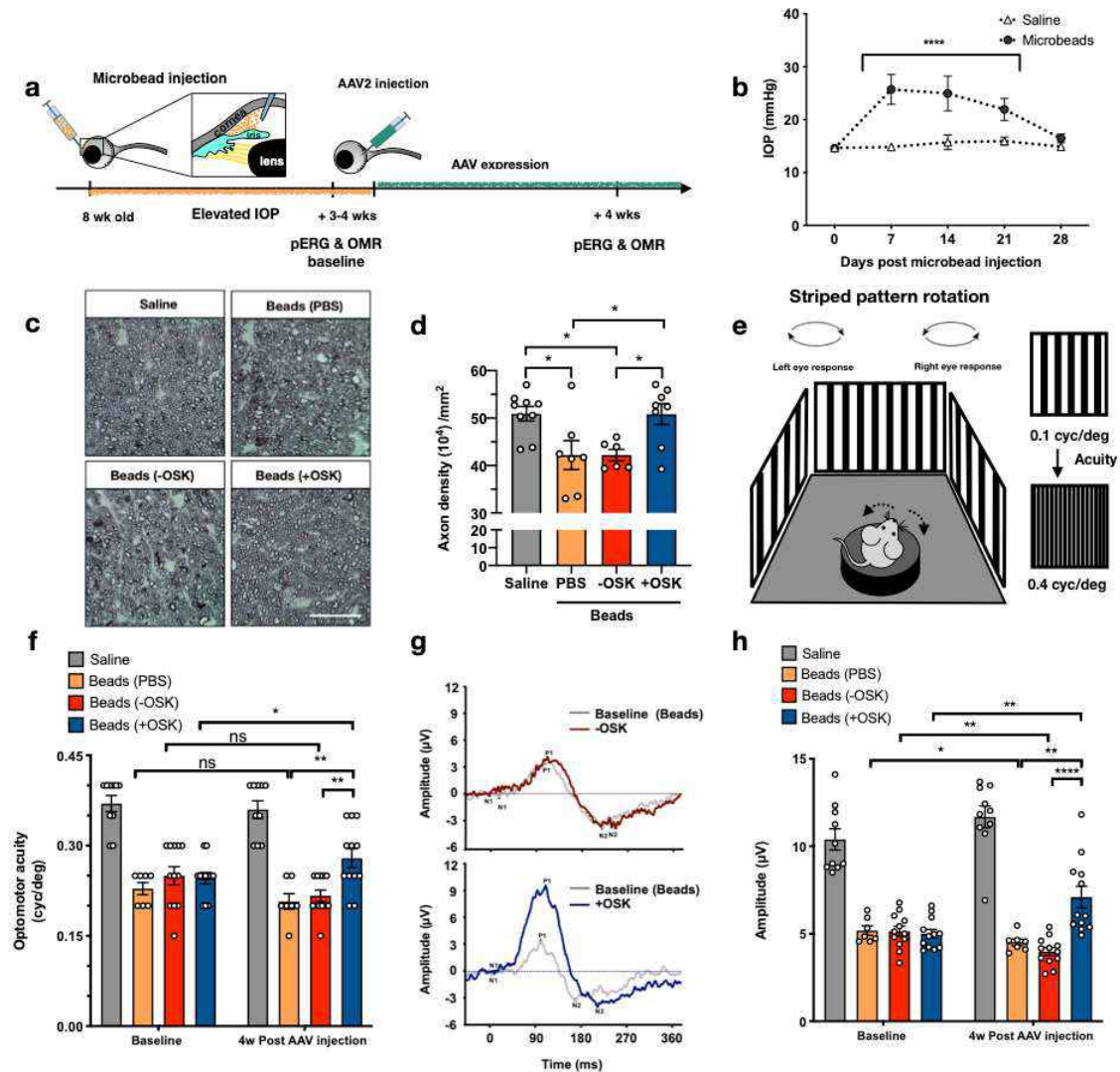


Figure 4.1 *In vivo* epigenetic reprogramming restores visual function at the late stage of glaucoma. **a**, Experimental outline of the induced glaucoma studies. **b**, Intraocular pressure (IOP) measured weekly by rebound tonometry for the first 4 weeks post-microbead injection. **c**, Representative micrographs of PPD-stained optic nerve cross-sections at 4 weeks after AAV2 or PBS injection. Scale, 50 μm . **d**, Quantification of axons 4 weeks after PBS or AAV injection. **e**, High-contrast visual stimulation to measure optomotor response. Reflexive head movements were tracked in response to the rotation of a moving stripe pattern that increases in spatial frequency. **f**, Spatial frequency threshold response of each mouse measured before treatment and 4 weeks after intravitreal injection of AAVs. **g**, Representative PERG waveforms recorded from the same eye both at pre-injection baseline and at 4 weeks after -OSK (upper graph) or +OSK (lower graph) AAV injection. **h**, Mean PERG amplitudes of recordings from each mouse in **f** at baseline before treatment and 4 weeks after intravitreal AAV injection. * $P < 0.05$; ** $P < 0.01$; *** $P < 0.001$, **** $P < 0.0001$. Two-way ANOVA with Bonferroni correction between groups was used for the overall effect of time and treatment for **b**, **f**, and **h**. Before and after treatments were analyzed using a paired two tailed student t-test in **f** and **h**. One-way ANOVA with Bonferroni's multiple comparison test for **d**.

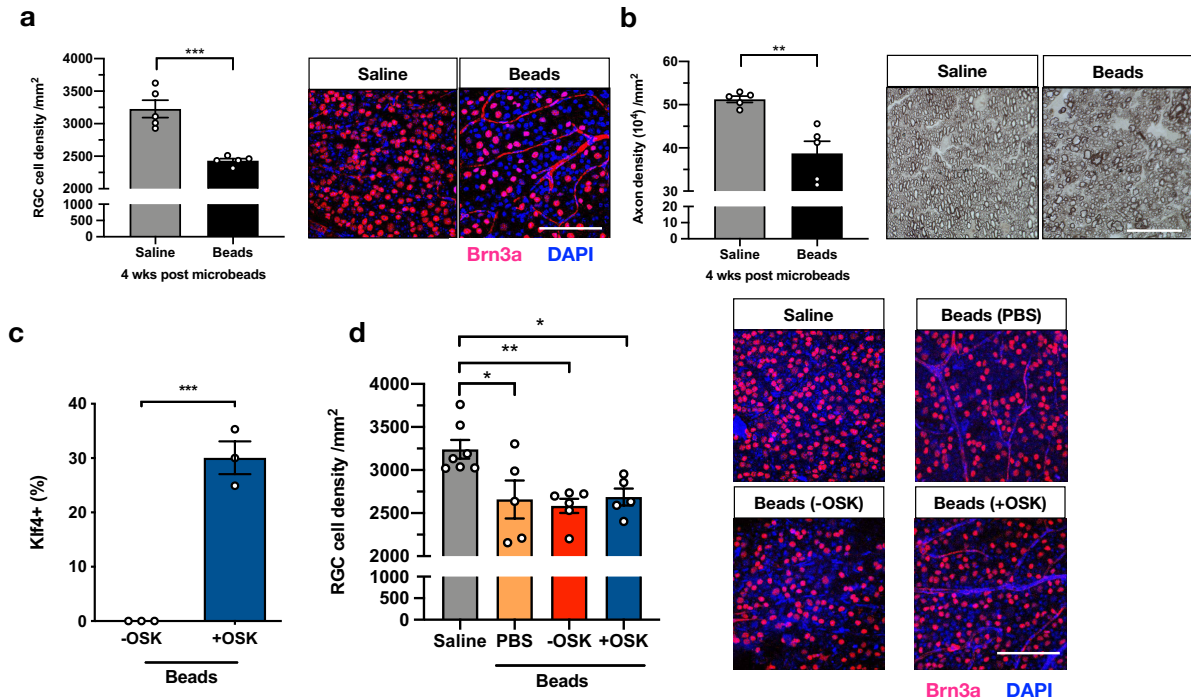


Figure 4.2 Vision restoration and regenerative effect of OSK in glaucoma is not dependent on RGC proliferation. **a**, Quantification of RGCs and representative confocal microscopic images from retinal flat-mounts stained with anti-Brn3a (red), an RGC-specific marker, and DAPI (blue), a nuclear stain, 4 weeks after microbead or saline injection. Scale bar, 100 μm . **b**, Quantification of healthy axons and representative photomicrographs of PPD-stained optic nerve cross-sections, 4 weeks after microbead or saline injection. Scale bars, 25 μm . **c**, OSK-positive frequency in the retina of microbead-induced glaucomatous mice, 4 weeks post AAV injection. -OSK: AAV2-rtTA+AAV2-TRE-OSK; +OSK: AAV2-tTA+AAV2-TRE-OSK. **d**, Quantification of RGCs and representative confocal microscopic images 4 weeks post-PBS or AAV injection (8 weeks after microbead or saline injection). Two tailed Student's t-test in **a-c**, One-way ANOVA with Bonferroni's multiple comparison test in **d**.

To determine whether the increased axon density in OSK-treated mice coincided with increased vision, we tracked the visual acuity of each mouse by measuring their optomotor response (OMR) (Figure 4.1e). Compared to mice that received either PBS or -OSK AAV, those that expressed OSK experienced a significant increase in visual acuity relative to the pre-treatment baseline measurement, restoring about half of the visual acuity loss in the OMR assay (Figure 4.1f). A readout of electrical waves generated by RGCs in response to a reversing contrast checkerboard pattern, known as pattern electroretinogram (PERG) analysis, showed that OSK treatment significantly improved RGC function relative to the pre-treatment baseline

measurements and PBS or -OSK AAV treatments (Figure 4.1g, h). Although other treatments initiated prior to, or during the initial stages of glaucoma can slow the progression via anti-inflammatory [2-9], anti-apoptotic [10-12], pro-survival [13-17], and metabolic [18, 19] pathways, to our knowledge, REVIVER is the first treatment to reverse vision loss at a late stage of glaucoma.

II. Restoration of youthful regenerative capacity and vision in aged mice by resetting epigenome

Many treatments that work well in young individuals often fail in aged individuals. For example, an approach to regenerate retinal rod photoreceptors was effective in 1-month-old mice but not in 7-month-olds [20]. Given the ability of REVIVER to regenerate axons and to restore vision after glaucomatous damage in young mice, we wondered if REVIVER might be effective in aged mice as well.

Optic nerve crush injury was performed on 12-month-old mice using the same protocol as in Figure 3.1a, according to the experimental design in Figure 4.3a. Two weeks after injury, OSK treatment using the Tet-Off system doubled RGC survival in aged mice, similar to that observed in 1- and 3-month-old mice (Figure 4.3b). Axon regeneration was slightly lower in aged mice (Figure 4.3c), but when treatment was extended three more weeks, axon regeneration was similar to that of young mice (Figure 4.3d, e), and again this occurred in the absence of RGC proliferation from analyzing a time-course of RGC survival post injury (Figure 4.3f). These data indicate that aging does not greatly diminish the effectiveness of OSK treatment in inducing axon regeneration following an optic nerve crush injury.

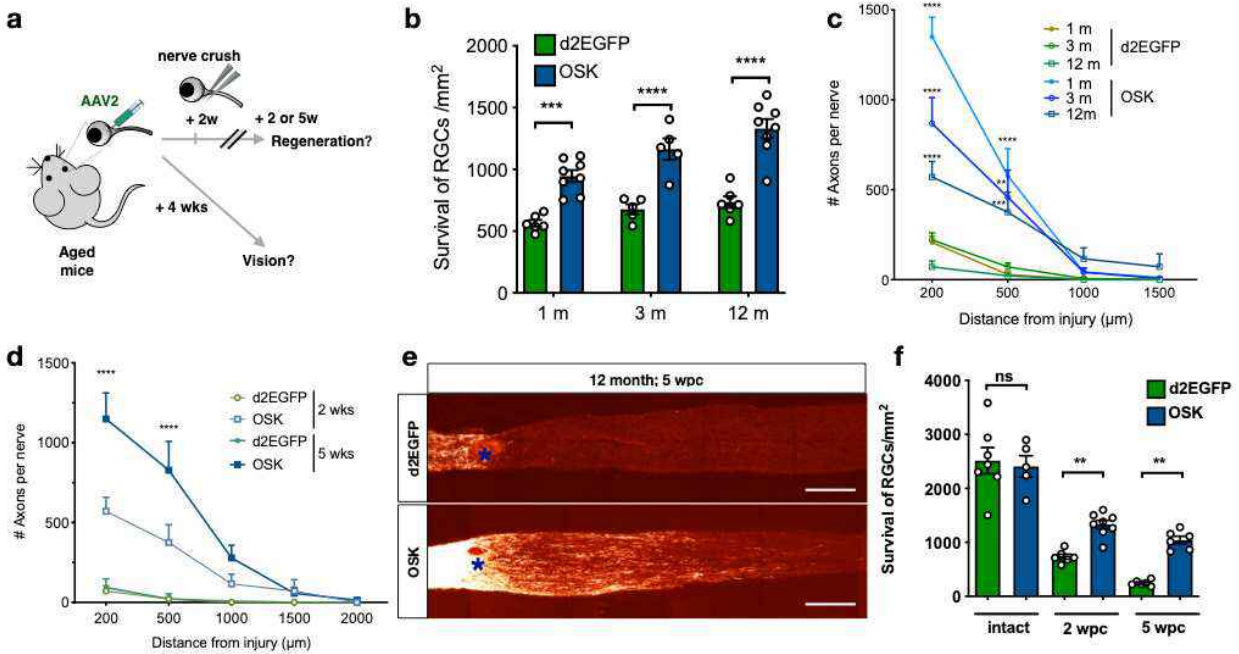


Figure 4.3 *In vivo* epigenetic reprogramming induces axon regeneration in aged mice following injury. **a**, Experimental outline for Figure 4.3 and 4.4. **b**, Effect of OSK expression on RGC survival in young, adult, and aged mice after optic nerve crush injury compared to expression of d2EGFP as a negative control. **c**, Axon regeneration after OSK expression compared to d2EGFP controls in young (1 m), adult (3 m), and aged (12 m) mice, 2 wpc. **d**, Axon regeneration in 12-month-old mice with OSK AAV or control AAV (d2EGFP) treatment, 2 or 5 wpc. **e**, Representative confocal images of longitudinal sections through the optic nerve showing CTB-labeled axons, 5 weeks after OSK treatment. Scale bar, 200 μm. **f**, Retinal RGC number of 12-month-old mice for intact, 2 or 5 wpc with OSK (AAV2-tTA+AAV2-TRE-OSK) or GFP (AAV2-tTA+AAV2-TRE-d2EGFP). **h**, Frequency of either GFP- or OSK-positive RGCs, 5 weeks post crush.

To test whether REVIVER could reverse vision loss associated with physiological aging, 4- and 12-month-old mice received intravitreal injections of -OSK or +OSK AAV (Figure 4.3a). Similar to the glaucoma study design, the -OSK group gets AAV2-rtTA and AAV2-TRE-OSK, where OSK is not induced; +OSK group gets AAV2-tTA and AAV2-TRE-OSK, where OSK is induced. Again, we did not choose TRE-d2EGFP as a replacement for TRE-OSK as control, concerning GFP autofluorescence may interfere with PERG.

Compared to the 4-month-olds, there was a significant reduction in visual acuity and RGC function at one year of age, as measured by OMR and PERG. Strikingly, this loss was completely restored by four weeks of OSK expression (Figure 4.4a, b). We did not see a

restorative effect in 18-month-old mice, likely due to the spontaneous corneal opacity that develops at that age [21] and interferes with OMR and PERG assessments.

Considering that there was no obvious increase in RGCs and axon density in the 12-month-old mice treated with +OSK AAV (Figure 4.4c, d), we suspected the increased vision was due to a functional improvement, one that could be revealed by analyzing the transcriptome. FACS-purified RGCs from 12-month-old mice, either untreated or treated with -OSK or +OSK AAV, were analyzed by RNA-seq. Compared to RGCs from 5-month-old young mice, we identified 464 genes that were differentially-expressed during aging and unaffected by empty AAV (Figure 4.5a and Supplemental Table 2), with following genes excluded: genes with low overall expression ($\log_2(\text{CPM}) < 2$), genes that did not significantly change with age (absolute \log_2 fold-change < 1) or genes altered by the virus (differentially expressed between Old and Old (-OSK)).

Remarkably, ~90 percent of the 464 age-deregulated genes were restored to youthful levels after 4 weeks of OSK expression (Figure 4.4e, f). Of the 268 age-downregulated genes, 116 are yet to be characterized and 44 are genes involved in sensory perception and axon targeting [22] (Figure 4.5b), suggesting a decline in sensory function during aging, one that can be restored by REVIVER (Figure 4.5c). Another 196 genes that were upregulated during aging are known or predicted to be involved in ion transport or negative regulation of neuronal projection development (Figure 4.5d, e), including *Efemp1*.

Efemp1 is a very interesting and relevant gene. For example, *Efemp1* transcription increases during aging, it is a known negative regulator of neuronal projection development. A missense variant of *Efemp1* is found in human open angle glaucoma cases [23], and the accumulation of *Efemp1* protein in RPE cells is linked to drusen formation in age-related macular degeneration (AMD) and Malattia Leventinese (ML) disease, a disease similar to AMD [24]. *Efemp1* has also been identified as a novel amyloidogenic protein in humans, as it frequently forms amyloid deposits in systemic venous walls of elderly people [25].

Using qPCR, we validated the RNA-seq results showing that *Efemp1* expression is two-fold higher in old vs young RGCs, and OSK treatment of aged RGCs reversed this age-dependent increase. In our newly prepared cDNA samples, we find that *Tet1* and *Tet2* are required for the restoration of *Efemp1* mRNA levels (Figure 4.5f).

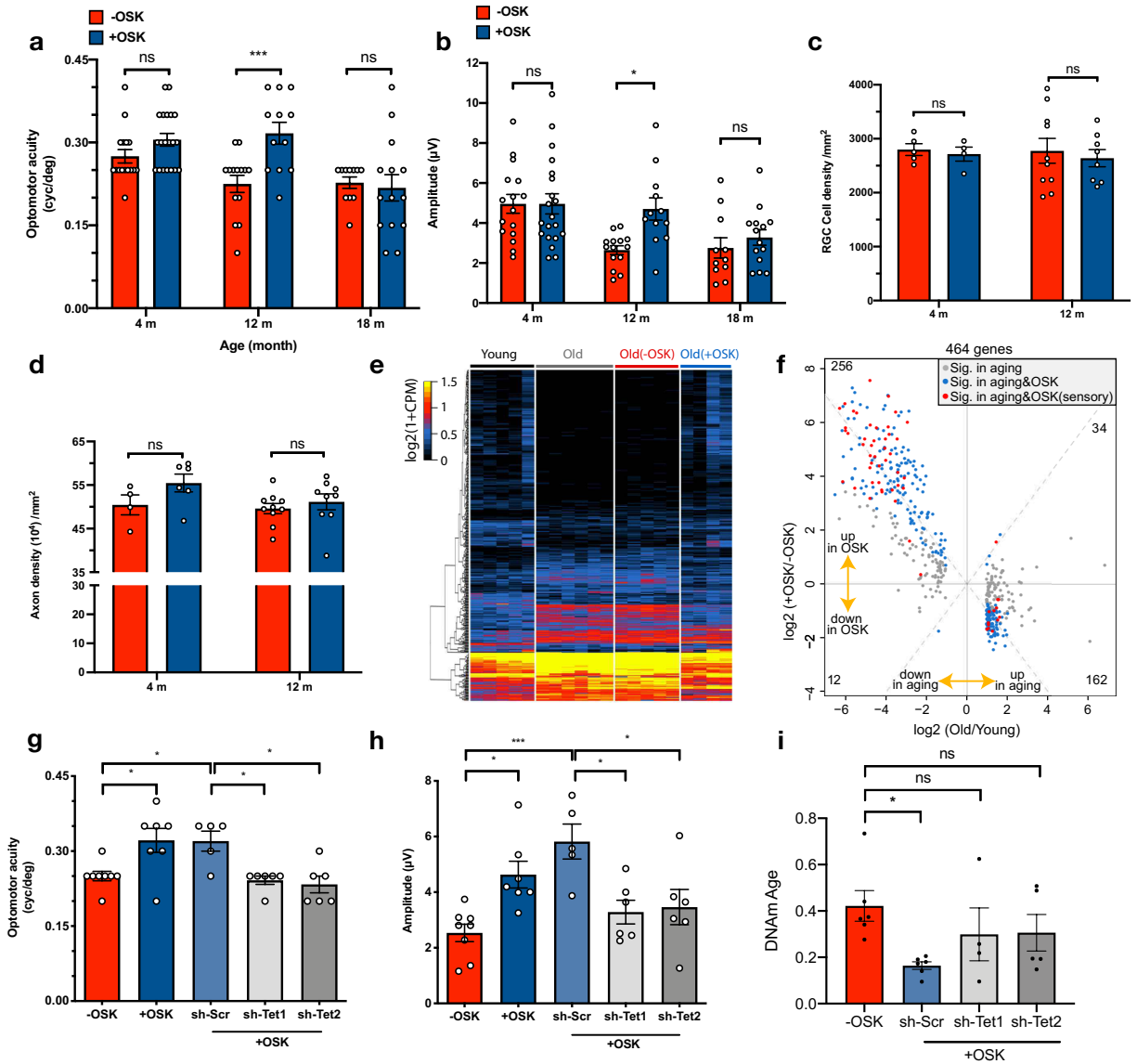


Figure 4.4 *In vivo* Tet-dependent epigenetic reprogramming restores visual function in uninjured aged mice. **a**, Spatial frequency threshold in young (4 months) and old mice (12 months, 18 months) with -OSK or +OSK AAV for 4 weeks. **b**, Comparison of PERG measurement in different ages 1 m after -OSK or +OSK treatment. **c**, RGC cell density in 4 and 12-month-old-mice, 1 month after -OSK or +OSK. **d**, Comparison of axon density in 4- and 12-month-old mice, 1 month after -OSK or +OSK. **e**, Hierarchical clustered heatmap showing mRNA level of 464 differentially expressed genes in sorted RGCs from intact young mice (5 months), intact old mice (12 months), or old mice treated with either -OSK or +OSK AAV. -OSK: AAV2-TRE-OSK; +OSK: AAV2-tTA+AAV2-TRE-OSK. **f**, Scatter plot of OSK-induced changes versus age-associated changes in mRNA levels. Dots represent significantly differentially expressed genes during aging in RGCs. Genes in top left and bottom right quadrants have been restored to youthful level in the old (+OSK) RGCs. **g** and **h**, Spatial frequency threshold and PERG amplitudes in old mice (12 months) treated with: (i) -OSK, (ii) +OSK, or (iii) +OSK together with either sh-Scr or sh-Tet1/sh-Tet2-mediated knockdown for 4

weeks. **i**, rDNA methylation age of 12-month-old RGCs FACS-isolated from retinas infected for 4 weeks with -OSK or +OSK AAV together with short hairpin RNAs targeting a scrambled sequence (sh-Scr), Tet1 (sh-Tet1) or Tet2 (sh-Tet2).

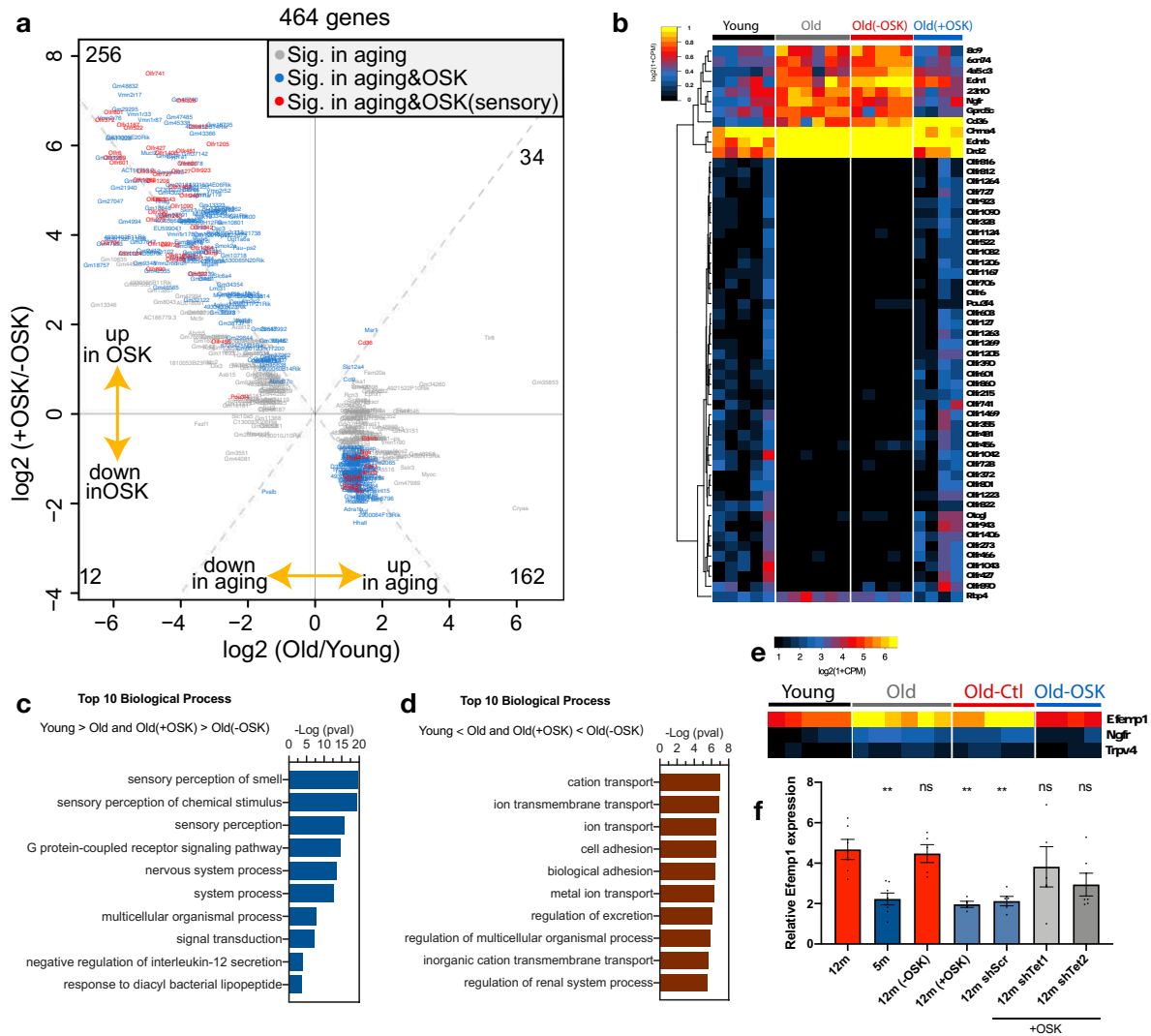


Figure 4.5 OSK expression in aged RGCs restores a youthful gene expression pattern. a, Scatter plot of OSK-induced changes and age-associated changes in mRNA levels in RGCs, with dots representing differentially expressed genes. **b**, Hierarchical clustered heatmap showing relative mRNA levels of sensory genes in FACS-sorted RGCs from young (5 m) or old mice (12 m), or old mice treated with either -OSK or +OSK AAV. **c**, Top 10 biological process that were lower in old compared to young and restored by OSK. **d**, Top 10 biological process that were higher in old compared to young and reduced by OSK. **e**, Heatmap showing relative mRNA levels of genes involved in neural projection development among the 464 differentially expressed genes during aging. *Efemp1* is a gene whose accumulation during aging is suspected to play a role in diseases of the retina. **f**, RGC *Efemp1* mRNA levels measured by qPCR (relative to GAPDH) compared between young, old and old treated with -OSK or + OSK AAV. Old RGCs with sh-Scr or sh-Tet1 or sh-Tet2 knockdown combined with +OSK AAV are included for comparison.

Consistent with the axon regeneration data in Chapter 3, the knockdown of Tet1 or Tet2 completely blocked the ability of REVIVER to restore vision in 12-month-old mice (Figure 4.4g, h). Also, four weeks of OSK expression significantly decreased DNAm age in a Tet1- and Tet2-dependent manner (Figure 4.4i). Together, these results demonstrate that Tet-dependent *in vivo* reprogramming can restore youthful gene expression patterns, reverse DNAm age, and restore the function and regenerative capacity of a tissue as complex as the retina.

III. Summary

Post-mitotic neurons in the CNS are some of the first cells in the body to lose their ability to regenerate. In this study, we show that *in vivo* reprogramming of aged CNS neurons can reverse DNAm age and allow them to regenerate and function as though they were young again. The requirement of active demethylation for this process indicates that altered DNA methylation patterns may not just be a measure of age but participants in aging, with the clock being a requisite component or an indicator of the site-specific DNA demethylation events that are necessary to reset the epigenome via OSK. These data lead us to conclude that mammalian cells retain a set of original epigenetic information that can be accessed in the adult to recover lost information [26]. How cells are able to mark and retain youthful DNA methylation patterns, then in late adulthood remove age-specific marks is unknown. Youthful epigenetic modifications may be resistant to removal by the Tets by the presence of specific proteins that bind DNA or covalent DNA modifications laid down early in life. Even in the absence of this knowledge, this work indicates that the restoration of a youthful epigenome could be an effective strategy, not just to restore vision, but to allow other tissues to recover from injury and reverse age-related decline.

IV. References

1. Krishnan, A. et al. (2016) Overexpression of Soluble Fas Ligand following Adeno-Associated Virus Gene Therapy Prevents Retinal Ganglion Cell Death in Chronic and Acute Murine Models of Glaucoma. *J Immunol* 197 (12), 4626-4638.
2. Anderson, M.G. et al. (2005) High-dose radiation with bone marrow transfer prevents neurodegeneration in an inherited glaucoma. *Proceedings of the National Academy of Sciences of the United States of America* 102 (12), 4566-71.
3. Howell, G.R. et al. (2012) Radiation treatment inhibits monocyte entry into the optic nerve head and prevents neuronal damage in a mouse model of glaucoma. *The Journal of clinical investigation* 122 (4), 1246-61.
4. Williams, P.A. et al. (2016) Inhibition of the classical pathway of the complement cascade prevents early dendritic and synaptic degeneration in glaucoma. *Molecular Neurodegeneration* 11 (1), 26.
5. Harder, J.M. et al. (2017) Early immune responses are independent of RGC dysfunction in glaucoma with complement component C3 being protective. *Proceedings of the National Academy of Sciences of the United States of America* 114 (19), E3839-E3848.
6. Nakazawa, T. et al. (2006) Tumor necrosis factor- α mediates oligodendrocyte death and delayed retinal ganglion cell loss in a mouse model of glaucoma. *The Journal of neuroscience: the official journal of the Society for Neuroscience* 26 (49), 12633-41.
7. Bosco, A. et al. (2008) Reduced Retina Microglial Activation and Improved Optic Nerve Integrity with Minocycline Treatment in the DBA/2J Mouse Model of Glaucoma. *Investigative Ophthalmology & Visual Science* 49 (4), 1437.
8. Roh, M. et al. (2012) Etanercept, a widely used inhibitor of tumor necrosis factor- α (TNF- α), prevents retinal ganglion cell loss in a rat model of glaucoma. *PloS one* 7 (7), e40065.
9. Williams, P.A. et al. (2019) Inhibition of monocyte-like cell extravasation protects from neurodegeneration in DBA/2J glaucoma. *Molecular Neurodegeneration* 14 (1), 6.
10. Libby, R.T. et al. (2005) Susceptibility to neurodegeneration in a glaucoma is modified by Bax gene dosage. *PLoS genetics* 1 (1), 17-26.
11. Krishnan, A. et al. (2019) A small peptide antagonist of the Fas receptor inhibits neuroinflammation and prevents axon degeneration and retinal ganglion cell death in an inducible mouse model of glaucoma. *Journal of neuroinflammation* 16 (1), 184.
12. Gregory, M.S. et al. (2011) Opposing roles for membrane bound and soluble Fas ligand in glaucoma-associated retinal ganglion cell death. *PloS one* 6 (3), e17659.
13. Zhong, L. et al. (2007) Erythropoietin Promotes Survival of Retinal Ganglion Cells in DBA/2J Glaucoma Mice. *Investigative Ophthalmology & Visual Science* 48 (3), 1212.
14. Jiang, C. et al. (2007) Intravitreal injections of GDNF-loaded biodegradable microspheres are neuroprotective in a rat model of glaucoma. PMID - 17960131. *Molecular vision* 13, 1783-92.
15. Fu, Q.L. et al. (2009) Combined effect of brain-derived neurotrophic factor and LINGO-1 fusion protein on long-term survival of retinal ganglion cells in chronic glaucoma. *Neuroscience* 162 (2), 375-382.
16. Yang, H. et al. (2009) Neuroprotective Effects of Angiotensin II Type 1 Receptor Blocker in a Rat Model of Chronic Glaucoma. *Investigative Ophthalmology & Visual Science* 50 (12), 5800.

17. Feng, L. et al. (2016) Long-Term Protection of Retinal Ganglion Cells and Visual Function by Brain-Derived Neurotrophic Factor in Mice With Ocular Hypertension. *Investigative Ophthalmology & Visual Science* 57 (8), 3793.
18. Kim, K.Y. et al. (2015) DRP1 inhibition rescues retinal ganglion cells and their axons by preserving mitochondrial integrity in a mouse model of glaucoma. *Cell death & disease* 6 (8), e1839.
19. Williams, P.A. et al. (2017) Vitamin B 3 modulates mitochondrial vulnerability and prevents glaucoma in aged mice. *Science* 355 (6326), 756-760.
20. Yao, K. et al. (2018) Restoration of vision after de novo genesis of rod photoreceptors in mammalian retinas. *Nature* 560 (7719), 484-488.
21. McClellan, A.J. et al. (2014) Ocular surface disease and dacryoadenitis in aging C57BL/6 mice. *Am J Pathol* 184 (3), 631-43.
22. Li, H. et al. (2020) Single-Cell Transcriptomes Reveal Diverse Regulatory Strategies for Olfactory Receptor Expression and Axon Targeting. *Curr Biol*.
23. Mackay, D.S. et al. (2015) Exome Sequencing Identifies a Missense Variant in EFEMP1 Co-Segregating in a Family with Autosomal Dominant Primary Open-Angle Glaucoma. *PLoS One* 10 (7), e0132529.
24. Marmorstein, L.Y. et al. (2002) Aberrant accumulation of EFEMP1 underlies drusen formation in Malattia Leventinese and age-related macular degeneration. *Proc Natl Acad Sci U S A* 99 (20), 13067-72.
25. Tasaki, M. et al. (2019) A novel age-related venous amyloidosis derived from EGF-containing fibulin-like extracellular matrix protein 1. *J Pathol* 247 (4), 444-455.
26. Shannon, C.E. (1948) A Mathematical Theory of Communication. *The Bell System Technical Journal* 27, 379-423.

Chapter 5: Mechanism and future directions of *in vivo* reprogramming

I. Active DNA demethylation is required for epigenetic correction

The observed decrease in DNA methylation age after OSK-mediated reprogramming indicated that remodeling of DNA methylation patterns is required for age reversal and functional improvement. The Ten-Eleven-Translocation dioxygenases, TET1-3, catalyze DNA demethylation either by replication-dependent passive dilution, or active enzymatic removal by the downstream enzyme thymine DNA glucosidase (TDG) [1]. In the case of *in vitro* iPSC derivation, active demethylation and passive demethylation both play a role. The mesenchymal-to-epithelial transition (MET), a necessary step in the early stages of reprogramming requires active demethylation, and that is why Tet-deficient and TDG-deficient MEFs cannot be reprogrammed [2]. At the later stages of reprogramming, replication-dependent passive demethylation promotes the formation of iPSC colonies by upregulating pluripotency genes such as Nanog, Esrrb, and Dppa2 [3]. Not surprisingly, somatic cell nuclear transfer (SCNT), the other classic age resetting process also requires DNA demethylation at gene promoters [4].

During *in vivo* reprogramming of the retina, Tet1 and Tet2 were found to be necessary for the restoration of vision by OSK in aged mice. For RGC survival and regeneration, Tet1 and Tet2 were also required, as was the downstream enzyme, TDG, showing active DNA demethylation is required for axon regrowth. Global changes in methylation were not seen after OSK treatment and overexpression of the Tet1 catalytic domain, which causes global demethylation, had no protective or regenerative effect. Together, these data strongly suggest that for OSK to protect RGCs and regenerate axons, site-specific, enzyme-dependent active demethylation is necessary.

Other studies also indicate that DNA demethylation may be important for degeneration and regeneration in the brain. For example, non-coding and loss-of-function variants in Tet2 are

associated with multiple neurodegenerative diseases [5] and the restoration of Tet2 in the adult hippocampal neurogenic niche counteracts age-related declines in neurogenesis [6].

In contrast to the CNS, the mammalian peripheral nervous system (PNS) has intrinsic axon regenerative capacity even in adulthood. Upon injury, adult PNS neurons can naturally switch from a dormant state with low regenerative capacity to a robust regeneration state. At the molecular level, this switch involves Tet3- and TDG-mediated DNA demethylation and expression of regeneration associated genes, and Tet3 is required for axon regeneration of dorsal root ganglion (DRG) neurons and following behavioral recovery of thermal withdrawal [7]. This suggests the exciting possibility that active DNA demethylation by OSK within the CNS may work by mimicking the PNS switch.

II. Alternative strategies for *in vivo* reprogramming

Moving from mice to retinal disease in humans is a big step. Currently, at least three AAV gene therapies, Glybera, Luxturna, and Zolgensma have been approved for use in humans [8]. Each method, however, has its limitations. The tissue tropism of each AAV serotype is an advantage for targeting tissue specific diseases (e.g. AAV2 for the retina [9]) but reliable and even delivery to the human brain (for neurodegenerative diseases) or to a broader distribution in multiple tissues simultaneously (for aging) is not yet possible. AAV9, a clinically approved AAV serotype [10], has the broadest tropism when introduced intravenously early in development of rodents [11], but when introduced at a late age, delivery is largely limited to the liver and pancreas [12]. A newly developed AAV9 variant, AAV.PHP.B, has enhanced CNS tropism [13] but the lack of a cellular receptor LY6A [14] [15] [16] in certain mouse strains and non-human primates limits its application [17]. Therefore, future directions for *in vivo*

reprogramming technologies must include the development of additional AAV serotypes that have new and broader tropisms.

It should also be possible to move away from using AAVs. Other cellular reprogramming strategies to avoid the use of nuclear transcription factors include CRISPR activation of endogenous locus, small molecules and secretory protein factors such as antibodies and peptides.

Targeted CRISPR activation of endogenous Oct4 or Sox2 locus is able to induce fully reprogramming *in vitro* [18]. However, *in vivo* delivery of dCas9-activator and guide RNA is still dependent on AAV system [11]. Consider the remodeling at promoter or enhancer does not require the long-term presence of the activation component, a transient expression through DNA plasmid or RNA-nanoparticle delivery is worth exploring.

Using small molecules for reprogramming is a promising strategy because they are cell-permeable and easier to manufacture than AAVs. A cocktail of 7 to 13 chemical compounds can reprogram mouse embryonic fibroblasts into pluripotent stem cells without any transcription factors [19, 20]. However, cells go through an extraembryonic endoderm (XEN)-like state that is fundamentally different from the transcription factor-based method. There is also a lack of knowledge about whether age-related epigenetic changes such as the DNA methylation clock are reset by chemical reprogramming, whether it is safe *in vivo*, or if tissue rejuvenation is even possible. In addition, the current cocktails are toxic to adult cells *in vitro*, so safer methods will be needed.

A list of small molecules has been identified that promote transcription factor-based reprogramming. They function either by targeting specific signaling pathways or by remodeling the chromatin state. For example, histone deacetylase inhibitors such as valproic acid (VPA), Trichostatin A (TSA) and suberoylanilide hydroxamic acid (SAHA) promote reprogramming

efficiency by increasing histone acetylation and decreasing histone methylation [21]. Vitamin C enhances the activity of histone demethylase such as KDM6B and DNA demethylases such as TET1-3 [22], the latter of which is also stimulated by their co-substrate α -ketoglutarate (α -KG), a key metabolite extended lifespan of worm [23] and mice [24]. DNMT inhibitors such as 5-azacytidine (5-aza) and RG108 promotes hypomethylation of the genome. It is yet to be determined whether these small molecules themselves are able to revert youthful epigenetic information and rejuvenate cells themselves or need the involvement of transcription factors.

The conventional reprogramming method uses Yamanaka transcription factors that act within the nucleus. In contrast, during development, signaling pathways are initiated at the cell membrane. Finding secretory factors that can act at the cell surface and induce reprogramming in the nucleus may solve the delivery issue for whole-body reprogramming. Secreted and membrane-bound antibodies that can replace either Sox2 and c-Myc or Oct4 have been found through screening. For example, the Sox2-replacing antibody can induce the expression of WT1, Esrrb and Lin28a independent of Sox2, through antagonism to membrane protein Basp1, a protein that translocates from the cell membrane to the nucleus [25]. The current challenge for this method is that the Oct4-replacing antibody is not very efficient, therefore finding antibodies to replace all factors will be challenging [26].

III. More applications of *in vivo* reprogramming

Direct reprogramming induces cell lineage change without going through pluripotency. It can be achieved through ectopic overexpression of transcription factor, which was first reported in 1987 [27], or miRNAs [28] and pure chemicals [29]. Recently, chemical induced photoreceptor-like cells, which were transformed from fibroblasts *in vitro*, partially restored vision in rod degeneration mice after transplantation [30].

When applied *in vivo*, direct reprogramming can convert fate of spare cells as an extra source to replace defective ones [31], such as reprogramming retinal Müller glial cells to generate rods [32] or turning pancreatic alpha cells into insulin produced beta cells [33]. However, such methods suffer from low conversion rate *in vivo*. Partial epigenetic reprogramming *in vivo* may be combined with direct reprogramming to lower the epigenetic barrier for the conversion and thus improve conversion *in vivo*.

Epigenetic reprogramming could also be applied to transplanted organs because the epigenetic age of the transplanted organ is intrinsic and will not be influenced by the recipient's age, exemplified by hematopoietic stem cell transplantation, in which the DNAm age of the reconstituted blood was not influenced by the recipient's age even after 17 years [34]. When a donated organ is from an older individual, *in vivo* reprogramming could be used to rejuvenate the organ pre- or post-transplantation and could help synchronize the epigenetic ages of the organ and recipient and, by making older organs suitable, making far more organs available for transplantation.

IV. Prospecction: What's the biological observer for aging reversal

In 1876, James Clarke Maxwell proposed a “demon” to prevent information loss due to entropy: an “observer” of initial and final states. Since then, physicists have highlighted the need for energy to record and replace the information collected by the observer, which is possible in the case of information in living organisms because they are open systems. In this way, a cell could theoretically reset itself by contacting the observer, so long as there was a supply of energy from outside the system.

Recent progress in the *in vivo* reprogramming field has led us to conclude that a biological observer indeed exists in mammalian cells. The cells retain a set of original epigenetic information that can be accessed in the adult to recover lost information (Figure 1) [35].

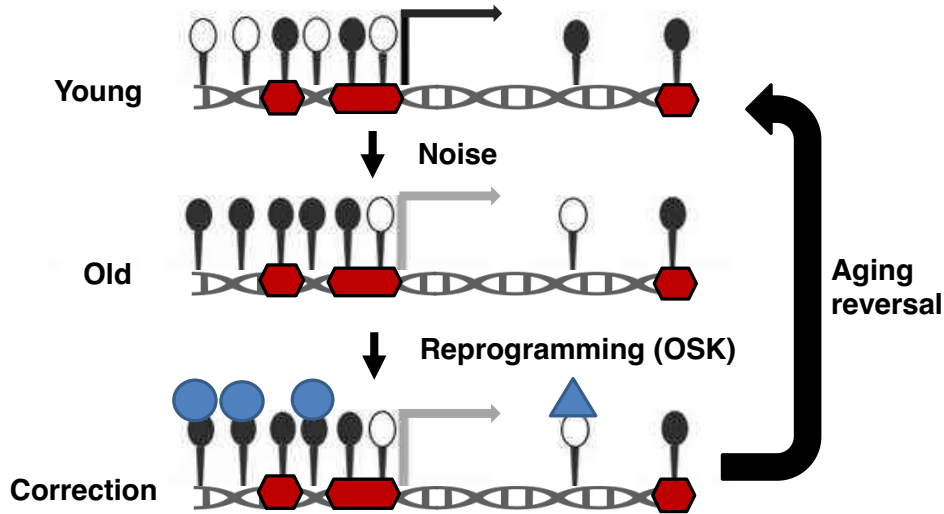
How does the biological observer work? It's the last missing piece in our information theory of aging. We propose the observer could work in either passive or active model, or both, during the epigenetic correction process (Figure 5):

In a passive model, the cells are able to mark and remember youthful DNA epigenetic patterns. The observer could be a covalent DNA modification or a specific protein that bind DNA early in life, then in late adulthood make that region inaccessible by the TETs and other modifiers. While the other DNA regions, such as bivalent promoters and methylation clock sites, get modified during aging, and are accessible by the TETs or other modifiers when signal is given by OSK. Therefore, the observer, does not directly cooperate with epigenetic modifier, plays a passive role during reprogramming. In an active model, the cells mark DNA regions that get modified gradually post development. The observer could be an epigenetic modification such as H3K27me3, that laid down during aging on the regions like bivalent promoters and methylation clock sites. In this way the observer directly recruits TETs or other modifiers when signal is given by OSK, thus plays an active role during reprogramming. We suspect that observer more likely fits in a passive model, where the observer should be stable, not dynamic.

The discovery of the observer would not only solve one of biology's most interesting questions, but also aid the design more precise and effective strategies to restore youthful epigenomes, not just to restore vision, but to allow other tissues to better recover from injury and resist age-related decline.

a. Passive model

▲ ● Modifiers ◆ Observer ○ Unmodified ● Modified



b. Active model

▲ ● Modifiers ◆ ◆ Observer ○ Unmodified ● Modified

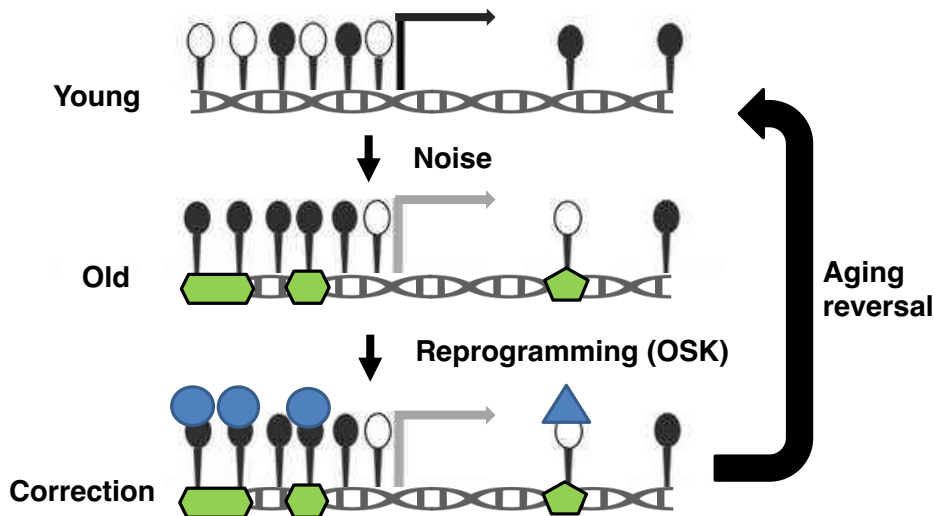


Figure 5. Hypothetical working models of the epigenetic observer during aging. **a**, In a passive model, the observer marks the DNA early in life and does not directly interact with epigenetic modifiers during reprogramming. **b**, In an active model, the observer marks the DNA during aging and interact with epigenetic modifiers directly during reprogramming. In **a** and **b**, grey arrows indicate weaker transcriptions than those indicated by black arrows.

V. References

1. Wu, X. and Zhang, Y. (2017) TET-mediated active DNA demethylation: mechanism, function and beyond. *Nat Rev Genet* 18 (9), 517-534.
2. Hu, X. et al. (2014) Tet and TDG mediate DNA demethylation essential for mesenchymal-to-epithelial transition in somatic cell reprogramming. *Cell Stem Cell* 14 (4), 512-22.
3. He, S. et al. (2017) Passive DNA demethylation preferentially up-regulates pluripotency-related genes and facilitates the generation of induced pluripotent stem cells. *J Biol Chem* 292 (45), 18542-18555.
4. Simonsson, S. and Gurdon, J. (2004) DNA demethylation is necessary for the epigenetic reprogramming of somatic cell nuclei. *Nat Cell Biol* 6 (10), 984-90.
5. Cochran, J.N. et al. (2019) Non-Coding and Loss-of-Function Coding Variants in TET2 are Associated with Multiple Neurodegenerative Diseases. *bioRxiv*.
6. Gontier, G. et al. (2018) Tet2 Rescues Age-Related Regenerative Decline and Enhances Cognitive Function in the Adult Mouse Brain. *Cell Rep* 22 (8), 1974-1981.
7. Weng, Y.-L. et al. (2017) An Intrinsic Epigenetic Barrier for Functional Axon Regeneration. *Neuron* 94 (2), 337-346.e6.
8. Wang, D. et al. (2019) Adeno-associated virus vector as a platform for gene therapy delivery. *Nat Rev Drug Discov* 18 (5), 358-378.
9. Smalley, E. (2017) First AAV gene therapy poised for landmark approval. *Nat Biotechnol* 35 (11), 998-999.
10. Al-Zaidy, S.A. et al. (2019) AVXS-101 (Onasemnogene Apeparvovec) for SMA1: Comparative Study with a Prospective Natural History Cohort. *J Neuromuscul Dis* 6 (3), 307-317.
11. Liao, H.K. et al. (2017) In Vivo Target Gene Activation via CRISPR/Cas9-Mediated Trans-epigenetic Modulation. *Cell* 171 (7), 1495-1507 e15.
12. Lu, Y. et al. (2019) Reversal of ageing- and injury-induced vision loss by Tet-dependent epigenetic reprogramming. *bioRxiv*.
13. Deverman, B.E. et al. (2016) Cre-dependent selection yields AAV variants for widespread gene transfer to the adult brain. *Nat Biotechnol* 34 (2), 204-9.
14. Hordeaux, J. et al. (2019) The GPI-Linked Protein LY6A Drives AAV-PHP.B Transport across the Blood-Brain Barrier. *Molecular Therapy* 27 (5), 912-921.
15. Batista, A.R. et al. (2020) Ly6a Differential Expression in Blood-Brain Barrier Is Responsible for Strain Specific Central Nervous System Transduction Profile of AAV-PHP.B. *Hum Gene Ther* 31 (1-2), 90-102.
16. Huang, Q. et al. (2019) Delivering genes across the blood-brain barrier: LY6A, a novel cellular receptor for AAV-PHP.B capsids. *PLoS One* 14 (11), e0225206.
17. Hordeaux, J. et al. (2018) The Neurotropic Properties of AAV-PHP.B Are Limited to C57BL/6J Mice. *Mol Ther* 26 (3), 664-668.
18. Liu, P. et al. (2018) CRISPR-Based Chromatin Remodeling of the Endogenous Oct4 or Sox2 Locus Enables Reprogramming to Pluripotency. *Cell Stem Cell* 22 (2), 252-261 e4.
19. Hou, P. et al. (2013) Pluripotent stem cells induced from mouse somatic cells by small-molecule compounds. *Science* 341 (6146), 651-4.
20. Zhao, Y. et al. (2015) A XEN-like State Bridges Somatic Cells to Pluripotency during Chemical Reprogramming. *Cell* 163 (7), 1678-91.

21. Huangfu, D. et al. (2008) Induction of pluripotent stem cells by defined factors is greatly improved by small-molecule compounds. *Nat Biotechnol* 26 (7), 795-7.
22. Lee Chong, T. et al. (2019) Reprogramming the Epigenome With Vitamin C. *Front Cell Dev Biol* 7, 128.
23. Chin, R.M. et al. (2014) The metabolite alpha-ketoglutarate extends lifespan by inhibiting ATP synthase and TOR. *Nature* 510 (7505), 397-401.
24. Shahmirzadi, A.A. et al. (2019) Alpha-ketoglutarate, an endogenous metabolite, extends lifespan and compresses morbidity in aging mice. *bioRxiv*.
25. Blanchard, J.W. et al. (2017) Replacing reprogramming factors with antibodies selected from combinatorial antibody libraries. *Nat Biotechnol* 35 (10), 960-968.
26. Rusk, N. (2017) Antibodies trigger reprogramming. *Nature Methods* 14 (11), 1035-1035.
27. Davis, R.L. et al. (1987) Expression of a single transfected cDNA converts fibroblasts to myoblasts. *Cell* 51 (6), 987-1000.
28. Yoo, A.S. et al. (2011) MicroRNA-mediated conversion of human fibroblasts to neurons. *Nature* 476 (7359), 228-31.
29. Ladewig, J. et al. (2012) Small molecules enable highly efficient neuronal conversion of human fibroblasts. *Nat Methods* 9 (6), 575-8.
30. Mahato, B. et al. (2020) Pharmacologic fibroblast reprogramming into photoreceptors restores vision. *Nature*.
31. Ofenbauer, A. and Tursun, B. (2019) Strategies for in vivo reprogramming. *Curr Opin Cell Biol* 61, 9-15.
32. Yao, K. et al. (2018) Restoration of vision after de novo genesis of rod photoreceptors in mammalian retinas. *Nature* 560 (7719), 484-488.
33. Xiao, X. et al. (2018) Endogenous Reprogramming of Alpha Cells into Beta Cells, Induced by Viral Gene Therapy, Reverses Autoimmune Diabetes. *Cell Stem Cell* 22 (1), 78-90 e4.
34. Soraas, A. et al. (2019) Epigenetic age is a cell-intrinsic property in transplanted human hematopoietic cells. *Aging Cell* 18 (2), e12897.
35. Shannon, C.E. (1948) A Mathematical Theory of Communication. *The Bell System Technical Journal* 27, 379-423.

Methods

Mouse lines

C57BL6/J wild type mice were purchased from Jackson Laboratory (000664) for optic nerve crush and glaucoma model experiments. For aging experiments, females from NIA Aged Rodent Colonies (<https://www.nia.nih.gov/research/dab/aged-rodent-colonies-handbook>) were used. Rosa26-M2rtTA/Col1a1-tetOP-OKS-mCherry alleles were a gift from the Hochedlinger lab (Harvard) [1]. Rosa-CAG-lox-STOP-lox-Tomato mice were provided by Fan Wang (Duke). Vglut2-IRES-Cre (016963), Vgat-IRES-Cre (016962), Tet2^f (017573) and Rosa26-M2rtTA/Col1a1-tetOP-OSKM (011011) were purchased from Jackson Laboratory. All animal work was approved by Harvard Medical School, Boston Children's Hospital, and Mass Eye and Ear Institutional animal care and use committees.

Surgery

Mice were anesthetized by intraperitoneal injection of a mixture of ketamine (100 mg/kg; Ketaset; Fort Dodge Animal Health, Fort Dodge, IA) and xylazine (10 mg/kg; TranquiVed; Vedco, Inc., St. Joseph, MO) supplemented by topical application of proparacaine to the ocular surface (0.5%; Bausch & Lomb, Tampa, FL). All animal procedures were approved by the IACUC of the respective institutions and according to appropriate animal welfare regulations.

Production of adeno associated viruses (AAVs)

Vectors of AAV-TRE-OSK were made by cloning mouse Oct4, Sox2 and Klf4 cDNA into an AAV plasmid consisting of the Tet Response Element (TRE3G promoter) and the SV40 element. The other vectors were made using similar strategy or directly chemically synthesized. All

pAAVs, as listed (Supplemental Table 3), were then packaged into AAVs of serotype 2/2 or 2/9 (titers: $> 5 \times 10^{12}$ genome copies/ml). AAVs were produced by Boston Children's Hospital Viral Core.

Systemic delivery of AAV9

Expression in internal organs was achieved through retro-orbital injection of AAV9: 7×10^{11} gc of UBC-rtTA and 3×10^{11} gc of TRE-OSK for 5-month-old mice; 7×10^{11} gc of UBC-rtTA and 5×10^{11} gc of TRE-OSK (or TRE-GFP) for 20-month-old mice. To induce OSK expression, doxycycline (1 mg/ml; MP Biochemicals) was given in drinking water continuously, 3 weeks post-AAV injection.

Cell culture and differentiation

Ear fibroblasts (EFs) were isolated from Reprogramming 4F (Jackson Laboratory 011011) or 3F (Hochedlinger lab, Harvard) mice and cultured at 37°C in DMEM (Invitrogen) containing GlutaMAX, non-essential amino acids, and 10% fetal bovine serum (FBS). EFs of transgenic OSKM and OSK mice were passaged to P3 and treated with doxycycline (2 mg/ml) for the indicated time periods in the culture medium. SH-SY5Y neuroblastoma cells were obtained from the American Tissue Culture Collection (ATCC, CRL-2266) and maintained according to ATCC recommendations. Cells were cultured in a 1:1 mixture of Eagle's Minimum Essential Medium (EMEM, ATCC, 30-2003) and F12 medium (ThermoFisher Scientific, 11765054) supplemented with 10% fetal bovine serum (FBS, Sigma, F0926) and 1X penicillin/streptomycin (ThermoFisher Scientific, 15140122). Cells were cultured at 37°C with 5% CO₂ and 3% O₂. Cells were passaged at ~80% confluency. SH-SY5Y cells were differentiated into neurons as

previously described [2] with modifications. Briefly, 1 day after plating, cell differentiation was induced for 3 days using EMEM/F12 medium (1:1) containing 2.5% FBS, 1× penicillin/streptomycin, and 10 μM all-trans retinoic acid (ATRA, Stemcell Technologies, 72264) (Differentiation Medium 1), followed by a 3 day incubation in EMEM/F12 (1:1) containing 1% FBS, 1 × penicillin/streptomycin, and 10 μM ATRA (Differentiation Medium 2). Cells were then split into 35 mm cell culture plates coated with poly-D-lysine (ThermoFisher Scientific, A3890401). A day after splitting, neurons were matured in serum-free neurobasal/B27 plus culture medium (ThermoFisher Scientific, A3653401) containing 1 × Glutamax (ThermoFisher Scientific, 35050061), 1 × penicillin/streptomycin, and 50 ng/ml BDNF (Alomone labs) (Differentiation Medium 3) for at least 5 days.

Real time PCR

qPCR primers used are in Supplementary Table 4.

Neurite regeneration assay

Differentiated SH-SY5Y cells were transduced with AAV.DJ vectors at 10^6 genome copies/cell. Five days after transduction, vincristine (100 nM; Sigma, V8879) was added for 24 hrs to induce neurite degeneration. Neurons were then washed once with PBS and fresh Differentiation Medium 3 (see above) was added back to the plates. Neurite outgrowth was monitored for 2-3 weeks by taking phase-contrast images at 100x magnification every 3-4 days. Neurite area, axon length, and branch points of each cluster of neurons were quantified using Image J. Alternatively, after vincristine damage, neurons were trypsinized to dissociate the clusters and transferred to new poly-D-lysine-coated plates to better visualize the morphology of neurons.

Cell cycle analysis

Cells were harvested and fixed with 70% cold ethanol for 16 hrs at 4°C. After fixation, cells were washed twice with PBS and incubated with PBS containing 50 µg/mL propidium iodide (Biotium, 40017) and 100 µg/mL RNase A (Omega) for 1 hr at room temperature. PI-stained samples were analyzed on a BD LSR II analyzer and only single cells were gated for analysis. Cell cycle profiles were analyzed using FCS Express 6 (De Novo Software).

Human neuron methylation and epigenetic clock analyses

DNA was extracted using the Zymo Quick DNA mini-prep plus kit (D4069) and DNA methylation levels were measured on Illumina 850 EPIC arrays. The Illumina BeadChip (EPIC) measured bisulfite-conversion-based, single-CpG resolution DNAm levels at different CpG sites in the human genome. Data were generated via the standard protocol of Illumina methylation assays, which quantifies methylation levels by the β value using the ratio of intensities between methylated and un-methylated alleles. Specifically, the β value was calculated from the intensity of the methylated (M corresponding to signal A) and un-methylated (U corresponding to signal B) alleles, as the ratio of fluorescent signals $\beta = \text{Max}(M,0)/(\text{Max}(M,0)+ \text{Max}(U,0)+100)$. Thus, β values ranged from 0 (completely un-methylated) to 1 (completely methylated). "Noob" normalization was implemented using the "minfi" R package [3, 4]. The mathematical algorithm and available software underlying the skin & blood clock for *in vitro* studies (based on 391 CpGs) was previously published [5].

AAV2 intravitreal injection

Adult animals were anesthetized with ketamine/xylazine (100/10 mg/kg) and then AAV (1-2 μ l) was injected intravitreally, just posterior to the limbus with a fine glass pipette attached to a Hamilton syringe using plastic tubing. In the elevated IOP model, mice received a 1 μ l intravitreal injection between 3-4 weeks following microbead injection. The injected volume of AAV-sh-RNA is 1/5th the volume of other AAVs.

Optical Coherence Tomography (OCT)

OCT images were taken with a Bioptigen Envisu R-Class OCT (Leica Microsystems). The animals were anesthetized with a ketamine/xylazine (100-200/20 mg/kg) cocktail and eyes were treated with a drop of 1% tropicamide solution to dilate the pupils and a drop of GenTeal gel to keep the lens hydrated. Full retinal OCT scans were obtained for all eyes (1000x100x10). 100 B-scans were converted into 7fps videos with ImageJ. Representative OCT images of the retina were taken near the optic nerve head, and the imaging location was marked on the volume intensity projection image with a white line. The retinal thickness of 4 B-scans from each eye was measured at a distance of 50 – 600 μ m on both sides of the optic nerve head and averaged using ImageJ.

Creation of retinoblastoma tumors

In order to create the space to inject the retinoblastoma tumor cells into the subretinal space, a transient retinal detachment was created. Intraocular pressure was decreased by first making a corneal incision, followed by a subretinal injection of 10,000 retinoblastoma tumor cells (Rb116) via a 30-gauge needle in a total volume of 10 μ l. Two weeks post-injection the mice were observed via OCT.

Optic nerve crush

Two weeks after intravitreal AAV injection, the optic nerve was accessed intraorbitally and crushed in anesthetized animals using a pair of Dumont #5 forceps (FST). Alexa-conjugated cholera toxin beta subunit (CTB-555, 1 mg/ml; 1-2 μ l) injection was performed 2-3 days before euthanasia to trace regenerating RGC axons. More detailed surgical methods were described previously [6].

In vivo doxycycline induction or suppression

Induction of the Tet-On or suppression of the Tet-Off AAV2 systems in the retina was performed by administration of doxycycline (2 mg/ml) (Sigma) in the drinking water. Induction of Tet-On AAV9 system systemically was performed by administration of doxycycline (1 mg/ml) (USP grade, MP Biomedicals 0219895505) in the drinking water.

Quantification of axon regeneration for the optic nerve crush model

The number of regenerating axons in the optic nerve was estimated by counting the number of CTB-labeled axons at different distances from the crush site as described previously [6].

Wholemout optic nerve preparation

Optic nerves and the connecting chiasm were dehydrated in methanol for 5 min, then incubated overnight with Visikol® HISTO-1™. Next day nerves were transferred to Visikol® HISTO-2™ and then incubated for 3 hrs. Finally, optic nerves and connecting chiasm were mounted with Visikol® HISTO-2™.

Immunofluorescence

Wholemount retinas were blocked with horse serum 4°C overnight then incubated at 4°C for 3 days with primary antibodies diluted in PBS, BSA (3%) Triton X-100 (0.5%). Then, tissues were incubated at 4°C overnight with appropriate Alexa Fluor-conjugated secondary antibodies (Alexa 405, 488, 567, 674; Invitrogen) diluted with the same blocking solution as the primary antibodies, generally used at 1:400 final dilution. Frozen sections were stained overnight with primary antibodies at 4°C and then secondary antibodies at room temperature for 2 h. Between changes of solutions, all wholemounts or slices were washed 3x 5min each time. Sections or wholemount retinas were mounted with Vectashield Antifade Mounting Medium. Antibodies used: Mouse anti-Oct4 (1:100, BD bioscience 611203), Rabbit anti-Sox2 (1:100, Cell signaling 14962), Goat anti-Klf4 (1:100, R&D system AF3158), Rabbit anti-phosphorylated S6 Ser235/236 (1:100, Cell Signaling 4857), Mouse anti-Brn3a (1:200, EMD Millipore MAB1585), Rabbit anti-Ki67(1:100, Abcam ab15580), Mouse anti-AP2 alpha (1:100, Developmental Studies Hybridoma Bank 3B5), Rabbit anti-pStat3 (Tyr705) (1:100, Cell signaling 9145S), Rat anti-HA (1:400, Roche 11867423001), Rabbit anti-5mC (1:100, Cell signaling 28692S), Rabbit anti-5hmC (1:100, Active Motif 39769), Rat anti-BrdU (1:200, Abcam ab6326), Rabbit anti-Olig2 (1:100, Novusbio NBP1-28667) and Chicken anti-GFP (1:10000, Aves Labs GFP-1020), and Guinea pig anti-RBPMS (1:400, Raygene custom order A008712 to peptide GGKAEKENTPSEANLQEEEVRC). Note that successful staining for anti-5mC, anti-5hmC, anti-Ki67, and anti-BrdU requires pre-treatment of 2N HCL for 30min at room temperature, followed by 3 washes of 0.1M Sodium Borate pH 8.3 and PBST each before the serum blocking.

5-Bromo-2'-deoxyuridine (BrdU) labelling

Post crush injury, mice were injected intraperitoneally with BrdU (Sigma, B5002) at a dose of 100 mg/kg daily the week before sacrifice. Optic nerves and retinas were collected either 1 or 2 wpc. Optic nerve sections and retina wholemounts were then performed with the same procedure in Immunofluorescence section (including HCL pre-treatment) to complete the staining.

Western blot

SDS-PAGE and Western blot analysis was performed according to standard procedures and detected with an ECL detection kit. Antibodies used: Rabbit anti-Sox2 (1:100, EMD Millipore, AB5603), Mouse anti-Klf4 (1:1000, ReproCell, 09-0021), Rabbit anti-p-S6 (S240/244) (1:1000, CST, 2215), Mouse anti-S6 (1:1000, CST, 2317), Mouse anti- β -Tubulin (1:1000, Sigma-Aldrich, 05-661), Mouse anti- β -Actin–Peroxidase antibody (1:20,000, Sigma-Aldrich, A3854).

RGC survival and phospho-S6 signal

BPMS-positive cells in the ganglion layer were stained with an anti-BPMS antibody (1:400, Raygene custom order A008712 to peptide GGKAEKENTPSEANLQEEEVRC) and a total of four 10X fields per retina, one in each quadrant, were enumerated. The average number per field was determined and the percentages of viable RGCs were obtained by comparing the values determined from the uninjured contralateral retinas. Phospho-S6 (1:100, Cell Signaling 4857) staining was performed under the same conditions and the densities of phospho-S6-positive RGCs were obtained by comparing the value to uninjured contralateral retinas.

Microbead-induced mouse model of elevated IOP (intraocular pressure)

Elevation of IOP was induced unilaterally by injection of polystyrene microbeads (FluoSpheres; Invitrogen, Carlsbad, CA; 15- μ m diameter) to the anterior chamber of the right eye of each animal under a surgical microscope, as previously reported [7]. Briefly, microbeads were prepared at a concentration of 5.0×10^6 beads/mL in sterile physiologic saline. A 2 μ L volume was injected into the anterior chamber through a trans-corneal incision using a sharp glass micropipette connected to a Hamilton syringe (World Precision Instruments Inc., Sarasota, FL) followed by an air bubble to prevent leakage. Any mice that developed signs of inflammation (clouding or an edematous cornea) were excluded.

IOP measurements

IOPs were measured with a rebound TonoLab tonometer (Colonial Medical Supply, Espoo, Finland), as previously described [7, 8]. Mice were anesthetized by 3% isoflurane in 100% oxygen (induction) followed by 1.5% isoflurane in 100% oxygen (maintenance) delivered with a precision vaporizer. IOP measurement was initiated within 2-3 min after the loss of a toe or tail pinch reflex. Anesthetized mice were placed on a platform and the tip of the pressure sensor was placed approximately 1/8 inch from the central cornea. Average IOP was displayed automatically after 6 measurements after elimination of the highest and lowest values. The machine-generated mean was considered as one reading, and six readings were obtained for each eye. All IOPs were taken at the same time of day (between 10:00 and 12:00 hrs) due to the variation of IOP throughout the day.

Optomotor response

Visual acuity of mice was measured using an optomotor reflex-based spatial frequency threshold test [9, 10]. Mice were able to freely move and were placed on a pedestal located in the center of an area formed by four computer monitors arranged in a quadrangle. The monitors displayed a moving vertical black and white sinusoidal grating pattern. A blinded observer, unable to see the direction of the moving bars, monitored the tracking behavior of the mouse. Tracking was considered positive when there was a movement of the head (motor response) to the direction of the bars or rotation of the body in the direction concordant with the stimulus. Each eye was tested separately depending on the direction of rotation of the grating. The staircase method was used to determine the spatial frequency start from 0.15 to 0.40 cycles/deg, with intervals of 0.05 cycles/deg. Rotation speed ($12^\circ/\text{s}$) and contrast (100%) were kept constant. Responses were measured before and after treatment by individuals blinded to the group of the animal and the treatment. Mice that had intravitreal bleeding or developed signs of inflammation (clouding or an edematous cornea) during or post intravitreal injection were excluded from OMR and histological analyses. Exclusion criteria were pre-determined before experimentation.

Pattern electroretinogram (PERG)

Mice were anesthetized with ketamine/xylazine (100mg/kg and 20mg/kg) and the pupils dilated with one drop of 1% tropicamide ophthalmic solution. The mice were kept under dim red light throughout the procedure on a built-in warming plate (Celeris, Full-Field and Pattern Stimulation for the rodent model) to maintain body temperature at 37°C . A black and white reversing checkerboard pattern with a check size of 1° was displayed on light guide electrode-stimulators placed directly on the ocular surface of both eyes and centered with the pupil. The visual stimuli

were presented at 98% contrast and constant mean luminance of 50 cd/m², spatial frequency: 0.05 cyc/deg; temporal frequency: 1Hz. A total of 300 complete contrast reversals of PERG were repeated twice in each eye and the 600 cycles were segmented and averaged and recorded. The averaged PERGs were analyzed to evaluate the peak to trough N1 to P1 (positive wave) amplitude.

Quantification of optic nerve axons for the glaucoma model

For quantification of axons, optic nerves were dissected and fixed overnight in Karnovsky's reagent (50% in phosphate buffer). Semi-thin cross-sections of the nerve were taken at 1.0 mm posterior to the globe and stained with 1% p-phenylenediamine (PPD) for evaluation by light microscopy. Optic nerve cross sections were imaged at 60x magnification using a Nikon microscope (Eclipse E800, Nikon, Japan) with the DPController software (Olympus, Japan) and 6-8 non-overlapping photomicrographs were taken to cover the entire area of each optic nerve cross-section. Using ImageJ (Version 2.0.0-rc-65/1.51u), a 100 μM x 100 μM square was placed on each 60x image and all axons within the square (0.01mm²) were counted using the threshold and analyze particles function in ImageJ as previously described [7-9]. Damaged axons stain darkly with PPD and are not counted. The average axon counts in the 6-8 images were used to calculate the axon density/mm² of optic nerve. Individuals performing axon counts were blinded to the experimental groups.

Quantification of retinal ganglion cells in glaucoma model

For ganglion cell counting, images of wholemount retinas were acquired using a 63x oil immersion objective of the Leica TCS SP5 confocal microscope (Leica Microsystems). The

retinal wholemount was divided into four quadrants and two to four images (248.53 μ m by 248.53 μ m in size) were taken from the midperipheral and peripheral regions of each quadrant, for a total of twelve to sixteen images per retina. The images were obtained as z-stacks (0.5 μ m) and all Brn3a positive cells in the ganglion cell layer of each image were counted manually as previously described [9]. Briefly, RGCs were counted using the “Cell Counter” plugin (http://fiji.sc/Cell_Counter) in Fiji (ImageJ Fiji, version 2.0.0-rc-69/1.52n). Each image was loaded into Fiji and a color counter type was chosen to mark all Brn3a stained RGCs within each image (0.025mm²). The average number of RGCs in the 12 to sixteen images were used to calculate the RGC density per square millimeter of retina. Two individuals blinded to the experimental groups performed all RGC counts.

RGC enrichment

Retinas were fresh dissected and dissociated in AMES media using papain, then triturated carefully and stained with Thy1.2-PE-Cy7 anti-body (Invitrogen 25-0902-81) and Calcein Blue live-dead cell stain, then flow sorted on a BD FACS Aria using an 130 μ m nozzle to collect over 10,000 Thy1.2+ and Calcein blue+ cells (1-2% of total events). Frozen cells were sent to GENEWIZ, LLC (South Plainfield, NJ, USA) for RNA extraction and ultra-low input RNA-seq, or to Zymo research (Irving, CA) for DNA extraction and genome-wide reduced representation bisulfite sequencing (RRBS).

RRBS library preparation

DNA was extracted using Quick-DNA Plus Kit Microprep Kit. 2-10 ng of starting input genomic DNA was digested with 30 units of *MspI* (NEB). Fragments were ligated to pre-annealed

adapters containing 5'-methyl-cytosine instead of cytosine according to Illumina's specified guidelines. Adaptor-ligated fragments ≥ 50 bp in size were recovered using the DNA Clean & ConcentratorTM-5 (Cat#: D4003). The fragments were then bisulfite-treated using the EZ DNA Methylation-LightningTM Kit (Cat#: D5030). Preparative-scale PCR products were purified with DNA Clean & ConcentratorTM-5 (Cat#: D4003) for sequencing on an Illumina HiSeq using 2x125 bp PE.

DNA methylation age analysis of mouse RGC

Reads were filtered using trim galore v0.4.1 and mapped to the mouse genome GRCm38 using Bismark v0.15.0. Methylation counts on both positions of each CpG site were combined. Only CpG sites covered in all samples were considered for analysis. This resulted in total of 708156 sites. For analyzing the rDNA methylation age, reads were mapped to BK000964 and the coordinates were adjusted accordingly [11]. 70/72 sites were covered for rDNA clock, compared to 102/435 sites of whole lifespan multi-tissue clock [12], or 248/582 and 77,342/ 193,651 sites (ridge) of two entire lifespan multi-tissue clocks [13]. The global DNA methylation comparisons, including CpG islands, gene promoters, and gene bodies was performed with RnBeads v2.0 using genome annotation version RnBeads.mm10[14].

Total RNA extraction and sample QC

Total RNA was extracted following the Trizol Reagent User Guide (Thermo Fisher Scientific). 1 μ l of 10 mg/ml Glycogen was added to the supernatant to increase RNA recovery. RNA was quantified using Qubit 2.0 Fluorometer (Life Technologies, Carlsbad, CA, USA) and RNA integrity was determined using TapeStation (Agilent Technologies, Palo Alto, CA, USA).

Ultra-low input RNA library preparation and multiplexing

RNA samples were quantified using Qubit 2.0 Fluorometer (Life Technologies, Carlsbad, CA, USA) and RNA integrity was ascertained using a 2100 TapeStation (Agilent Technologies, Palo Alto, CA, USA). RNA library preparations, sequencing reactions, and initial bioinformatics analysis were conducted at Genewiz (South Plainfield, NJ, USA). A SMART-Seq v4 Ultra Low Input Kit for Sequencing was used for full-length cDNA synthesis and amplification (Clontech, Mountain View, CA), and Illumina Nextera XT library was used for sequencing library preparation. Briefly, cDNA was fragmented, and adaptors were added using Transposase, followed by limited-cycle PCR to enrich and add an index to the cDNA fragments. The final library was assessed by a Qubit 2.0 Fluorometer and Agilent TapeStation.

Paired End Sequencing

The sequencing libraries were multiplexed and clustered on two lanes of a flowcell. After clustering, the flowcell were loaded on the Illumina HiSeq instrument according to manufacturer's instructions. Samples were sequenced using a 2x150 Paired End (PE) configuration. Image analysis and base calling were conducted by the HiSeq Control Software (HCS) on the HiSeq instrument. Raw sequence data (.bcl files) generated from an Illumina HiSeq was converted into fastq files and de-multiplexed using Illumina bcl2fastq v2.17 program. One mismatch was allowed for index sequence identification.

RNA-seq analysis

Paired-end reads were aligned with hisat2 v2.1.0[15] to the Ensembl GRCm38 primary assembly using splice junctions from the Ensembl release 84 annotation. Paired read counts were quantified using featureCounts v1.6.4[16] using reads with a MAPQ ≥ 20 . Differentially-expressed genes for each pairwise comparison were identified with edgeR v3.26[17], testing only genes with at least 0.1 counts-per-million (CPM) in at least three samples. Gene ontology analysis of differentially-expressed genes was performed with AmiGO v2.5.12[18-20]. Age-associated sensory perception genes were extracted from the mouse Sensory Perception (GO:0007600) category the Gene Ontology database, including genes that were differentially expressed ($q \leq 0.05$) in 12 versus 5-month-old mice, excluding genes that were induced by the Control virus alone ($q \leq 0.1$).

Statistical analysis

Statistical analyses were performed with GraphPad Prism 8, using two-tailed Student's t-tests, one-way or two-way ANOVA. All of the statistical tests performed are indicated in the figure legends. The data are presented as mean \pm S.E.M. Although no statistical methods were used to predetermine sample size, we took into account previous experience to estimate the number of animals needed in each experiment.

Data availability

RRBS data for DNA methylation analysis and RNA-seq data are available in the Biosample database (NCBI) and under BioProject ID PRJNA555100. Illumina Human Methylation EPIC array data is available under GSE147436.

References

1. Bar-Nur, O. et al. (2014) Small molecules facilitate rapid and synchronous iPSC generation. *Nat Methods* 11 (11), 1170-6.
2. Shipley, M.M. et al. (2016) Differentiation of the SH-SY5Y Human Neuroblastoma Cell Line. *J Vis Exp* (108), 53193.
3. Triche, T.J., Jr. et al. (2013) Low-level processing of Illumina Infinium DNA Methylation BeadArrays. *Nucleic Acids Res* 41 (7), e90.
4. Fortin, J.P. et al. (2017) Preprocessing, normalization and integration of the Illumina HumanMethylationEPIC array with minfi. *Bioinformatics* 33 (4), 558-560.
5. Horvath, S. et al. (2018) Epigenetic clock for skin and blood cells applied to Hutchinson Gilford Progeria Syndrome and ex vivo studies. *Aging (Albany NY)* 10 (7), 1758-1775.
6. Park, K.K. et al. (2008) Promoting axon regeneration in the adult CNS by modulation of the PTEN/mTOR pathway. *Science* 322 (5903), 963-6.
7. Krishnan, A. et al. (2016) Overexpression of Soluble Fas Ligand following Adeno-Associated Virus Gene Therapy Prevents Retinal Ganglion Cell Death in Chronic and Acute Murine Models of Glaucoma. *J Immunol* 197 (12), 4626-4638.
8. Dordea, A.C. et al. (2016) An open-source computational tool to automatically quantify immunolabeled retinal ganglion cells. *Exp Eye Res* 147, 50-56.
9. Gao, S. and Jakobs, T.C. (2016) Mice Homozygous for a Deletion in the Glaucoma Susceptibility Locus INK4 Show Increased Vulnerability of Retinal Ganglion Cells to Elevated Intraocular Pressure. *Am J Pathol* 186 (4), 985-1005.
10. Sun, D. et al. (2013) Reversible reactivity by optic nerve astrocytes. *Glia* 61 (8), 1218-1235.
11. Wang, M. and Lemos, B. (2019) Ribosomal DNA harbors an evolutionarily conserved clock of biological aging. *Genome Res* 29 (3), 325-333.
12. Meer, M.V. et al. (2018) A whole lifespan mouse multi-tissue DNA methylation clock. *Elife* 7.
13. Thompson, M.J. et al. (2018) A multi-tissue full lifespan epigenetic clock for mice. *Aging (Albany NY)* 10 (10), 2832-2854.
14. Muller, F. et al. (2019) RnBeads 2.0: comprehensive analysis of DNA methylation data. *Genome Biol* 20 (1), 55.
15. Kim, D. et al. (2015) HISAT: a fast spliced aligner with low memory requirements. *Nat Methods* 12 (4), 357-60.
16. Liao, Y. et al. (2014) featureCounts: an efficient general purpose program for assigning sequence reads to genomic features. *Bioinformatics* 30 (7), 923-30.
17. Robinson, M.D. et al. (2010) edgeR: a Bioconductor package for differential expression analysis of digital gene expression data. *Bioinformatics* 26 (1), 139-40.
18. Carbon, S. et al. (2009) AmiGO: online access to ontology and annotation data. *Bioinformatics* 25 (2), 288-9.
19. Ashburner, M. et al. (2000) Gene ontology: tool for the unification of biology. The Gene Ontology Consortium. *Nat Genet* 25 (1), 25-9.
20. The Gene Ontology, C. (2019) The Gene Ontology Resource: 20 years and still GOing strong. *Nucleic Acids Res* 47 (D1), D330-D338.

Supplementary Tables

Supplementary Table 1| List of axon regeneration related genes and their changes in OSK treatment

OSK/-OSK	logFC	QValue
Stat3	1.14	5.84E-13
RhoA	0.52	1.46E-05
CREB1	0.64	1.94E-05
SRF	0.71	0.00276158
ASCL1	-1.45	0.00394945
KLF7	-0.56	0.01105991
KLF6	0.46	0.02200404
SOCS3	0.61	0.09081721
SOX11	-1.00	0.15063212
PTEN	-0.20	0.20517764
c-JUN	-0.23	0.4980782
HIF1a	0.14	0.61787927
SMAD1	-0.14	0.64625121
ATF3	0.14	0.91788819

Supplementary Table 2| List of genes differentially expressed during RGC aging

Genes down during aging	Genes up during aging
1700031P21Rik	0610040J01Rik
1810053B23Rik	1700080N15Rik
2900045O20Rik	2900064F13Rik
2900060B14Rik	4833417C18Rik
4921504E06Rik	4921522P10Rik
4930402F11Rik	4930447C04Rik
4930453C13Rik	4930488N15Rik
4930455B14Rik	Ace
4930500H12Rik	Ackr1
4930549P19Rik	Acot10
4930555B11Rik	Acvr1
4930556J02Rik	Adamts17
4932442E05Rik	Adra1b
4933431K23Rik	AI504432
4933438K21Rik	Best3
6720475M21Rik	Boc
9830132P13Rik	Cadm3
A430010J10Rik	Cand2
A530064D06Rik	Ccl9
A530065N20Rik	Cd14
Abcb5	Cd36
Abhd17c	Cfh
AC116759.2	Chrm3
AC131705.1	Chrna4
AC166779.3	Cntn4
Acot12	Cracr2b
Adig	Cryaa
Akr1cl	CT573017.2
Ankrd1	Cyp26a1
Asb15	Cyp27a1
Atp2c2	D330050G23Rik
AU018091	D930007P13Rik
AW822073	Ddo
Btnl10	Dgkg
C130093G08Rik	Dlk2
C730027H18Rik	Dnaja1-ps

Ccdc162	Drd2
Chil6	Dsel
Col26a1	Dytn
Corin	Ecsr
Crls1	Edn1
Cybrd1	Ednrb
Cyp2d12	Efemp1
Cyp7a1	Elfn2
D830005E20Rik	Epha10
Dlx3	Ephx1
Dnah14	Erbp4
Dsc3	Fam20a
Dthd1	Fbxw21
Eid2	Ffar4
Eps811	Flt4
EU599041	Fmod
Fam90a1a	Foxp4
Fancf	Fzd7
Fau-ps2	Gabrd
Fezfl	Galnt15
Gja5	Galnt18
Gm10248	Gfra2
Gm10513	Ggt1
Gm10635	Gm10416
Gm10638	Gm14964
Gm10718	Gm17634
Gm10722	Gm2065
Gm10800	Gm32352
Gm10801	Gm33172
Gm11228	Gm34280
Gm11251	Gm35853
Gm11264	Gm36298
Gm11337	Gm36356
Gm11368	Gm36937
Gm11485	Gm3898
Gm11693	Gm42303
Gm12793	Gm42484
Gm13050	Gm42537
Gm13066	Gm42743

Gm13323	Gm43151
Gm13339	Gm43843
Gm13346	Gm44545
Gm13857	Gm44722
Gm14387	Gm45516
Gm14770	Gm45532
Gm15638	Gm47494
Gm16072	Gm47982
Gm16161	Gm47989
Gm16181	Gm48398
Gm17200	Gm48495
Gm17791	Gm48593
Gm18025	Gm48958
Gm18757	Gm49089
Gm18795	Gm49326
Gm18848	Gm49331
Gm19719	Gm49760
Gm20121	Gm5796
Gm20356	Gm6374
Gm2093	Gm7276
Gm21738	Gm8237
Gm21940	Gm9796
Gm22933	Gm9954
Gm24000	Gpr75
Gm24119	Gpre5c
Gm25394	Grid2ip
Gm26555	Gsg112
Gm27047	Hapln4
Gm28262	Hcn3
Gm28530	Hcn4
Gm29295	Hhatl
Gm29825	Hs6st2
Gm29844	Htr3a
Gm3081	Il1rap
Gm32051	Il1rapl2
Gm32122	Inka1
Gm33056	Kbtbd12
Gm33680	Kcnj11
Gm34354	Kenk4

Gm34643	Kdelc2
Gm3551	Klhl33
Gm36660	Lamc3
Gm36948	Lilra5
Gm37052	Lman11
Gm37142	Lrfn2
Gm37262	Lrrc38
Gm37535	Lrrn4cl
Gm37569	Ltc4s
Gm37589	Mansc1
Gm37647	Mir344c
Gm37648	Msr1
Gm37762	Mycbpap
Gm38058	Myoc
Gm38069	Ngfr
Gm38137	Nipal2
Gm38218	Olfr1372-ps1
Gm39139	Otop3
Gm42535	P2rx5
Gm42680	P2ry12
Gm42895	P4ha2
Gm42994	Pcdha12
Gm43027	Pcdha2
Gm43158	Pcdhac2
Gm43288	Pcdhb18
Gm43366	Pcdhb5
Gm44044	Pcsk2os1
Gm44081	Pcsk6
Gm44187	Perp
Gm44280	Pkp1
Gm44535	Plxna4
Gm45338	Prickle2
Gm45644	Qsox1
Gm45740	Rapgef4os2
Gm46555	Rbp4
Gm46565	Rcn3
Gm4742	Sec14l5
Gm47485	Sel1l3
Gm47853	Serpinh1

Gm47992	Sgpp2
Gm48225	Shisa6
Gm48314	Siah3
Gm48383	Siglech
Gm48673	Slc12a4
Gm48804	Slc24a2
Gm48832	Slc2a5
Gm4994	Slc4a4
Gm5487	Slitrk3
Gm5724	Smagp
Gm595	Smoc2
Gm6012	Speer4b
Gm6024	Spon2
Gm7669	Sstr2
Gm7730	Sstr3
Gm8043	St3gal3
Gm8953	Stc1
Gm9348	Stc2
Gm9369	Syndig1
Gm9495	Syt10
H2al2a	Thsd7a
Ido2	Tlr8
Igfbp1	Tmem132a
Kif7	Tmem132d
Klhl31	Tmem200a
Lrrc31	Tmem44
Mc5r	Trpc4
Mgam	Trpv4
Msh4	Unc5b
Muc12	Vgf
Mug1	Vmn1r90
Mybl2	Vwc2l
Myh15	Wfikkn2
Nek10	Wnt11
Neurod6	Wnt6
Nr1h5	Zeb2os
Olfr1042	Zfp608
Olfr1043	Zfp976
Olfr1082	

Olfr1090
Olfr1124
Olfr1167
Olfr1205
Olfr1206
Olfr1223
Olfr1263
Olfr1264
Olfr1269
Olfr127
Olfr1291-ps1
Olfr1406
Olfr1469
Olfr215
Olfr273
Olfr328
Olfr355
Olfr372
Olfr390
Olfr427
Olfr456
Olfr466
Olfr481
Olfr522
Olfr6
Olfr601
Olfr603
Olfr706
Olfr727
Olfr728
Olfr741
Olfr801
Olfr812
Olfr816
Olfr822
Olfr860
Olfr890
Olfr923
Olfr943

Otogl
Pi15
Pkhd1
Pkhd111
Platr6
Pou3f4
Prr9
Pvalb
Rhag
Sav1
Serpib9b
Skint1
Skint3
Skint5
Slc10a5
Slc6a4
Smok2a
Tcaf3
Tomm20l
Trcgl
Trdn
Ugt1a6a
Usp17la
Vmn1r178
Vmn1r179
Vmn1r33
Vmn1r74
Vmn1r87
Vmn2r102
Vmn2r113
Vmn2r17
Vmn2r52
Vmn2r66
Vmn2r68
Vmn2r76
Vmn2r78
Wnt16

Supplementary Table 3| AAV vectors used in this study

Vector	qPCR Primer for measuring titer	Source
pAAV-TRE-Oct4	TRE3G	This paper
pAAV-TRE-Sox2	TRE3G	This paper
pAAV-TRE-Klf4	TRE3G	This paper
pAAV-TRE-Oct4-Sox2	TRE3G	This paper
pAAV-TRE-OSK	TRE3G	This paper
pAAV-TRE-d2EGFP	TRE3G	This paper
pAAV-TRE-Luc	TRE3G	This paper
pAAV-CMV-rtTAV16	WPRE	This paper
pAAV-UBC-rtTA4	WPRE	This paper
pAAV-CAG-tTA	hGH	This paper
pAAV-sh-Scr-YFP	WPRE	Addgene #85741
pAAV-Sh-Tet1-YFP	WPRE	Addgene #85742
pAAV-sh-Tet2-YFP	WPRE	Addgene #85743
pAAV-EF1a-HA-hTet1CD-WPRE-PolyA	WPRE	Addgene #39454
pAAV-EF1a-HA-hTet1CDmu-WPRE-PolyA	WPRE	Addgene #39455
pAAV-CAG-FLEX2-tTA2-WPRE-bGHpA	WPRE	Addgene #65458
pAAV-sh-Scr-H2BGFP	hGH	Weng et al., 2017, Neuron
pAAV-sh-TDG-H2BGFP	hGH	Weng et al., 2017, Neuron

Primer name	Sequence
TRE3G F	AACGTATCTACAGTTTACT CCCTATC
TRE3G R	GGTAGGAAGTGGTACGGA AAG
WPRE F	CACTGACAATTCCGTGGTG T
WPRE R	GAGATCCGACTCGTCTGAG G
hGH F	TGGGAAGACAACCTGTAGG G
hGH R	TGAAACCCCGTCTCTACCA A

Supplementary Table 4| Primers used for RT-PCR

Gene	Primer sequence
mOct4 F	ACA TCG CCA ATC AGC TTG G
mOct4 R	AGA ACC ATA CTC GAA CCA CAT CC
mSox2 F	ACA GAT GCA ACC GAT GCA CC
mSox2 R	TGG AGT TGT ACT GCA GGG CG
mKlf4 F	GTGCCCCGACTAACCGTTG
mKlf4 R	GTCGTTGAACTCCTCGGTCT
mMyc F	ATGCCCTCAACGTGAACTTC
mMyc R	CGCAACATAGGATGGAGAGCA
mHist1 h2a F	GCG ACA ACA AGA AGA CGC GCA T
mHist1 h2a R	CTG GAT GTT GGG CAG GAC GCC
mHist1 h2b F	AAG AAG GAC GGC AAG AAG CGC A
mHist1 h2b R	CGC TCG AAG ATG TCG TTC ACG A
mHIST1 H3.1/H3.2 F	GAA GAA GCC TCA CCG CTA CCG
mHIST1 H3.1/H3.2 R	GGT TGG TGT CCT CAA ACA GAC CC
mHist1 h4 F	AAC ATC CAG GGC ATC ACC AAG C
mHist1 h4 R	GTT CTC CAG GAA CAC CTT CAG C
mLmnb1 F	CCG GCC TCA AGG CTC TCT A
mLmnb1 R	TGC CGC CTC ATA CTC TCG AA
mActb F	AGT GTG ACG TTG ACA TCC GT
mActb R	TGC TAG GAG CCA GAG CAG TA
mNanog F	TCTTCCTGGTCCCCACAGTTT
mNanog R	GCAAGAATAGTTCTCGGGATGAA
mChaf1a R	GTG TCT TCC TCA ACT TTC TCC TTG G
mChaf1a F	CGC GGA CAG CCG CGG CCG TGG ATT GC
mChaf1b R	GGC TCC TTG CTG TCA TTC ATC TTC CAC
mChaf1b F	CAC CGC CGT CAG GAT CTG GAA GTT GG
mLmnb1 F	CCG GCC TCA AGG CTC TCT A
mLmnb1 R	TGC CGC CTC ATA CTC TCG AA
mp16 (Cdkn2a) F	ACA TCA AGA CAT CGT GCG ATA TT
mp16 (Cdkn2a) R	CCA GCG GTA CAC AAA GAC CA
mApob F	AAG CAC CTC CGA AAG TAC GTG

mApob R	CTC CAG CTC TAC CTT ACA GTT GA
hTet2 F	GATAGAACCAACCATGTTGAGGG
hTet2 R	TGGAGCTTTGTAGCCAGAGGT
hActb F	CACCATTGGCAATGAGCGGTTC
hActb R	AGGTCTTTGCGGATGTCCACGT
mTet1 F	TCAAGCAATGGACCACTGGG
mTet1 R	TCTCCATGAGCTCCCTGACA
mTet2 F	ACT CCT GGT GAA CAA AGT CAG A
mTet2 R	CAT CCC TGA GAG CTC TTG CC
mTet3-F	CCGGATTGAGAAGGTCATCTAC
mTet3-R	AAGATAACAATCACGGCGTTCT
mGAPDH F	CCA ATG TGT CCG TCG TGG ATC T
mGAPDH R	GTT GAA GTC GCA GGA GAC AAC C
mStat3-F	CAATACCATTGACCTGCCGAT
mStat3-R	GAGCGACTCAAACCTGCCCT
mKlf6-F	GTTTCTGCTCGGACTCCTGAT
mKlf6-R	TTCCTGGAAGATGCTACACATTG
Efemp1-F	GCGCTGGTCAAGTCACAGTA
Efemp1-R	AAGCATCTGGGACAATGTCAC